



Norwegian University of
Science and Technology

Snow Production Equipment at Ambient Temperatures Above Zero Degrees Celsius

Jon-Brede Rykkje Dieseth

Master of Science in Mechanical Engineering

Submission date: June 2016

Supervisor: Trygve Magne Eikevik, EPT

Co-supervisor: Ignat Tolstorebrov, EPT

Norwegian University of Science and Technology
Department of Energy and Process Engineering

EPT-M-2016-32

MASTER THESIS

for

Student Jon-Brede Rykkje Dieseth

Spring 2016

Snow Production equipment at Ambient Temperatures above 0°C*Snøproduksjonsutstyr for lufttemperaturer over 0°C***Background and objective**

In the perspective of increasing global temperatures, there is a challenge having available snow close to the cities and villages in the mountain for a reasonable winter season. The periods of natural snow is shorter and in areas, the snow in the winter is disappearing. In Europe the facilities is moving to higher locations to be able to arrange winter games.

In the Nordic countries, it is also a tradition for doing winter activities in snow like kinder gardens, schools and for the families to go skiing in weekends and holidays. If the trend with milder winters is going on the distance, the individual homes to areas with snow will grow. To be able to maintain the snow activity close to the cities it will be of importance to produce snow at temperatures above 0°C. Since this is an energy consuming process, the energy efficiency of the equipment is of importance and the possibility to utilize the heat for space heating or hot tap water, with emphasize on reducing the operational costs.

This master thesis work is a cooperation with Trondheim Kommune and the Norwegian Ski Association within the scope of "Snow for the future". Trondheim Kommune will in the near future build a center in Granåsen that will give possibilities for future winter games and give the people possibility to enjoy the winter activity in the period from November to March.

This master thesis will focus on energy efficient and environmentally friendly machinery for making snow at ambient air temperatures above 0°C, with emphasis on utilization of the surplus heat. The capacity of the system in this project should be 50 tons per day.

The following tasks are to be consider:

1. Literature review of snow production at temperatures above 0°C both components and systems
2. Developing a simulation tool for the ice production unit, including both flake ice and vacuum ice. The model should include pipe and component design with pressure drop

3. Modelling and design of an indirect CO₂ ice producing system, connected to a heat recovery refrigeration unit. The same heat recovery unit should cool the vacuum ice maker.
4. Evaluation of energy use at different ambient temperatures, comparing new solutions with existing solutions
5. Make a draft scientific paper with the main results for the thesis
6. Make proposal for further work within the topic

-- " --

Within 14 days of receiving the written text on the master thesis, the candidate shall submit a research plan for his project to the department.

When the thesis is evaluated, emphasis is put on processing of the results, and that they are presented in tabular and/or graphic form in a clear manner, and that they are analyzed carefully.

The thesis should be formulated as a research report with summary both in English and Norwegian, conclusion, literature references, table of contents etc. During the preparation of the text, the candidate should make an effort to produce a well-structured and easily readable report. In order to ease the evaluation of the thesis, it is important that the cross-references are correct. In the making of the report, strong emphasis should be placed on both a thorough discussion of the results and an orderly presentation.

The candidate is requested to initiate and keep close contact with his/her academic supervisor(s) throughout the working period. The candidate must follow the rules and regulations of NTNU as well as passive directions given by the Department of Energy and Process Engineering.

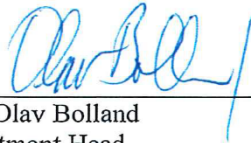
Risk assessment of the candidate's work shall be carried out according to the department's procedures. The risk assessment must be documented and included as part of the final report. Events related to the candidate's work adversely affecting the health, safety or security, must be documented and included as part of the final report. If the documentation on risk assessment represents a large number of pages, the full version is to be submitted electronically to the supervisor and an excerpt is included in the report.

Pursuant to "Regulations concerning the supplementary provisions to the technology study program/Master of Science" at NTNU §20, the Department reserves the permission to utilize all the results and data for teaching and research purposes as well as in future publications.

The final report is to be submitted digitally in DAIM. An executive summary of the thesis including title, student's name, supervisor's name, year, department name, and NTNU's logo and name, shall be submitted to the department as a separate pdf file. Based on an agreement with the supervisor, the final report and other material and documents must be given to the supervisor in digital format. All relevant data collected and produced during the project shall be delivered to the supervisor on a Memory stick at the end of the Master Thesis work.

- Work to be done in lab (Water power lab, Fluids engineering lab, Thermal engineering lab)
- Field work

Department of Energy and Process Engineering, January 15th 2016



Prof. Olav Bolland
Department Head

Research Advisor:
Dr. Ignat Tolstorebrov



Prof Trygve M. Eikevik
Academic Supervisor
e-mail: Trygve.m.eikevik@ntnu.no

e-mails
ignat.tolstorebrov@ntnu.no

Preface

This master thesis is a part of the Mechanical Engineering study programme at Norwegian University of Science and Technology(NTNU), and is written during the spring of 2016. The thesis is within the scope of “Snow for the future” and is in coordination with Trondheim Kommune, Norwegian Ski Federation, SINTEF and NTNU. The thesis investigates machinery for making snow at ambient air temperatures above 0°C.

I would like to thank my supervisor Professor Trygve M. Eikevik for his great guidance and dedication to the project during the work on the master thesis.

A special thank also goes to my co-supervisor Ignat Tolstorebrov for being available during the work.

Trondheim, 10.06.2016

Jon-Brede R. Dieseth

Abstract

In the perspective of increasing global temperatures, the periods with natural snow is shorter and in areas, the snow in the winter is disappearing. Therefore, it is important to produce snow at temperatures above 0°C to be able to maintain the snow activity close to the cities. Today, temperature independent snow machines(TIS) produce plate ice, flake ice and ice slurry in temperatures above 0°C. There are four manufacturers of TIS, IDE Technologies, TechnoAlpin(TA), SnowTech and SnowMagic Inc. The machines are using refrigerants with challenging properties, and CO₂ is investigated as a substitute for these.

Vacuum and flake ice systems with a production capacity of 50 tons/day are modelled in EES, to investigate the thermodynamic performance at different ambient temperatures. The flake ice model shows that a single stage system(SCS) consumes less energy than a two-stage system(TCS) in ambient temperatures below 14°C. The U-value and ice growth rate for the flake ice drum(FID) are highly dependent on the ice thickness. Ice has high thermal resistance, and dictates the heat transfer from water to CO₂ rather than the metals or the refrigerants. The vacuum model shows that a two stage system(TVS) is more efficient than a single stage system(SVS) regardless of the ambient temperature. A cascade system with CO₂ is more energy intensive than the two previous systems. The most efficient vacuum system consumes just 20,8% of the energy required by the least efficient flake ice system. In terms of operation costs, the snow from the flake ice system is 4,8 times more expensive than from the vacuum systems. However, the investment costs are much higher for the vacuum system. Both the SCS and TCS is more energy efficient than the TA SF100. The energy consumption is 3,4% and 1,8% lower, respectively. A comparison between the vacuum models and existing machines is difficult, due to little known information about the existing machine.

COMSOL was used to do calculations on the FID. The results reveal that increasing the number of refrigerant pipes in the FID above 200, do not affect the temperature distribution on the freezing surface too much. In addition, the thickness can be optimized regarding the structural strength, rather than the heat transfer.

It is suggested to work further with improving the EES- and COMSOL models, investigate heat recovery possibilities, improving the efficiency of the systems, estimating the life cycle cost, look into operation strategies to minimize the energy consumption, and to build prototypes.

Sammendrag

I perspektiv av økte globale temperaturer, er perioden med naturlig snø er kortere, og i noen områder er snøen i ferd med å forsvinne helt. For å opprettholde snøaktivitetene rundt byene er det derfor viktig å kunne produsere snø i temperaturer over 0°C. I dag produserer temperatur uavhengige snømaskiner flakis, plateis og slush is i temperaturer over 0°C. Det finnes fire produsenter, IDE Technologies, TechnoAlpin(TA), SnowTech and SnowMagic Inc. Maskinene bruker kjølemedier med utfordrende egenskaper, og CO₂ blir utforsket som en substitutt for disse.

Vakuump og flakis systemer med en produksjonskapasitet på 50 tonn/dag er modellert i EES, for å undersøke den termodynamiske ytelsen i forskjellige utendørstemperaturer. Flakis modellen viser at et system med ett-trinns kompresjon(SCS) forbruker mindre energi enn et to-trinns system(TCS) i temperaturer under 14°C. Varmeovergangstallet og vekst raten til islaget på flakistrommelen(FID) henger tett sammen med tykkelsen på islaget. Is har lav termisk ledningsevne, og dikterer varmeovergangen fra vannet til CO₂ i mye større grad enn egenskapene til metallene og kjølemediene. Vakuump modellen viser at et to-trinns kompresjons system er mer effektivt enn en ett-trinns system uavhengig av utendørs temperaturen. Et kaskade-system av vakuump og CO₂ krever mer energi enn de to foregående systemene. Det mest effektive vakuump systemet forbruker kun 20,8% av energien det minst effektive flakis systemet behøver. Det betyr at flakis systemet er 4,8 ganger dyrere i drift enn vakuump systemet. Investeringskostnadene er imidlertid mye høyere for vakuump systemene. Sammenlignet med TA SF100, bruker SCS og TCS henholdsvis 3,4% og 1,8% mindre energi. En sammenligning mellom eksisterende vakuump løsning og utviklet modell er vanskelig, da systemkonfigurasjonen til det eksisterende system er ukjent.

COMSOL ble brukt til å kjøre beregninger på flakis trommelen. Resultatene viser at temperaturfordelingen på fryseflaten ikke endrer seg mye ved å øke antall rør med CO₂ til over 200. I tillegg, kan tykkelsen på trommelen optimeres med tanke på styrke fremfor varmeoverføring, da temperaturfordelingen ikke påvirkes særlig av endring av tykkelsen.

Videreutvikling av EES- og COMSOL-modellene, undersøke varmegjenvinnings mulighetene, forbedre effektiviteten av systemene, estimere livssyklus kostnader, se på driftsstrategier for å optimere energiforbruk og produksjon, og å bygge en prototype er foreslått som videre arbeid.

Contents

| | |
|---|------------|
| PREFACE | I |
| ABSTRACT | III |
| SAMMENDRAG | IV |
| CONTENTS | V |
| LIST OF FIGURES | VII |
| LIST OF TABLES | IX |
| NOMENCLATURE | X |
| 1 INTRODUCTION | 1 |
| 1.1 Background | 1 |
| 1.2 Objective | 2 |
| 1.3 Outline of the Thesis | 2 |
| 2 ICE PRODUCTION SYSTEMS | 3 |
| 2.1 Flake Ice | 3 |
| 2.2 Plate Ice | 5 |
| 2.3 Ice Slurry | 6 |
| 2.4 Status of the Ice Production Technology | 9 |
| 2.5 Alternative Snow Production: Nitrogen | 10 |
| 2.6 Water Additives | 11 |
| 3 EXISTING TEMPERATURE INDEPENDENT SNOW MAKERS (TIS) | 12 |
| 3.1 TechnoAlpin AG (TA) | 12 |
| 3.2 SnowMagic Inc. | 13 |
| 3.3 IDE Technologies (IDE) | 15 |
| 3.4 SnowTek | 17 |
| 3.5 Comparison between the manufacturers | 18 |
| 4 THEORY | 19 |
| 4.1 Basic refrigeration cycle | 19 |
| 4.2 Working fluids | 22 |
| 4.2.1 Natural working fluids | 23 |
| 4.3 Heat recovery from CO ₂ -systems | 27 |

| | | |
|----------|--|-----------|
| 4.4 | Materials in the flake ice drum..... | 30 |
| 4.5 | Heat transfer mechanisms in a flake ice drum | 31 |
| 5 | EES SIMULATION MODELS OF VACUUM AND FLAKE ICE MAKERS..... | 32 |
| 5.1 | General calculations for the vacuum and flake ice model | 32 |
| 5.2 | Modelling of the Vacuum Ice Maker | 39 |
| 5.2.1 | Results | 42 |
| 5.2.2 | Discussion | 46 |
| 5.3 | Modelling of the Flake Ice Maker | 49 |
| 5.3.1 | Modelling of the flake ice drum (FID)..... | 50 |
| 5.3.2 | Heat exchangers | 55 |
| 5.3.3 | Compressor..... | 56 |
| 5.3.4 | Results | 58 |
| 5.3.5 | Discussion | 63 |
| 5.4 | Comparison between the vacuum and flake ice model | 65 |
| 6 | CALCULATIONS OF THE FLAKE ICE DRUM USING COMSOL..... | 66 |
| 6.1 | General | 66 |
| 6.1.1 | Results | 67 |
| 6.1.2 | Discussion | 70 |
| 7 | CONCLUSIONS AND SUGGESTIONS FOR FURTHER WORK..... | 71 |
| 7.1 | Conclusions | 71 |
| 7.2 | Suggestions for further work..... | 73 |
| | BIBLIOGRAPHY | 74 |
| | APPENDIX | 78 |
| A. | Log p-h diagram | 78 |
| B. | Thermodynamic data. EES simulation models | 79 |
| C. | Input variables COMSOL model | 84 |
| D. | Heat transfer coefficients heat exchangers..... | 84 |
| E. | EES Code. Vacuum ice maker | 85 |
| F. | EES Code. Flake ice maker..... | 93 |
| G. | Scientific paper..... | 115 |

List of Figures

| | |
|---|----|
| Figure 2-1 Schematic diagram of the FID in flake ice maker..... | 4 |
| Figure 2-2 Schematic diagram of a plate ice machine (Graham et al., 1993)..... | 5 |
| Figure 2-3 Phase diagram for water (Anon, 2008)..... | 7 |
| Figure 2-4 Schematic of the vacuum ice making (VIM) | 8 |
| Figure 2-5 Scraped surface plate heat exchanger(Stamatiou et al., 2005) | 9 |
| Figure 3-1 The Snowfactory SF220 from TA (technoalpin.com, 2015)..... | 12 |
| Figure 3-2 Patented apparatus for crushing of ice (Fujiwara, 2003)..... | 14 |
| Figure 3-3 VIM100. | 16 |
| Figure 3-4 SnowGen, | 17 |
| Figure 4-1 Working principle of a simple heat refrigeration cycle (Eikevik, 2015)..... | 20 |
| Figure 4-2 Radial compressor used in a vacuum ice maker (Ophir, 2007)..... | 24 |
| Figure 4-3 Simple trans-critical and sub-critical CO ₂ cycle | 25 |
| Figure 4-4 Basic schematics of two arrangements for indirect CO ₂ systems(Reulens, 2009). 26 | |
| Figure 4-5 CO ₂ compared to other working fluids in high stage operation (Reulens, 2009)... 27 | |
| Figure 4-6 CO ₂ compared to other working fluids in low stage operation(Reulens, 2009)..... 27 | |
| Figure 4-7 De-superheater heat recovery method (Sawalha and Chen, 2010)..... | 28 |
| Figure 4-8 Heat pump cascade method for heat recovery (Sawalha and Chen, 2010) | 28 |
| Figure 4-9 Heat pump cascade for sub-cooling for heat recovery (Sawalha and Chen, 2010) 29 | |
| Figure 4-10 Schematic diagram of the process of flake ice maker (Cao et al., 2015) | 31 |
| Figure 5-1 Ambient temperatures at Voll observation station | 32 |
| Figure 5-2 Schematic of the model of a vacuum ice maker..... | 39 |
| Figure 5-3 Mass balance of the vacuum freezer and snow separator..... | 40 |
| Figure 5-4 Comparison of COP for the different system configurations. | 43 |
| Figure 5-5 Work vs ambient temperature. Vacuum systems | 44 |
| Figure 5-6 Outlet temp and pressure ratios vs ambient temp. Vacuum systems. | 44 |
| Figure 5-7 Energy consumption during the production period. Vacuum systems..... | 45 |
| Figure 5-8 Diameter of vacuum vessel with varying evaporation coefficient | 45 |
| Figure 5-9 Wall thickness of the vacuum vessel..... | 45 |
| Figure 5-10 Schematic of flake ice machine | 49 |
| Figure 5-11 Geometry of FID | 50 |
| Figure 5-12 Operating limits low stage compressor, model HGX4..... | 57 |
| Figure 5-13 Operating limits high stage compressors, model HGX2. | 57 |

| | |
|---|----|
| Figure 5-14 Comparison of COP for one- and two stage systems. Flake ice | 58 |
| Figure 5-15 Comparison of work for one- and two stage systems. Flake ice | 59 |
| Figure 5-16 Comparison of outlet temperature and pressure ratios. Flake ice. | 59 |
| Figure 5-17 Energy consumption at T=-30°C. Flake ice machine..... | 60 |
| Figure 5-18 Variation of the overall heat transfer coefficient for different | 61 |
| Figure 5-19 Ice growth rate [m/s] vs ice thickness [m] at T=-30°C | 61 |
| Figure 5-20 Variation of ice thickness with time at T=-30°C..... | 61 |
| Figure 5-21 Ice layer thickness for carbon steel constructions vs time | 62 |
| Figure 5-22 Capacity as function of refrigerant temperature | 62 |
| Figure 6-1 Temperature distribution between the refrigerant pipes with different width..... | 68 |
| Figure 6-2 Temperature distribution at varying depth of model. Width=26mm | 68 |
| Figure 6-3 Total displacement at depth=15mm | 69 |
| Figure 6-4 Displacement at different model thickness..... | 69 |
| Figure 6-5 Von Mises stress at depth=15mm | 70 |
| Figure 6-6 Von Mises stress at different model thickness | 70 |
| Figure A-1 Log P-h diagram of the vacuum cycle. T _{amb} =5°C | 78 |
| Figure A-2 Log P-h diagram Flake ice system. T _{amb} =5°C..... | 78 |

List of Tables

| | |
|--|----|
| Table 1 General information about the TA machines | 12 |
| Table 2 Technical data for machines from TA | 13 |
| Table 3 General information about the SnowMagic machines | 13 |
| Table 4 Technical data for the machines from SnowMagic Inc. | 14 |
| Table 5 General information for the IDE machines | 15 |
| Table 6 Technical data for machines from IDE Technologies..... | 16 |
| Table 7 General information about the SnowGen..... | 17 |
| Table 8 Technical data for the machine from SnowTek | 18 |
| Table 9 Comparison between the four manufacturers | 18 |
| Table 10 Material properties of metals | 30 |
| Table 11 Area of heat exchangers at $T_{amb}=5^{\circ}\text{C}$ and $T_{water}=5^{\circ}\text{C}$. Two-stage compression..... | 34 |
| Table 12 Heat exchanger pressure drop | 36 |
| Table 13 Pressure drop in pipes in the vacuum model at $T_{cond}=5^{\circ}\text{C}$ | 37 |
| Table 14 Pressure drop in pipes in the flake ice refrigeration system at $T_{cond}=5^{\circ}\text{C}$ | 38 |
| Table 15 Pressure drop in pipes in the FID circuit at $T_{cond}=5^{\circ}\text{C}$ | 38 |
| Table 16 Pump work | 38 |
| Table 17 Input variables vacuum machine..... | 42 |
| Table 18 Volume flow compressors..... | 57 |
| Table 19 Input variables vacuum machine..... | 58 |
| Table 20 At $T_{amb}=5^{\circ}\text{C}$ | 79 |
| Table 21 At $T_{amb}=20^{\circ}\text{C}$ | 79 |
| Table 22 At $T_{amb}=5^{\circ}\text{C}$ | 80 |
| Table 23 At $T_{amb}=20^{\circ}\text{C}$ | 80 |
| Table 24 Vacuum system. $T_{cond}=5^{\circ}\text{C}$ | 81 |
| Table 25 CO2 system. $T_{evap}=-5^{\circ}\text{C}$. $T_{cond}=5^{\circ}\text{C}$ | 81 |
| Table 26 CO2 system. $T_{evap}=-5^{\circ}\text{C}$. $T_{cond}=20^{\circ}\text{C}$ | 81 |
| Table 27 At $T_{amb}=5^{\circ}\text{C}$ | 82 |
| Table 28 At $T_{amb}=20^{\circ}\text{C}$ | 82 |
| Table 29 At $T_{amb}=5^{\circ}\text{C}$ | 83 |
| Table 30 At $T_{amb}=20^{\circ}\text{C}$ | 83 |
| Table 31 COMSOL input variables | 84 |

Nomenclature

Latin letters

| | | |
|-----------------|---|------------------------|
| A | Area | [m ²] |
| B | Constant, water heat transfer | [-] |
| C | Chisholm factor | [-] |
| C _p | Specific heat capacity | [kJ/kg·K] |
| d | Diameter | [m] |
| F | Correction factor evaporating CO ₂ | [-] |
| f | Friction factor | [-] |
| f _{ec} | Evaporation coefficient | [-] |
| G | Mass flux | [kg/m ² ·s] |
| h | Height | [m] |
| k | Thermal conductivity | [W/m·K] |
| L | Latent heat of fusion | [kJ/kg·K] |
| M | Molecular weight | [kg/kmol] |
| N _{ch} | Number of plate pairs | [-] |
| P | Pressure | [Pa] |
| Q | Heat transfer | [kW] |
| q | Heat flux | [kW] |
| R | Thermal resistance | [K/W] |
| R _g | Universal gas constant | [kJ/kmol·K] |
| S | Nucleate boiling suppression factor | [-] |
| sc | Sub-cooling | [K] |
| T | Temperature | [C] |
| t | Thickness | [m] |
| U | Overall heat transfer coefficient | [W/m ² ·K] |
| u | Velocity | [m/s] |
| x | Ice thickness | [m] |
| X _{tt} | Lockhart Martinelli parameter | [-] |
| z | Gas quality | [-] |

Abbreviations

| | | |
|------|-------------------------------------|-----|
| Al | Aluminium | [-] |
| Bo | Boiling number | [-] |
| CFC | Chlorofluorocarbon | [-] |
| COP | Coefficient of performance | [-] |
| CS | Carbon steel | [-] |
| EES | Engineering equation solver | [-] |
| FID | Flake ice drum | [-] |
| FIS | International ski federation | [-] |
| GWP | Global warming potential | [-] |
| HFC | Halofluorocarbons | [-] |
| HVAC | Heat, ventilation, air-conditioning | [-] |
| Nu | Nusselt number | [-] |
| ODP | Ozone depletion potential | [-] |
| Pr | Prandtl number | [-] |
| PR | Pressure ratio | [-] |
| Re | Reynolds number | [-] |
| SCS | Single-stage flake ice | [-] |

| | | |
|------|-----------------------------------|-------|
| SF | SnowFactory | [-] |
| SGHX | Suction gas heat exchanger | [-] |
| SST | Stainless steel | [-] |
| SVS | Single-stage vacuum system | [-] |
| TCS | Two-stage flake ice | [-] |
| TIS | Temperature independent snowmaker | [-] |
| TVS | Two-stage vacuum system | [-] |
| UTS | Ultimate tensile strength | [MPa] |
| VIM | Vacuum ice maker | [-] |

Greek letters

| | | |
|------------|---------------------------------|-----------------------|
| α | Heat transfer coefficient | [W/m ² ·K] |
| β | Chevron angle | [deg] |
| δ | Wall thickness | [m] |
| λ | Volumetric efficiency | [-] |
| μ | Dynamic viscosity | [kg/m·s] |
| ρ | Density | [kg/m ³] |
| ϵ | Roughness | [m] |
| ϕ | Two-phase frictional multiplier | [-] |

Subscripts

| | | |
|------|-----------------------------|-----|
| acc | acceleration/deceleration | [-] |
| amb | ambient | [-] |
| b | boundary | [-] |
| c | condenser | [-] |
| comp | compressor | [-] |
| e | equivalent | [-] |
| evap | evaporation | [-] |
| f | fluid | [-] |
| fg | liquid-gas phase transition | [-] |
| fl | flake ice | [-] |
| fric | friction | [-] |
| g | gas | [-] |
| gr | gravity | [-] |
| h | hydraulic | [-] |
| ht | heat transfer | [-] |
| i | inner | [-] |
| is | isentropic | [-] |
| l | liquid | [-] |
| lim | limit | [-] |
| LMTD | log mean temp difference | [-] |
| m | mean | [-] |
| man | manifold | [-] |
| nb | nucleate boiling | [-] |
| o | outer | [-] |
| r | reduced | [-] |
| SST | stainless steel | [-] |
| tp | two-phase | [-] |
| w | water | [-] |

1 Introduction

1.1 Background

In the perspective of increasing global temperatures, there is a challenge having snow available close to the cities and villages in the mountain for a reasonable long winter season. The periods with natural snow is shorter and in areas, the snow in the winter is disappearing. In Europe the facilities are moving to higher locations to be able to arrange winter games. In the Nordic countries, it is also a tradition for doing winter activities in the snow in kinder gardens, schools and for the families to go skiing in weekends and holidays. If the trend with milder winters is continuing, the distance from individual homes to areas with snow will grow. To be able to maintain the snow activity close to the cities it will be of importance to produce snow at temperatures above 0°C.

Snow is a basic need for ski resorts and Nordic skiing arenas, and the will to produce artificial snow has increased with the effects of global warming. The average air temperatures on earth has increased by 0,74°C during the 20th century, and is expected to increase further at a much higher rate than previously (Anon, 2015). As an example, the number of days with skiing conditions in Oslo has been reduced by one to two months over the last century. In 2050 it is assumed that the length of the winter will be halved compared to the 1980s (Larsen, 2014). The climate changes are already noticeable, and 24 out of 66 cross-country competitions were cancelled in Nord-Trøndelag during the winter of 2014-2015.

Trondheim hosted the FIS Nordic World Ski Championships in Granåsen in 1997, and several World Cup events have been held in Granåsen in ski jumping, Nordic combined, biathlon and cross country skiing. Unfortunately, Trondheim was not chosen to host the FIS Nordic World Ski Championships in 2021. However, Trondheim will apply for the Championships in 2023. The facilities in Granåsen are to be expanded, and a strategy for having snow in the tracks from November 1. is to be determined.

1.2 Objective

The object of this thesis is to get an overview of snow and ice producing equipment, with focus on the machinery for making snow at ambient air temperatures above 0°C. Based on this, models for snow making systems utilizing vacuum and flake ice technology will be developed, in order to evaluate the thermodynamic performance at different ambient temperatures. CO₂ will be used as the refrigerant in the flake ice maker. The models include pipe and component design with pressure drop. Based on the result from the models, proposals for further work will be made. Highlights from the thesis will end in a scientific paper.

1.3 Outline of the Thesis

Chapter 2 presents an overview of the current technologies for producing ice in temperatures above 0°C.

Chapter 3 gives an overview of the different temperature independent manufacturer, and what technology they utilize. In addition, the machines with equivalent production capacity are compared.

Chapter 4 presents theory relevant for the vacuum and flake ice models.

Chapter 5 explains the setup of the models. Equations and the components in the system are presented. The results from the models are evaluated and discussed.

Chapter 6 presents calculations done in COMSOL. The design of the flake ice drum is evaluated, and the results are evaluated and discussed.

Chapter 7 comprises the conclusion and suggestions for further work.

2 Ice Production Systems

The ice production systems can be divided into two groups, machines that produce dry subcooled ice or wet ice (Graham et al., 1993). Generally, dry subcooled ice is produced in machines that mechanically remove the ice from the evaporator surface, while wet ice is made in machines utilizing a defrost procedure to release the ice. The defroster partially melts the ice at the evaporator surface allowing the ice to detach. Unless the ice is being subcooled, the surface of the ice will remain wet. In some machines, the ice is formed and collected to produce an ice slurry, which is an ice and water mixture.

2.1 Flake Ice

Flake ice is harvested as dry subcooled ice flakes that typically can be up to 3 mm thick (Graham et al., 1993). The water is fed into a tank above the flake ice drum (FID), which operates as the evaporator in the system, from which it is evenly sprinkled onto the inner wall of the FID through a series of distribution tubes, resulting in an ice layer on the FID wall (Cao et al., 2015). Any water not frozen falls into a collection disk, and is pumped back into the tank. A schematic diagram of the flake ice maker is presented in Figure 2-1. The flake ice makers require a refrigeration system. The temperature of the working fluid flowing inside the FID may be as low as -30°C , while the sub-cooled walls of the FID are at around -20°C . No water is added in front of the scraper, allowing the ice to reach a sub-cooled temperature of around -8°C (Carpenter, 1995). This ensures that only dry ice falls into the storage space below the scraper. Flake ice makers are used in the industry for controlling chemical reactions, cool concrete and in the fishing industry for cooling purposes (Cao et al., 2015). In addition, flake ice is the most commonly used snow substitute (Paul, 2002). Salt may be added to increase the number of impurities in the water to accelerate the freezing process.

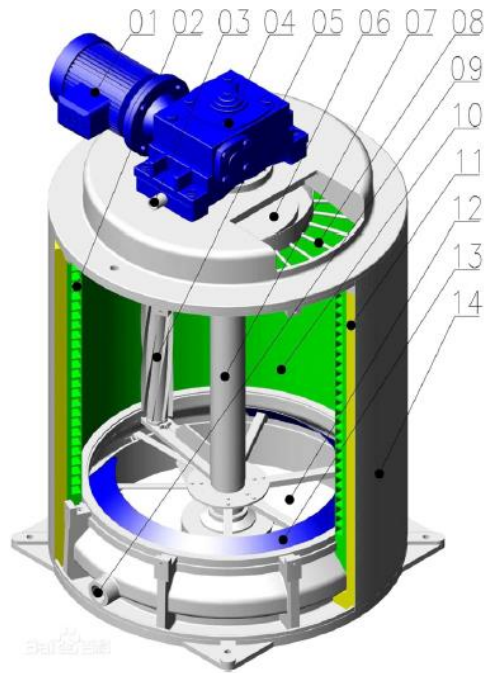


Figure 2-1 Schematic diagram of the FID in flake ice maker. 01—motor, 02—spiral evaporation pipelines, 03—water supply inlet, 04—reducer, 05—ice blade, 06—water distribution pan, 07—main shaft, 08—water distribution tubes, 09—exit of water collection dish, 10—inner wall of evaporator, 11—insulation material, 12—ice storage bin, 13—ice drop opening, 14—outer shell. (Cao et al., 2015)

In some models, the FID rotates and the scraper on the outer surface remains stationary. In others, the scraper rotates and removes the ice from the inner surface of a stationary FID, as seen in Figure 2-1. Usually, the FID rotates in a vertical plane, but some models have drums rotating in a horizontal plane. One advantage of the rotating FID method is that the ice-forming surface and the ice scraper are exposed, and the operator can easily observe if the plant is operating correctly. In contrast to machines with rotating scraper, these machines require a rotating seal on the refrigerant supply and return pipes. This can be a weak spot, but in modern machines, the seal has a high degree of reliability (Graham et al., 1993).

The temperature of the working fluid in a flake ice machine is substantially lower than in other types of ice machines, often up to 15⁰C lower. On the other hand, a flake ice machine does not require a defrost system, and the extra power required for operating at low temperatures is therefore somewhat compensated compared to other ice machines.

For the flake ice machines, the refrigerant temperature, the feed water temperature, degree of sub-cooling and speed of rotation of the drum or scraper are all variables, that affect the capacity of the machine and the thickness of the ice produced. The temperature in the FID dictates the ice production rate, and the lower the evaporator temperature is, the more ice can be produced. Low temperatures are necessary to keep the machines small and compact.

2.2 Plate Ice

Plate ice is formed by spraying water over the face of a refrigerated vertical plate. The plates are released by running water on the other face of the vertical plate. Other types of machines form ice on both surfaces and use an internal defrost process, illustrated in Figure 2-2. The harvesting time of the ice may vary, depending on the operational conditions, but is normally 8 to 10% of the total cycle time. Multiple vertical plates are arranged to form the ice-making machine, and the capacity of the machine can be adjusted by removing or adding more plates. An ice crusher is required to break the ice into a suitable size for storage and use (Graham et al., 1993).

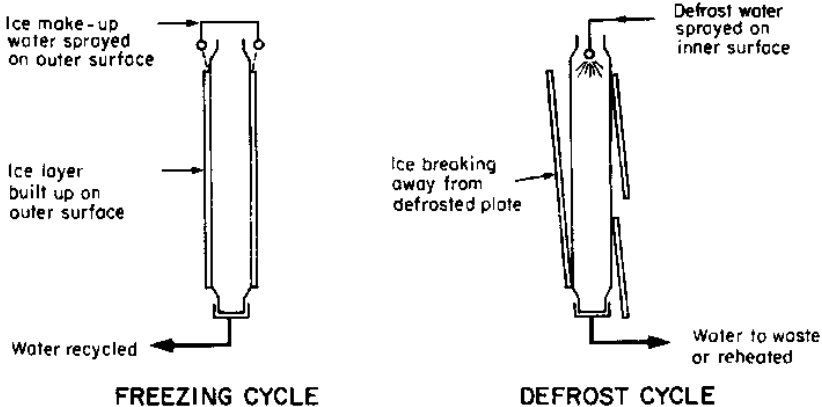


Figure 2-2 Schematic diagram of a plate ice machine (Graham et al., 1993)

Defrost equipment is required when making plate ice, and this will increase the energy consumption. Thus, plate ice plants will have an additional factor increasing the energy consumption compared to flake ice plants. This factor is the main reason why an plate ice plant needs to make ice with a thickness of 10 to 12 mm (Graham et al., 1993). The energy consumption compared to the amount of ice produced makes it economically unprofitable to produce thinner ice.

The production capacity of plate ice machines highly depends on feed water temperature and evaporating temperature. Today, regulation systems adjust the evaporating temperature according to the desired production rate and the compressor power is reduced when the machine is running on part load (Samuelsen, 2015).

To increase the efficiency, it is desirable to have as high evaporation temperature as possible. Due to heat losses to the surroundings and losses from the ice harvest, which is relatively large compared to the increased efficiency of higher evaporating temperature, it is unprofitable with an evaporation temperature above -12°C . If the evaporation temperature is too high the, ice will have high core temperature and it will feel wet. Therefore, an evaporation temperature of around -15°C is desirable (Samuelsen, 2015).

2.3 Ice Slurry

Ice slurry is a mixture of ice particles and a liquid, containing up to 40% ice particles (Stamatiou et al., 2005). The size of the ice particles can be between 0.1 and 1 mm in diameter (Hägg et al., 2005). The liquid can be pure water, or a brine of water and freezing point depressant. Due to the latent heat of fusion of the ice crystals, ice slurry has a high energy storage density and the temperature remains constant during the cooling process. This provides a higher heat transfer coefficient compared to water and other single-phase liquids. In addition, it has a fast cooling rate due to the large heat transfer surface area created by its numerous particles. (Kauffeld et al., 2010). Ice slurry has many areas of application, such as comfort cooling, commercial refrigeration, industrial production processes, medicine and artificial snow production (Bellas and Tassou, 2005). Ice slurry can be an excellent snow substitute, and it can provide a better skiing surface than flake ice (Paul, 2007a, Paul, 2002).

Vacuum Ice Maker

A typical system consists of a vacuum freeze evaporator, compressor, condenser and a vacuum pump (Asaoka et al., 2009). Air is introduced with the water entering the system, and the vacuum pump is used to deaerate the system in case of leakage into the system (Orshoven et al., 1993). Presence of air in the system will reduce the heat transfer of the condenser and reduce the capacity of the compressor (Chamoun et al., 2012a). The operating principal for the vacuum ice maker is to bring water to triple-point conditions, where the vapour pressure of water is 611,7 Pa and the temperature is $0,01^{\circ}\text{C}$ (Orshoven et al., 1993). Figure 2-3 shows this relation. A vapour pressure of 611,7 Pa is characterized as a medium vacuum (Anon, 2016).

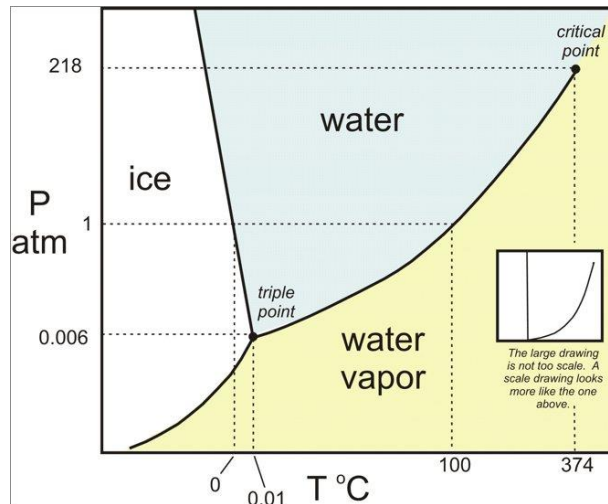


Figure 2-3 Phase diagram for water (Anon, 2008)

When water is brought to triple-point conditions, the water starts to boil and some of it evaporates. Energy in the shape of heat is released, causing the temperature in the remaining water to decrease. Eventually it will freeze, and create an ice slurry. The latent heat of fusion and vaporization is 333 kJ/kg and 2500 kJ/kg, respectively. This means that the mass of ice produced is 7,5 times the mass of water vapour (Orshoven et al., 1993).

To maintain the vacuum, the vapour has to be evacuated, and this is done by the compressor. The compressed vapour is brought to the condenser, where heat may be recovered, before being injected back into the evaporator. Another method to maintain vacuum, is to deposit the water vapour on refrigerated plates inside the vacuum freezer. The vapour will condense and reject heat. Frequent defrosting of the plates is necessary in order to maintain the vapour condensation (ide-snowmaker.com, 2015).

A circulation pump is installed in the evaporator in order to agitate the slurry. As long as there is no agitation, the freezer specific capacity and crystal quality are poor (Pachter and Barak, 1967). The ice slurry is continuously removed from the evaporator and collected in a tank, where ice and water can be separated. The working fluid in these machines are the water itself, and no separate refrigeration system are required. Figure 2-4 shows a schematic of a vacuum ice maker.

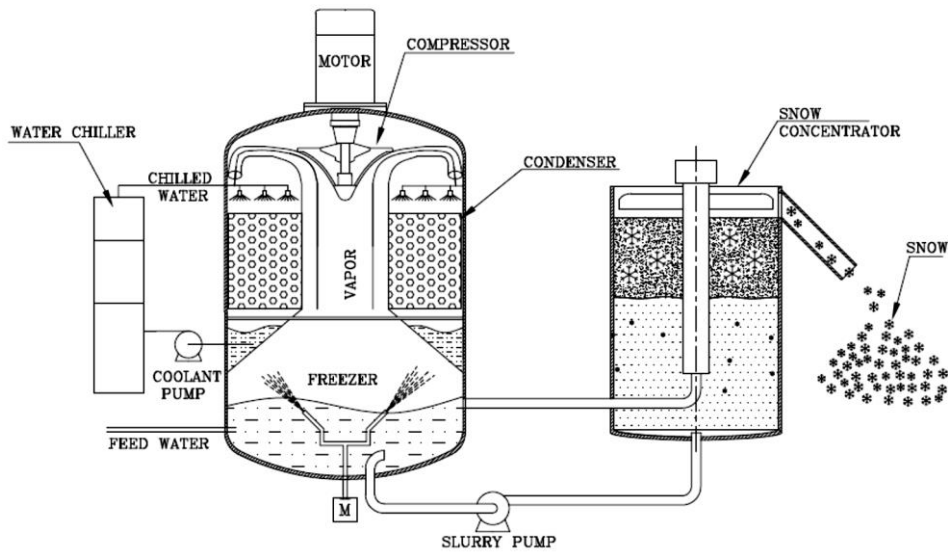


Figure 2-4 Schematic of the vacuum ice making (VIM) plant from IDE Technologies (ide-snowmaker.com, 2015)

Like flake ice makers, the vacuum ice maker production capacity depends on the water temperature. Each 1°C increase in the temperature of the feed water reduces the snow production capacity by 1,5% (IDE Technologies, 2015).

Scraped Surface

The scraped surface ice slurry generator is currently the most technologically developed and widely accepted ice slurry generation method over the last 20 years (Stamatiou et al., 2005). Typically, the scraped surface ice slurry generator is a circular shell-and-tube heat exchanger through which water flows. Between the inner and outer cylinder wall the working fluid flows. Another method is to submerge plates, through which the working fluid flows, in water inside a vessel. The ice is created on the walls of the cylinders or plates, and are mechanically removed by rotating blades, as seen in Figure 2-5. It is possible to use scrapers made of both metals and polymers. In other types of generators, the ice is produced in tubes and removed by turning screws. (Egolf and Kauffeld, 2005, Mouneer et al., 2010). Freezing point depressants, like salt, glycol and alcohol are added to the water to lower the freezing point.. These generators can be both horizontal and vertical (Martínez et al., 2014). The scraped surface generator has a large surface for ice creation, and is therefore used when high ice production rates are required. Scraped surface evaporators is quite expensive and have high maintenance costs (Bédécarrats et al., 2010).

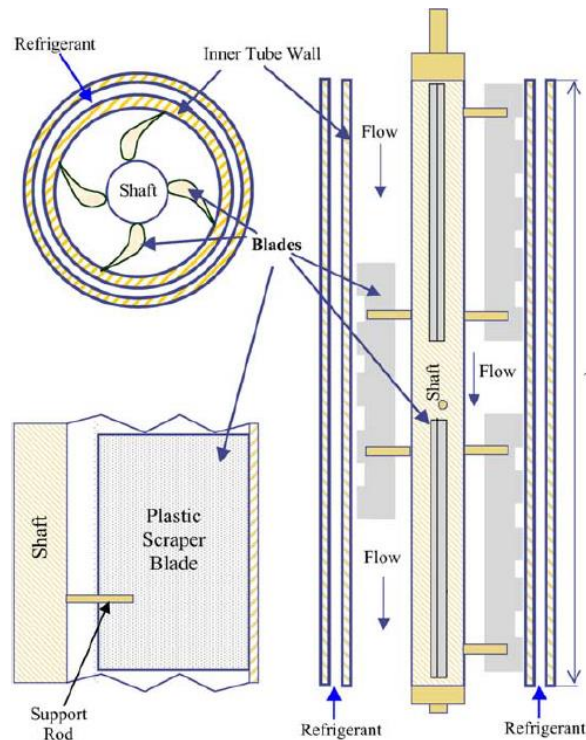


Figure 2-5 Scraped surface plate heat exchanger(Stamatiou et al., 2005)

2.4 Status of the Ice Production Technology

In this section an overview of the research related to the different ice production technologies are presented. There are no published articles about the different commercially available temperature independent snow machines. Therefore, the machines had to be split into subsystems that are a field of research.

The methods for producing ice, presented in section 2.1 and 2.2, have existed for several years. Therefore, the research on new ways to produce flake ice and plate ice is limited. The work related to these machines are more focused on improving the production methods. The trend is to develop systems with environmental friendly working fluids, like CO₂, ammonia and propane, that satisfy the EU F-gas directive, in addition to improve of the energy efficiency (Karstensen, 2015). In addition, it is important to lower the cost of the machines. The investment cost of such machines are often more important to costumers, than the energy consumption (Samuelsen, 2015).

Regarding ice slurries, the majority of applications utilizing ice slurries are concentrated in Europe and Japan. In Japan, the interest has mainly been in air conditioning with thermal storage and electrical load shifting to off-peak periods. In Europe, the applications vary widely

from air conditioning to process cooling (Bellas and Tassou, 2005). The research on ice slurries are mainly focused on system design, to develop new methods to produce ice slurry or to improve existing technology (Wang et al., 2016). It appears that the performance of the systems, in addition to being simple and reliable, are prioritized before the energy consumption. In addition, the heat transfer mechanisms between the water or brine and the heat exchanger is a field of study (Martínez et al., 2014, Mouneer et al., 2010, Singh and Kachhwaha, 2015). Even though the production of ice is the purpose of this machines, researchers seem to focus on methods to improve the ice production rather than maximize the ice production rate (Bail and Havet, 2015, Fumoto et al., 2015). In addition, new application areas of ice slurries are being studied. This lead to new ways of producing ice slurry, which are being developed to suit the desired demands.

Using water as working fluid requires compressors that can handle large amounts of water vapour. Although water vapour compression can be performed by several industrial compressors, the performance is not satisfactory, with poor efficiency, high cost and not sufficient compression ratios (Chamoun et al., 2012b). Therefore, the field of research has been to find suitable compressors with satisfying performance, compact design and a moderate cost. Both turbo, screw, centrifugal and axial compressors have been assessed in the research (Li et al., 2011a, Wobst et al., 2004, Madsboell et al., 2015). The research also states that systems using water as working fluid are very efficient, with energy savings up to 30% compared to conventional working fluids (Paul, 2007b, Li et al., 2011b).

2.5 Alternative Snow Production: Nitrogen

By using compressed air, water and liquid nitrogen Polar Technologies and AGA can produce up to 1100 m³ of snow in two days (Haugsvær, 2016). By direct heat exchange between the water and the nitrogen, the water is cooled down below its freezing point by the nitrogen, which evaporates. The process can operate in temperatures up to 30°C. The snow is produced inside large tents, which insulates against the ambient air. To produce 1100 m³ of snow, around 400 tons of liquid nitrogen is used. Today's price of liquid nitrogen is around 1,38 NOK/kg (AGA, 2016), meaning this method has high operating costs. On the other side, the investment cost of the system is rather low.

2.6 Water Additives

Normally water freezes at 0°C , while distilled supercooled water has a freezing point of around -48°C (Moore and Molinero, 2011). The water freezes around impurities, thus making polluted water more suitable for snow production than pure water. The impurities are called nucleators and these can be added to the clean water to help the freezing process. Impurities lower the freezing point, and extra energy is required to cool the water. However, this energy is small compared to the energy of phase change. The motivation for adding impurities is therefore to have more nucleators in the water. Sodium chloride, sodium chloride, ethanol, ethylene glycol and propylene glycol are examples of freezing point depressants commonly used in the industry (Kauffeld et al., 2010).

Snomax is a natural natural protein that also can be added to the water. In addition of being a nucleator, Snomax lower the temperature of the water, allowing snow production in marginal temperatures. The amount of the protein being added to the water is approximately 0,9 g per 1000 L (Gjerland and Olsen, 2014). Snomax may increase the amount of snow produced by up to 40% and there are no detected negative environmental consequences (snomax.com, 2015).

DRIFT is another additive that is used in the snow production industry. DRIFT is injected into the snowmaking water, and it lowers the tension of the water. The water molecules will not stick together as tightly, allowing the water to freeze more rapidly because of larger surface area. The water freezes more rapidly since the energy keeping the water molecules together is lowered by DRIFT. DRIFT is dispersed into the water at 3-5 ppm (aquatrols.com, 2016).

Snomax and DRIFT are normally used in traditional sub-zero snow machines, while salts glycols and alcohols are more common in temperature independent ice making.

3 Existing Temperature Independent Snow Makers (TIS)

Based on the ice production methods presented in section 2, manufacturers are able to produce ice at temperatures above 0°C. Below follows an overview of some TIS manufacturers. The focus is on machines producing the ice itself, rather than just crushing pre-made ice.

3.1 TechnoAlpin AG (TA)

TA from Italy released SnowFactory in 2014. The SnowFactory produces flake ice and exists in three variants, SF70, SF100 and SF220. Information about the SF70 has not been provided from TA, except that it has been sold to Bangkok, Thailand.

| | SF100 (2014) | SF220 (2014) |
|----------------------|--|---|
| Principle | Flake ice machine | Flake ice machine |
| Type | Mobile | Stationary |
| Working fluid | R404A (HFC) | R717 (Natural working fluid) |
| Size | 1 x 40' container | 2 x 40' container + 1 x evaporative condenser |
| Customers | Geilo, Idre Fjäll, German ski federation | Winterberg, Sjusjøen |
| Price | Ca. 4 mill SEK (Idre Fjäll) | Ca. 6 mill NOK (Sjusjøen) |

Table 1 General information about the TA machines

The system contains of a refrigeration system, flake ice makers, an ice transportation system, air fan and an ice crusher. The ice is harvested in the snow distribution system below the flake ice drums, before being transported to the ice crusher. Due to the fact that the ice is dry and has no liquid in it, the snow can be blown out to the ambient by the air fan.

SF100 is a mobile unit that is delivered in a 40 feet container and does not require extensive building work or fittings. It only needs to be connected to power and a water supply. SF220, shown in Figure 3-1, is a permanent unit consisting of two 40 feet containers and one evaporative condenser.

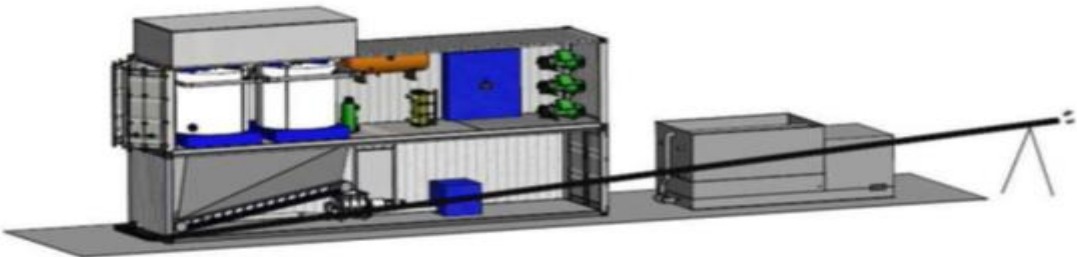


Figure 3-1 The Snowfactory SF220 from TA (technoalpin.com, 2015)

The power consumption and production capacities of the machines from TA are presented in Table 2 below.

| | SF100 (2014) | SF220 (2014) |
|--------------------------------------|-------------------------|-------------------------|
| Cooling Capacity | 206 kW | 640 kW |
| Capacity | 100 m ³ /day | 220 m ³ /day |
| Power consumption¹ | 130 kW | 230 kW |
| Water consumption | 0,8 L/s | 1,5 L/s |
| Energy per m³ | 31,2 kWh/m ³ | 25,1 kWh/m ³ |
| Operating air temperatures | -5°C to + 25°C | -5°C to + 25°C |

Table 2 Technical data for machines from TA

TA has not included details about what equipment that is included in the power consumption calculations. It is reasonable to assume that the whole system is included. The energy consumption is based on 24 hours of production every day.

3.2 SnowMagic Inc.

SnowMagic Inc. from USA was the first manufacturer to offer a TIS in 1993. The machines from SnowMagic Inc. utilize plate ice to produce artificial snow, and exists of four models with different capacities.

| Model | 50 | 100 | 150 | 200 |
|----------------------|--------------------|-------------------|-------------------|-------------------|
| Principle | Plate ice | Plate ice | Plate ice | Plate ice |
| Type | Mobile | Mobile | Stationary | Stationary |
| Working fluid | - | - | - | - |
| Size | 40' container | 40' container | 40' container | 40' container |
| Customers | Ski resorts Japan, | Ski resorts Japan | Ski resorts Japan | Ski resorts Japan |

Table 3 General information about the SnowMagic machines

After the ice is released from the refrigerated plates, the ice is first crushed into coarse particles by an ice crusher. Secondly, the ice is crushed into even finer particles by the patented apparatus shown in Figure 3-2. The apparatus consists of a high-speed rotor blade that beats and crushes the ice into particles sizing from 0,1mm to 0,3mm in diameter.

¹ The numbers for power consumption is based on an inlet water temperature of 5°C and an air temperature of 15°C. The temperature of the refrigerant is -30°C.

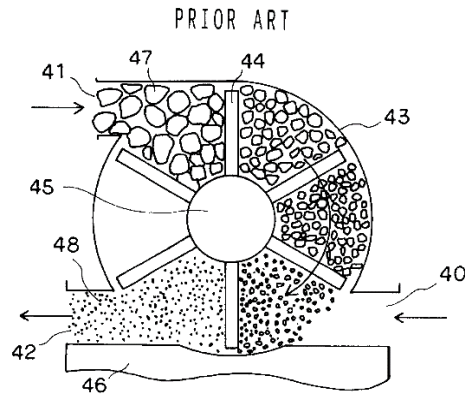


FIG. 8

Figure 3-2 Patented apparatus for crushing of ice (Fujiwara, 2003)

These machines were installed in many ski resorts in Japan in the late 1990's, in addition to venues in Saudi Arabia, Mexico and USA. Like the machines from TA, SnowMagic Inc. also uses containers to house the equipment (snowmagic.com, 2015).

The power consumption and production capacities for the machines from SnowMagic Inc. are presented in Table 4.

| Model | 50 | 100 | 150 | 200 |
|---------------------------------|-------------------------|-------------------------|-------------------------|-------------------------|
| Capacity | 50 tons/day | 100 tons/day | 150 tons/day | 200 tons/day |
| Capacity² | 100 m ³ /day | 200 m ³ /day | 300 m ³ /day | 400 m ³ /day |
| Power consumption | 151 kW | 248 kW | 362 kW | 545 kW |
| Water consumption | 0,8 l/s | 1,6 l/s | 2,4 l/s | 3,2 l/s |
| Energy per m³ | 36,2 kWh/m ³ | 29,8 kWh/m ³ | 29 kWh/m ³ | 32,7 kWh/m ³ |

Table 4 Technical data for the machines from SnowMagic Inc.

The energy consumption is based on 24 hours of production every day. Limited information is available on SnowMagics's website. SnowMagic Inc. has been contacted, but no more information could be provided.

² The density of the ice is assumed to be 500 kg/m³

3.3 IDE Technologies (IDE)

The Israeli company IDE Technologies developed their first TIS in 2005. IDE uses ice slurry produced by a vacuum ice maker to make artificial snow. IDE has been a pioneer regarding centrifugal water vapour compressors since the idea of water turbo compressor refrigeration systems started in the end of 1980s (Sarevski and Sarevski, 2016). They have a portfolio of three ice makers, VIM100, VIM400 and VIM850.

| IDE Technologies | VIM100 Snowmaker2go (2013) | VIM400 all weather snowmaker (2009) | VIM850 all weather snowmaker (2005) |
|----------------------|--|--|--|
| Principle | Vacuum ice slurry | Vacuum ice slurry | Vacuum ice slurry |
| Type | Mobile | Stationary | Stationary |
| Working fluid | Water | Water | Water |
| Size | 1 x 40' container + 1 x 20' container + snow separator | - | - |
| Customers | - | Pitztal, Austria and Zermatt, Switzerland | - |

Table 5 General information for the IDE machines

The freezer and the compressor are called the VIM unit. To maintain the vacuum in the freezer, VIM400 and VIM850 uses a compressor to evacuate the vapour, while VIM100 deposits the vapour on cold plates that are regularly defrosted. The ice slurry is then pumped into a snow separator, which separates the water and ice particles.

VIM100 is a mobile unit that is delivered in a 40 feet container, a 20 feet container and a snow separator. Like SF100, it does not require extensive building work or fittings. It only needs to be connected to power and a water supply. VIM400 and VIM 850 are much larger units that are stationary.

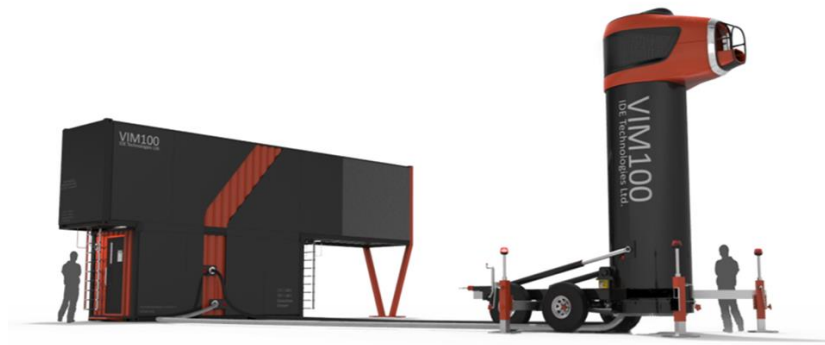


Figure 3-3 VIM100. The ice slurry production unit to the left and snow separator to the right (ide-snowmaker.com, 2015)

The power consumption and production capacities for the machines from IDE Technologies are presented in Table 6.

| | VIM100 Snowmaker2go (2013) | VIM400 all weather snowmaker (2009) | VIM850 all weather snowmaker (2005) |
|---------------------------------|---|--|--|
| Cooling capacity | 350 kW | 1750 kW | 3500kW |
| Capacity³ | 200 m ³ /day | 860 m ³ /day | 1720 m ³ /day |
| Power consumption | <250 kW | <235 kW | <397 kW |
| Water consumption | 1,3 l/s | 6,5 l/s | 12,9 l/s |
| Energy per m³ | 30 kWh/m ³ | 6,6 kWh/m ³ | 5,5 kWh/m ³ |

Table 6 Technical data for machines from IDE Technologies

For the two largest machines from IDE Technologies, the power consumption refers to the VIM unit only and does not include the supporting cooling system, like chiller, cooling tower and cooling tower circulation pump. Therefore, the energy consumption of these machines will be higher. The energy consumption is based on 24 hours of production every day.

³ Feed water temperature at 4.5°C.

3.4 SnowTek

Another manufacturer that produces artificial snow from ice slurry is SnowTek from Finland. Their machine, SnowGen, uses a scraped surface ice slurry generator from the Canadian company IceGen Inc. to produce the ice slurry.

| SnowTek | SnowGen (2014) |
|----------------------|------------------------------------|
| Principle | Scraped surface, ice slurry |
| Type | Mobile |
| Working fluid | R717 (Natural working fluid) |
| Size | 1 x 40' container + snow separator |
| Customers | Olympics Sochi 2014 |

Table 7 General information about the SnowGen

The ice particles are created on cold plates before being scraped of and transported to a snow separator. About 2,5% salt is added to the water to increase the number of nucleates in the water. This machine produced snow to the disciplines ski jumping and combined in the 2014 Olympic Games in Sochi. In Sochi, three units where used in order to increase the production rate. The system is shown in Figure 3-4.



Figure 3-4 SnowGen, showing the ice slurry generator in the container and the snow separator behind (Tucker, 2014)

The power consumption and production capacities for the machine from SnowTek are presented in Table 8.

| | SnowGen (2014) |
|---------------------------------|-------------------------|
| Capacity | 220 m ³ /day |
| Power consumption | 280kW |
| Water consumption | 1,4 l/s |
| Energy per m³ | 30,5 kWh/m ³ |

Table 8 Technical data for the machine from SnowTek

Limited information is available on SnowGen’s website. SnowGen has been contacted, but they were restrictive with the information they could provide. The energy consumption is based on 24 hours of production every day.

3.5 Comparison between the Manufacturers

A comparison between the temperature independent machines with the same production capacity are presented in Table 9.

| | SnowGen (2014) | TechnoAlpin SF220 (2014) | IDE VIM100 (2013) | SnowMagic Inc, 100 |
|---------------------------------|------------------------------------|---------------------------------|---|---------------------------------------|
| Principle | Scraped surface, ice slurry | Flake ice | Vacuum ice maker, ice slurry | Flake ice |
| Type | Mobile | Stationary | Mobile | Mobile |
| Power consumption | 280 kW | 230 kW | <250 kW | 248 kW |
| Capacity | 220 m ³ /day | 220 m ³ /day | 200 m ³ /day | 200 m ³ /day |
| Water consumption | 1,4 l/s | 1,5 l/s | 1,3 l/s | 1,6 l/s |
| Working fluid | R717 | R717 | Water | - |
| Size | 1 x 40’ container + snow separator | 2 x 40’ containers | 1 x 40’ and 1 x 20’ containers + snow separator | - |
| Energy per m³ | 30,5 kWh/m ³ | 25,1 kWh/m ³ | <30 kWh/m ³ | 29,8 kWh/m ³ |
| Customers | Sochi 2014 | Winterberg, Sjusjøen | - | Ski resorts in Japan, Stadiums in USA |

Table 9 Comparison between the four manufacturers

The energy consumption calculations are based on the power consumption and capacity given in the manufacturers specifications, and 24 hours of production every day.

4 Theory

4.1 Basic Refrigeration Cycle

The working principle of a refrigeration system is seen in Figure 4-1, and the main components in a refrigeration system are:

- Compressor
- Condenser
- Expansion valve
- Evaporator

According to the second law of thermodynamics, heat flows naturally in the direction of decreasing temperature. Heat from a heat source, \dot{Q}_0 , is received in the evaporator. The working fluid in the evaporator, which has lower temperature than the heat source, is evaporated and cooling is provided. The gas enters the compressor, where energy, \dot{W}_{comp} , is added to increase the temperature and pressure of the working fluid. In the condenser, heat from the working fluid, \dot{Q}_{cond} , is rejected to a heat sink at lower temperature. Then, the condensed working fluid is expanded back into the evaporator. The heat \dot{Q}_{cond} may be recovered and utilized for e.g. space heating and hot water heating (Zsebik et al., 2014, Sawalha, 2013). The heat rejected in the gas cooler or the condenser equals the work supplied to the compressor and the heat received in the evaporator, shown in Equation (4.1).

$$\dot{Q}_{cond} = \dot{Q}_{evap} + \dot{W}_{comp} \quad (4.1)$$

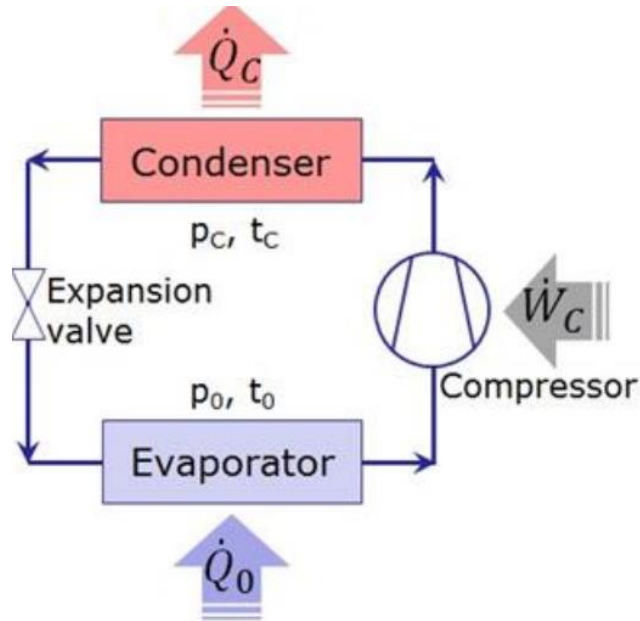


Figure 4-1 Working principle of a simple heat refrigeration cycle (Eikevik, 2015)

The coefficient of performance, COP, is the amount of heating/cooling energy that can be produced by 1 kW of applied energy, and is a measure of how energy efficient a refrigeration cycle is. Equation (4.2) and (4.3) defines the COP for a refrigerator and heat pump, respectively, and equation (4.4) defines the energy saving compared to an alternative electric system.

$$COP_{evap} = \frac{Q_{evap}}{\sum_{i=1}^n W_i} = \frac{\dot{m}_f (h_{out} - h_{in})}{\sum_{i=1}^n W_i} \quad (4.2)$$

$$COP_{cond} = \frac{Q_{cond}}{\sum_{i=1}^n W_i} = \frac{\dot{m}_f (h_{in} - h_{out})}{\sum_{i=1}^n W_i} \quad (4.3)$$

$$\Delta E = \left(1 - \frac{1}{COP}\right) * 100\% \quad (4.4)$$

The refrigeration capacity of the system is calculated by the amount of refrigerant circulated in the system and the enthalpy difference before and after the evaporator.

$$\dot{Q}_o = \dot{m}_f (h_1 - h_2) \quad (4.5)$$

The size of the compressor is determined by the volume flow of the refrigerant required to achieve the desired refrigeration capacity. The suction volume is the volume that needs to be removed from the evaporator. Due to volumetric losses, the required volume of the compressor, also known as the swept volume, is larger than the suction volume. The volumetric efficiency of the compressor is defined as the ratio between the suction and swept volume, as seen in equation (4.6). In addition to volumetric, energy losses in the compressor result in a higher power demand than the theoretical. The energy losses are given by the isentropic efficiency given in equation (4.8).

$$V_{suction} = \dot{m}_f \cdot v_1 \quad (4.6)$$

$$\lambda = \frac{V_{suction}}{V_s} \rightarrow V_s = \frac{\dot{m}_f \cdot v_1}{\lambda} \quad (4.7)$$

$$\eta_{is} = \frac{W_{theo}}{W} \rightarrow W = \frac{W_{theo}}{\eta_{is}} = \frac{\dot{m}(h_{2,is} - h_1)}{\eta_{is}} \quad (4.8)$$

Including heat loss in the compressor, two different discharge enthalpies have to be calculated, as seen in equation (4.9) and (4.10). The heat is produced by e.g. friction between movable parts or gas molecules in the compressor, which results in an increased compressor work. In addition, the heat loss results in less heat in the condenser. The resulting compressor work is calculated in equation (4.11).

$$h_2 = h_1 + \frac{h_{2,is} - h_1}{\eta_{is}} \quad (4.9)$$

$$h_2' = h_1 + \frac{h_{2,is} - h_1}{\eta_{is}} (1 - Q_{loss}) \quad (4.10)$$

$$\dot{W}_{comp} = \dot{m}_f (h_2 - h_1) \quad (4.11)$$

4.2 Working Fluids

According to the EU F-Gas Regulations, the amount of halo fluorocarbons (HFC) on the European market will be gradually capped. By 2030, the volume of HFCs on the market is expected to be reduced to 21% of today's levels. In addition, the EU has agreed to ban HFCs in new equipment in commercial refrigeration by 2022. From 2020, HFCs with GWP-value of over 2500 and with a larger charge size than 40 tons of CO₂ equivalent will no longer be used to service and maintain refrigeration systems. HFC's have high global warming potential (GWP), often up to many thousands times higher than CO₂. Emissions of HFC currently accounts for about 2% of European emissions of greenhouse gases and this is growing rapidly (EU, 2014). Therefore, TA SF100 have to be redesign in order to legally be maintained and serviced after 2022.

Some criteria for choosing a working fluid are (Palm, 2014)

- Flammable and toxicity
- Chemical and thermal stability
- Suitable thermodynamic and physical properties
- Compatibility with materials and lubricants
- Low cost
- Environmental impact (GWP, ODP)

Based on these criteria and the EU F-Gas Regulations it is desirable to use a natural working fluid in the refrigeration system. Natural working fluids are molecular structures already existing in the biosphere. The development of new refrigeration systems is focused around implementing natural working fluids with ODP- and GWP-values close to zero. Generally, systems with natural working fluids achieve higher COP than systems charged with HFC's (Stene, 2015). Every working fluid have one or more negative attributes, whether it is flammability, toxicity, poor thermodynamic properties, chemical instability, or very high operating pressures. Hence, it is a trade-off between the attributes when choosing the suitable working fluid (McLinden et al., 2014).

4.2.1 Natural Working Fluids

Hydrocarbons

Hydrocarbons are interesting as working fluid, since it is environmentally safe and have ODP and GWP-values equal to zero. Due to high enthalpy of evaporation, the mass flow in the system is low, leading to a small charge size. In addition, the temperature after the compression is low, and the pressure level is low. The volumetric refrigeration capacity is moderate, leading to moderate compressor volumes. The challenge with hydrocarbons are that they are flammable, and cautions have to be made when designing the system (Stene, 2015). Propane, butane and isobutane are examples of hydrocarbons commonly used as refrigerants.

Ammonia - NH₃

Ammonia, which is used in TechnoAlpin SF220 and SnowGen, is widely used as a refrigerant in industrial systems for food refrigeration, distribution warehousing and process cooling. Due to extremely high enthalpy of evaporation, the mass flow in the system is very low. The discharge gas temperature is very high for an ammonia system, and the pressure level is moderate. The volumetric refrigeration capacity is relatively high, leading to relatively low compressor volumes. Ammonia is very toxic even at small concentrations. Thus, the design of the system is very important in order to prevent leakages. In addition, ammonia is not compatible with all materials, e.g copper (Stene, 2015).

Water

Water as a refrigerant is one of the oldest refrigerants being used for refrigeration applications above 0°C (Kilicarslan and Müller, 2005). Water is easily accessible, it is cheap and has excellent thermodynamic and chemical properties. It is environmentally safe, with ODP and GWP-values equal to zero, it is non-toxic, non-flammable and non-explosive. In addition, systems with water have high COP.

However, there are some technical challenges using water as refrigerant. The low operating pressure in the vacuum process results in a very large specific volume of the water vapour. Therefore, the compressor needs to handle large amounts of gas, which influence the dimensions of the compressor. In addition, the need of large compression ratios, makes the application of standard compressors expensive (Orshoven et al., 1993), and has been the major reason for why water as a refrigerant in air conditioning systems have not been used more

frequent (Li et al., 2011b). Since the operating pressure of the evaporator is low, the lift in pressure is small, even with large pressure ratio. The small pressure difference results in small aerodynamic forces on the compressor components. Hence, it is possible to build a lightweight construction using composites or titanium. Figure 4-2 shows a turbo compressor successfully implemented in a vacuum ice making maker. The diameter is 2,6m, and the titanium alloy blades are only 1,5mm thick. Two such compressors in series are suggested in a vacuum ice maker with cooling capacity of 3500kW. The pressure ratio of each compressor is between 2 and 3 (Orshoven et al., 1993) (Ophir, 2007). Another challenge with water is the high compressor outlet temperature. The complex construction leads to high investment costs. Lachner Jr et al. (2007) investigated the life-cycle cost of a water based cycles against a R134a cycle, and for a system with refrigeration capacity of 3500kW, the investment cost of the water vapour compressors was around 1 million USD compared to 22500 USD for the R134a compressor.



Figure 4-2 Radial compressor used in a vacuum ice maker (Ophir, 2007)

CO₂

CO₂ was a commonly used working fluid in installations in late 1800's and in the beginning of the 20th century. Due to the introduction of CFCs in the 1930s, CO₂ as a working fluid was almost forgotten until the end of the last century (Lorentzen, 1994). CO₂ is one of the few natural working fluids, which is neither flammable nor toxic. It is widely available, inexpensive and does not affect the global environment, with GWP and OPD-values equal to zero. The GWP value is zero when used a technical gas (Nekså, 2002). In addition, it is compatible with all materials, unlike ammonia (Pearson, 2008).

CO₂ has high critical pressure of 73,8 bar, which is high compared to other working fluids. This leads to a very high volumetric refrigeration capacity, yielding low compressor volumes. CO₂ systems operate at high pressure, meaning that special compressors and components must be utilized. In addition, CO₂ systems are compact, due to high vapour density, have low viscosity and low $\frac{\Delta T}{\Delta P}$, which leads to small pipe dimensions and the relatively small compressor volume (Stene, 2015).

The critical temperature is only 31,1°C, which implies that sub-critical operation is only possible when the average heat sink temperature is rather low. The practical upper limit of condensation, refers to a condensing temperature of 28°C for subcritical operation. However, sub-critical CO₂ systems performs well compared to systems using other working fluids (Nekså, 2002). At average heat sink temperature above the critical temperature, the cycle operates trans-critical. The difference between the operation modes is shown in Figure 4-3. To increase the efficiency and to reduce the power consumption at higher temperature lifts, multi-staging of compressors with intercooling and sub-cooling are often employed in the industry (Bansal, 2012).



Figure 4-3 Simple trans-critical and sub-critical CO₂ cycle

During trans-critical heat rejection, the pressure and temperature are independent properties, unlike sub-critical heat rejection. This means that the heat rejection occurs at relatively constant pressure and a gliding CO₂ temperature (Stene, 2015). This property makes CO₂ ideal for water

heating purposes when the water temperature difference is large. For trans-critical CO₂ systems, the heat exchanger is called gas cooler, while it is a condenser for sub-critical systems.

When expanding the CO₂ into the two-phase area, significant amounts of gas is creates. This leads to large thermodynamic losses. However, some of the expansion loss may be recovered by including an expander or an ejector into the system. An expander utilizes the expansion energy to produce mechanical work, while an ejector utilizes the expansion energy to increase the compressor suction pressure. Expansion work recovery could partially compensate for the large throttling losses in trans-critical CO₂ cycles (Austin and Sumathy, 2011). In addition, throttling losses can be minimized by sub-cooling the CO₂ before the expansion, by a suction gas heat exchanger(SGHX) or a separate sub-cooling heat exchanger (Stene, 2015).

CO₂ as a secondary working fluid in indirect systems was the first CO₂ refrigeration system to be commercially applied. The CO₂ circuit is connected to the primary refrigerant cycle through a heat exchanger. The circuit contains a vessel that acts as a receiver and accumulates the CO₂ returning from the condenser/evaporator (Reulens, 2009). Two possible arrangements are shown in Figure 4-4. Arrangement (A) may operate unstable, because two-phase CO₂ enters the condenser. Therefore, arrangement (B) is more favourable, where one-phase CO₂ vapour enters the condenser.

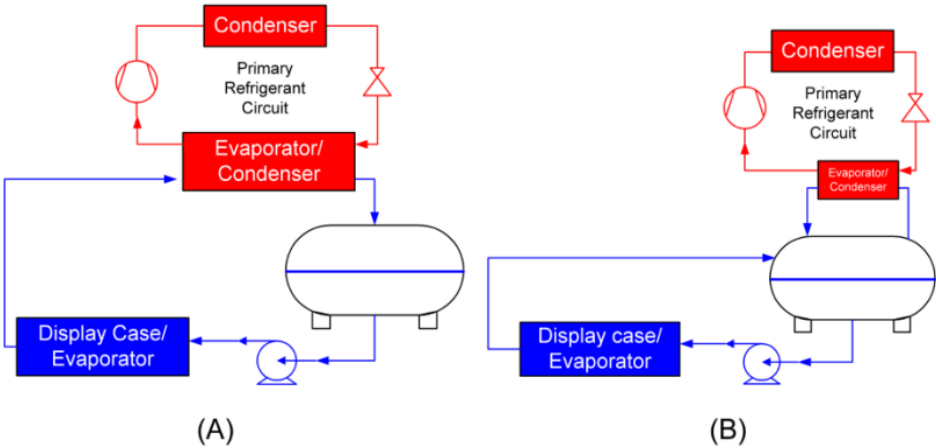


Figure 4-4 Basic schematics of two arrangements for indirect CO₂ systems(Reulens, 2009)

Regarding the safety, the high pressure level is not dangerous, and in case of leakage, only dry ice will be formed (Stene, 2015). Compared to other natural working fluids like ammonia and hydrocarbons, CO₂ has favourable safety properties.

4.3 Heat Recovery From CO₂-Systems

When producing snow, excess heat will be produced from the system. Today, this excess heat is released into the ambient, meaning the temperature of the waste heat is rather low. Instead of wasting this heat, a heat recovery system can be applied. As described previously, the flake and plate ice machines include a refrigeration system, while the vacuum ice machine needs an external refrigeration unit to be able to recover the heat. The refrigeration system can upgrade this waste heat to the desired end-use temperature. The same refrigeration unit may be utilized for the different ice production methods.

Heat recovery from refrigeration systems has typically been done by floating condensing pressure according to the ambient temperature (Arias and Lundqvist, 2006). The condensing temperature follows the ambient temperature to a minimum condensing level, usually $\Delta T = 10K$ (Sawalha and Chen, 2010). Another method is to combine this method with fixed condensing pressure method, which adjusts the condensing pressure to match the required temperature for the heating system. The latter method is mostly being used with systems running with HFCs. This heat recovery method is not suitable for systems running with CO₂ as working fluid, e.g. trans-critical systems, mainly because trans-critical CO₂ systems have relatively low COP at high heat sink temperatures compared to conventional working fluids, as seen in Figure 4-5 and Figure 4-6. Therefore, trans-critical systems have been installed mainly in cold climates with direct heat rejection to the ambient air where the operation is mostly sub-critical (Sawalha, 2013).

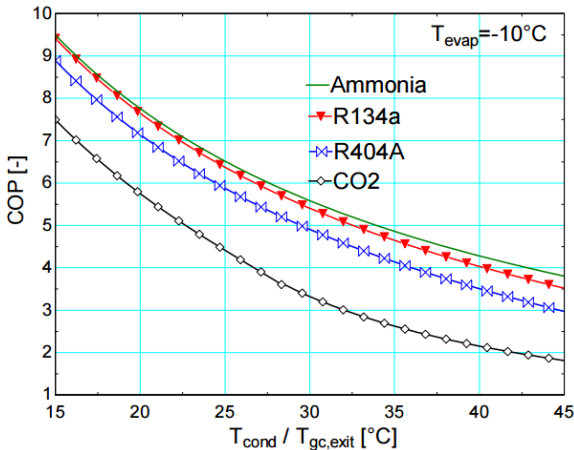


Figure 4-5 CO₂ compared to other working fluids in high stage operation (Reulens, 2009)

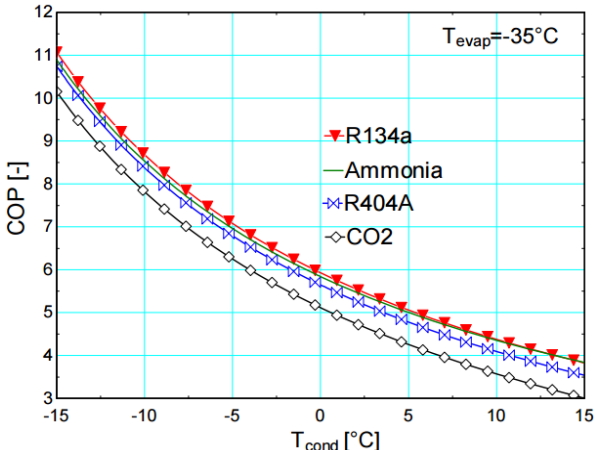


Figure 4-6 CO₂ compared to other working fluids in low stage operation (Reulens, 2009)

De-superheater (DSH)

In this system, Figure 4-7, heat is rejected in a de-superheater which is installed before the gas cooler/condenser. The system can provide heat to HVAC system or floor heating which requires lower operating temperature. The condensing pressure in the system is controlled according to the heating needs. This method is suitable for systems utilizing working fluids with high discharge gas temperatures, which is the case for CO₂ when operated trans-critically.

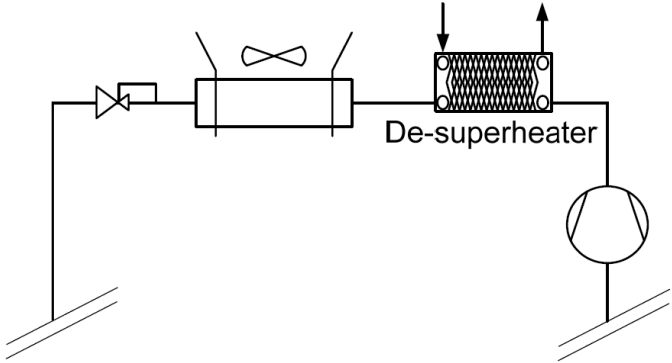


Figure 4-7 De-superheater heat recovery method (Sawalha and Chen, 2010)

Heat Pump Cascade (HPC)

Another concept of heat recovery from refrigeration system is to use a heat pump to recover heat from the condenser at low temperature, and elevate the temperature before transferring it to the HVAC system. This system uses the rejected heat and at the same time allowing the refrigeration system to operate at relatively low condensing pressure.

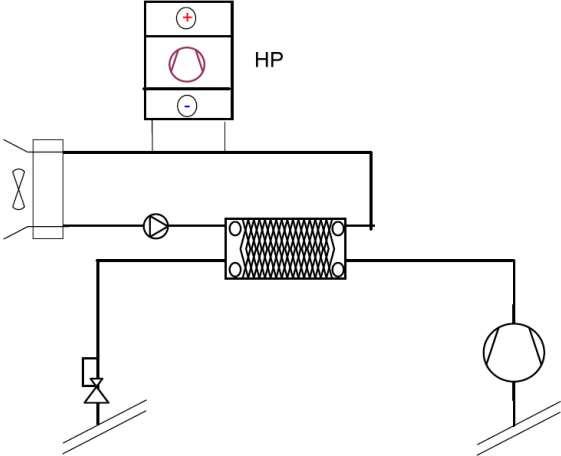


Figure 4-8 Heat pump cascade method for heat recovery (Sawalha and Chen, 2010)

Heat Pump Cascade for Sub-Cooling (HPSC)

A similar arrangement to a HPC system, is to connect a heat pump to the sub-cooling heat exchanger after the gas cooler so the refrigeration system operates at low condensing pressure when the ambient temperature is low and heating is needed. In addition to recover heat from the refrigeration system, it provides further sub-cooling of the CO₂ and improve its efficiency.

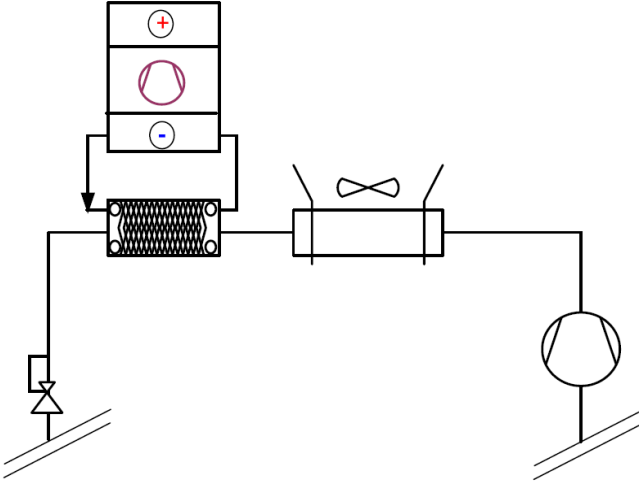


Figure 4-9 Heat pump cascade for sub-cooling for heat recovery (Sawalha and Chen, 2010)

4.4 Materials in the Flake Ice Drum

The materials used in the FID is important in order to maximize the heat transfer between the water and the working fluid. Carbon steel exhibits a higher thermal conductivity than stainless steel, as seen in Table 10. Aluminium exhibits superior thermal conductivity compared to both carbon steel and stainless steel. Ultimate tensile strength (UTS) is measured by the maximum stress that a material can withstand while being compressed or pulled before breaking. Steel is capable of withstanding much higher stresses than aluminium. The cost of carbon steel is 26,8% of aluminium, and 15,5% of stainless steel (meps.co.uk, 2016, indexmundi.com, 2016).

| Material | Thermal conductivity | Ultimate Tensile strength | Price |
|-----------------|--------------------------|---------------------------|--------------|
| Carbon steel | $k = 70,63 \frac{W}{mK}$ | - | 371 €/tonne |
| Stainless steel | $k = 15,0 \frac{W}{mK}$ | UTS = 515MPa | 2398 €/tonne |
| Aluminium | $k = 233,5 \frac{W}{mK}$ | UTS = 45 MPa | 1385 €/tonne |

Table 10 Material properties of metals⁴

EU regulations dictate what materials that can be utilized in the FID to produce ice. For food processing equipment the machines must be easily cleanable, corrosion resistant when in contact with food, and have smoothly bonded seams free of pits. For these purposes, stainless steel is accepted as a suitable material with satisfying hygienic properties (Jullien et al., 2003). For non-food related applications, carbons steel is a suitable material (northstar.com, 2015).

⁴ Properties from built-in data in EES. UTS for carbon steel is not available in the built-in library in EES

4.5 Heat Transfer Mechanisms in a Flake Ice Drum

The heat transfer mechanisms involved in the flake ice maker is convection and conduction. Through convection, heat is transferred from the chilled water to the ice layer. Then the heat is conducted through the ice layer to the FID wall, and through the wall. Lastly, the heat is transferred by convection from the FID to the working fluid, which provides the energy for the working fluid to evaporate. A schematic of the process is shown in Figure 4-10.

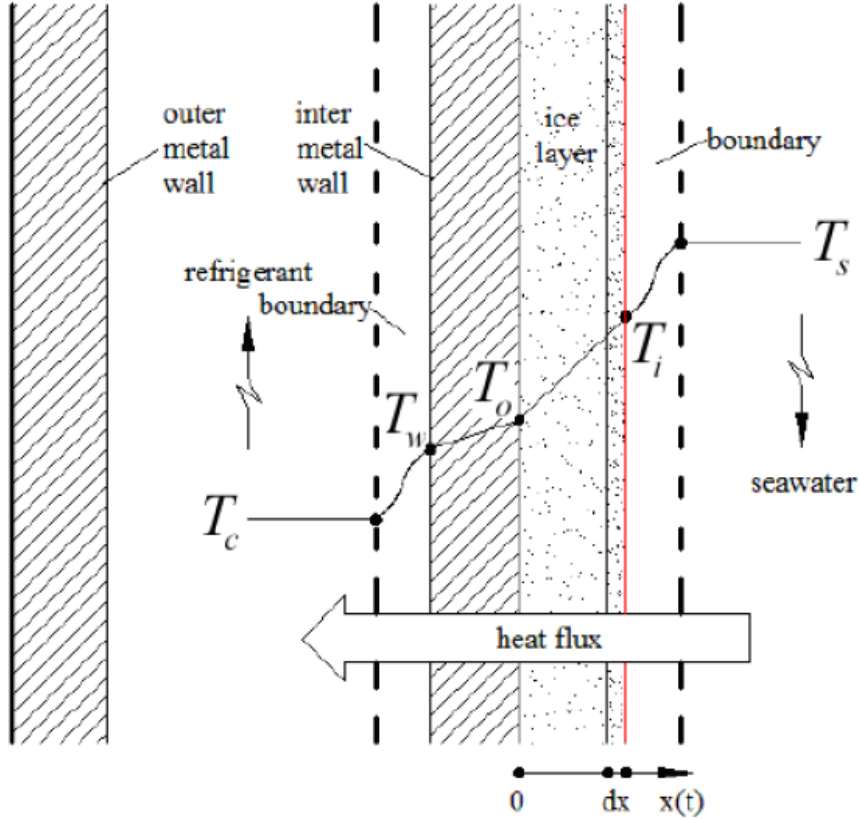


Figure 4-10 Schematic diagram of the process of flake ice maker (Cao et al., 2015)

The period of ice making is a phase-changing heat transfer process. It can be considered as a one-dimension freezing process. In the heat transfer model, there is a migrating interface between solid ice and liquid water during the process, and the latent heat of fusion is released at this interface (Zhao et al., 2008). The phase-change process begins from $x=0$, and migrates along the x -axis. The position is a time dependent property. As the ice boundary migrates, the heat transfer decreases due to increased resistance in the ice layer. Before the ice scraper, there is only ice left on the FID, allowing the ice to be sub-cooled.

5 EES Simulation Models of Vacuum and Flake Ice Makers

To assess snow making systems based on vacuum and flake ice technology, computer simulation models were made. The purpose of the models is to evaluate the thermodynamic performance of the machines. The models are developed in Engineering Equation Solver (EES). EES is a general equation-solving program that can numerically solve coupled non-linear algebraic and differential equations. A major feature of EES is the high accuracy thermodynamic and transport property database that allows it to be used with the equation solving capability. EES code for the vacuum and flake ice machines is given in appendix E and F, respectively.

The main focus in the thesis is on the flake ice maker. The vacuum ice model is an improved model from the project work. Only subcritical operation of the CO₂ unit and heat rejection to air or water is discussed in this thesis. However, the systems are designed such that a heat recovery system can be connected. The models are designed to produce $50 \frac{\text{tons}}{\text{day}}$.

5.1 General Calculations for the Vacuum and Flake Ice Model

Ambient temperatures

The simulations are based on the average ambient temperatures in the period from September 1. to November 1. at Voll observation station in Trondheim, since the ski tracks are supposed to open November 1. Voll observation station is the closest weather observation station to Granåsen. Assuming a 2,5km long, 6m wide and 0,4m deep track, which requires 6000m³ of snow, the machines need to produce snow for 60 days. The temperatures in this period in 2015 is presented in Figure 5-1. It is necessary to store the produced snow, but snow storage is not included in this thesis. In addition, snow production after November 1. is not included.

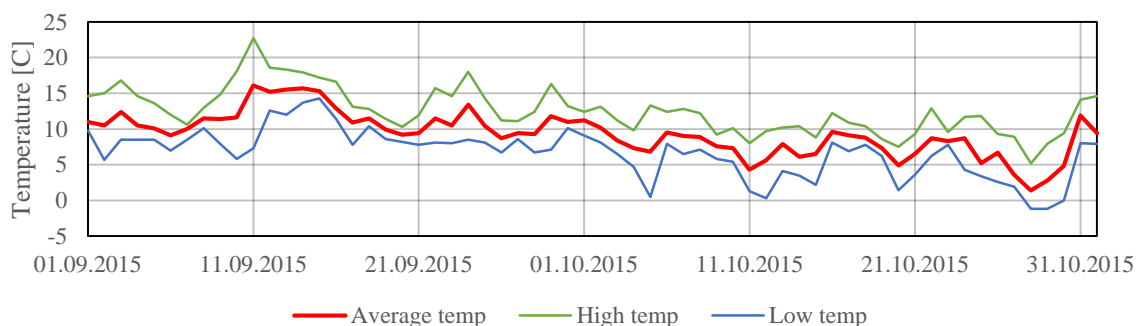


Figure 5-1 Ambient temperatures at Voll observation station in Trondheim from September to November (yr.no, 2016)

Overall heat transfer coefficient

The overall heat transfer coefficient, U-value, of the heat exchangers is determined by the resistances of the cold fluid side, the plate wall, and the warm fluid side. Brazed plate and gasketed plate heat exchangers are utilized in the systems. The U-value is calculated to be able to calculate the size of the heat exchangers.

$$U = \frac{1}{R_{warm} + R_{wall} + R_{cold}} = \frac{1}{\frac{1}{\alpha_{warm}} + \frac{\delta}{k_{wall}} + \frac{1}{\alpha_{cold}}} \quad (5.1)$$

where δ are the thickness of the plate, k_{wall} are the heat conductivity coefficient of the wall and α is the heat transfer coefficient.

Correlation for heat transfer coefficient calculations

The heat transfer coefficient of each fluid is calculated in order to determine the U-value. The SGHX, intercooler, superheat heat exchanger and water-side of the condenser, shown in Figure 5-2 and Figure 5-10, deal with one-phase fluids, and the Martin correlation for one-phase flow in plate heat exchangers is utilized.

$$Nu = 0,122 * Pr^{\frac{1}{3}} * \frac{\mu_f^{\frac{1}{6}}}{\mu_{wall}} * (f * Re^2 * \sin(2\beta))^{0,374} \quad (5.2)$$

where f is the friction factor found in (5.4), and β is the chevron angle of the heat exchanger plates (García-Cascales et al., 2007). A chevron angle of 45° is assumed. Using the definition of the Nusselt number, the heat transfer coefficient α_f is found

$$Nu = \frac{\alpha_f d_e}{k_f} \quad (5.3)$$

$$\frac{1}{\sqrt{f}} = \frac{\cos\beta}{\left(0,18 * \tan\beta + 0,36 * \sin\beta + \frac{f_0}{\cos\beta}\right)^{0,5}} + \frac{1 - \cos\beta}{\sqrt{3,8 * f_1}} \quad (5.4)$$

where f_0 and f_1 are defined by the Reynolds number of the fluid stream.

$$f_0 = \begin{cases} \frac{64}{Re}, & Re < 2000 \\ (1,8 * \log_{10} Re - 1,5)^{-2}, & Re \geq 2000 \end{cases} \quad (5.5)$$

$$f_1 = \begin{cases} \frac{597}{Re} + 3,85, & Re < 2000 \\ \frac{39}{Re^{0,289}}, & Re \geq 2000 \end{cases} \quad (5.6)$$

Area of heat exchangers

The area is calculated for water-cooled counter current plate heat exchangers, and is based on the known Q , ΔT_{LMTD} and U -values. For air-cooled heat exchangers the area is larger, due to lower heat transfer coefficient. The outlet temperatures of the water are determined using an energy balance. An initial U -value is guessed, and the number of plates, based on the size of commercially available plate heat exchangers from Alfa Laval, are determined. A new U -value based on this number is then calculated, and the guessed U -value is updated. The iterative process continues until the guessed value equals the calculated.

$$Q = UA\Delta T_{LMTD} \leftrightarrow A = \frac{Q}{U\Delta T_{LMTD}} \quad (5.7)$$

$$\Delta T_{LMTD} = \frac{(T_{h,in} - T_{c,in}) - (T_{h,out} - T_{c,out})}{\ln\left(\frac{T_{h,in} - T_{c,in}}{T_{h,out} - T_{c,out}}\right)} \quad (5.8)$$

| Heat exchanger | Model | Width [mm] | Height [mm] | # of plates | Q [kW] | \dot{m}_w [kg/s] | U-value [W/m ² K] | ΔT_{LMTD} [K] | Area [m ²] |
|-------------------------|----------|------------|-------------|-------------|--------|--------------------|------------------------------|-----------------------|------------------------|
| Condenser/evap | AC112 | 92 | 519 | 165 | 213,9 | - | 2764 | 5,00 | 15,48 |
| Intercooler | AC120EQ | 90 | 269 | 39 | 16 | 2 | 549,3 | 15,47 | 1,88 |
| Superheat HX | AXP112 | 150 | 519 | 62 | 90,43 | 10 | 384 | 24,46 | 9,63 |
| Condenser | AXP112 | 150 | 519 | 285 | 185,9 | 15 | 1277 | 3,28 | 44,42 |
| SGHX | AXP52 | 70 | 154 | 46 | 15,66 | - | 449,7 | 34,85 | 1,00 |
| Condenser Vacuum | AlfaCond | 1658 | 500 | 4 | 213,2 | 10 | 3243 | 11,17 | 5,89 |

Table 11 Area of heat exchangers at $T_{amb}=5^{\circ}\text{C}$ and $T_{water}=5^{\circ}\text{C}$. Two-stage compression

Pressure drop in heat exchangers

The total pressure drop in the heat exchangers is the sum of several smaller pressure drops (Shah and Sekulić, 2007)

- Frictional pressure loss, ΔP_{fric}
- Gravitational pressure loss, ΔP_g
- Acceleration pressure loss, ΔP_{acc}
- Manifold pressure loss, ΔP_{man}

The total pressure loss on the evaporation side is given by

$$\Delta P_{tot} = \Delta P_{fric} + \Delta P_{man} + \Delta P_{acc} + \Delta P_{gr} \quad (5.9)$$

The total pressure loss on the condensation side is given by

$$\Delta P_{tot} = \Delta P_{fric} + \Delta P_{man} - \Delta P_{acc} - \Delta P_{gr} \quad (5.10)$$

The frictional pressure drop is the pressure drop due to the roughness of the channel walls and colliding molecules. It is given by,

$$\Delta P_{fric} = \frac{2fG^2 h_{plate}}{d_e \rho_m} \quad (5.11)$$

where f is a friction factor depending on whether the pressure drop is in a one- or two-phase fluid, G is the mass flux, h is the height of the plate, d_e is the equivalent diameter and ρ_m is the mean density

$$G = \frac{\dot{m}}{A_0 N_{ch}} \quad (5.12)$$

A_0 is the cross sectional area of the space between the plates and N_{ch} is the number of plate pairs.

$$\rho_m = \frac{1}{\frac{z_m}{\rho_g} + \frac{1-z_m}{\rho_f}} \quad (5.13)$$

z_m is the average gas quality.

$$f = 0,8Re^{-0,25} \quad (5.14)$$

Equation (5.14) calculates the friction factor for single phase flow.

Gravitational pressure loss, ΔP_g , is the loss or gain of pressure due to the effects of gravity. In the condenser the fluid enters at the top of the heat exchanger. Thus, pressure is gained, while the opposite occurs in the evaporator.

$$\Delta P_{gr} = \rho_m g h_{plate} \quad (5.15)$$

ΔP_{acc} is the loss or gain of pressure due to either acceleration or deceleration. In the condenser the gas is decelerated and pressure is gained. In the evaporator, there is a pressure loss due to acceleration.

$$\Delta P_{acc} = G^2 \Delta z \left(\frac{1}{\rho_g} - \frac{1}{\rho_f} \right) \quad (5.16)$$

where Δz is the difference in quality of the fluid.

The manifold pressure loss ΔP_{man} is the loss due the fluid entering the inlet and outlet ports and manifolds.

$$\Delta P_{man} = 0,75 * \frac{G^2}{\rho_m} \quad (5.17)$$

The pressure drop in the different heat exchangers are presented in Table 12.

| Heat exchanger | ΔP_{fric} | ΔP_g | ΔP_{acc} | ΔP_{man} | ΔP_{total} |
|----------------------------|-------------------|--------------|------------------|------------------|--------------------|
| Condenser/evap warm | 0,31 Pa | 2840 Pa | 4,92 Pa | 4622 Pa | 1,77 kPa |
| Condenser/evap cold | 2711 Pa | 236,3 Pa | 0,42 Pa | 3184 Pa | 6,13 kPa |
| Intercooler | 574,8 Pa | 121,5 Pa | - | 3211 Pa | 3,66 kPa |
| Superheat HX | 89,11 Pa | 544,9 Pa | - | 1381 Pa | 2,02 kPa |
| Condenser | 0,28 Pa | 686,5 Pa | 0 Pa | 1096 Pa | 0,41 kPa |
| SGHX warm | - | - | - | - | 22,45 kPa |
| SGHX cold | - | - | - | - | 5,764 kPa |
| FID | 31404 Pa | 923,1 Pa | 3,114 Pa | 815,1 Pa | 33,15 kPa |
| Condenser Vacuum | - | - | - | - | - |

Table 12 Heat exchanger pressure drop

The manifold pressure losses, ΔP_{man} , are the major losses in most of the heat exchangers. The diameter is set to 5,2 cm for all heat exchangers, due to unknown inlet manifold diameter. Hence, the pressure drop may be incorrect. In addition, the space between the plates in the plate heat exchanger are set to 3,5mm, leading to an equivalent diameter, d_e , of 7mm.

The pressure drop in the vacuum system condenser is not included due to problems with very large ΔP_{fric} . Alfa Laval was asked for advice, but no feedback was given. However, a pressure drop analysis of steam in a tube bundle executed by O'Donovan and Grimes (2015) at pressures from 0,05 to 0,14 bar, which is 10 times higher than in the model, showed the overall losses to be relatively small, and in the region of 120-250 Pa. The main reason was that momentum recovery balanced the frictional losses. Although the cases are not totally comparable, the expected pressure drop is rather low, even though the magnitude of each pressure drop component is significant.

Pressure drop in pipes

The pressure loss in the pipes are given by the Darcy-Weisbach equation

$$\Delta P = f \frac{L}{D} \frac{\rho u^2}{2} \quad (5.18)$$

The pressure drop in the pipes is calculated using the built-in EES-function “PipeFlow”

CALL PipeFlow(R\$;T_{co2};P_{co2};m_{pipe};D_{pipe};L_{pipe};RelRough: ;ΔP_{pipe};;)

The equation takes the working fluid, temperature, pressure, mass flow, pipe diameter, pipe length and relative roughness as inputs, and gives the pressure drop as output. Pressure drop in the pipe after the expansion valve is neglected.

| Segment | T _{in,co2} [°C] | P _{in,co2} [Pa] | L _{pipe} [m] | D _{pipe} [cm] | RelRough [-] ⁵ | ΔP _{pipe} [Pa] |
|---------|--------------------------|--------------------------|-----------------------|------------------------|---------------------------|-------------------------|
| 2-3 | 44,42 | 865,4 | 1 | 40 | 3,75·10 ⁻⁵ | 3,49 |
| 4-5 | 59,15 | 1228 | 1 | 35 | 4,29·10 ⁻⁵ | 4,76 |
| 6-7 | 10,00 | 1223 | 1 | 35 | 4,29·10 ⁻⁵ | 3,94 |
| 10-1 | 0,01 | 611,7 | 1 | 5 | 3·10 ⁻⁵ | 1,882 |

Table 13 Pressure drop in pipes in the vacuum model at T_{cond}=5°C

⁵ A roughness, ϵ , of $1,5 \cdot 10^{-5}$ is assumed

| Segment | T _{in,co2} [°C] | P _{in,co2} [kPa] | L _{pipe} [m] | D _{pipe} [cm] | RelRough [-] ⁶ | ΔP _{pipe} [kPa] |
|---------|--------------------------|---------------------------|-----------------------|------------------------|---------------------------|--------------------------|
| 2-3 | 42,10 | 1143 | 1 | 4,2 | 6,82·10 ⁻⁴ | 2,29 |
| 4-5 | 10,00 | 2263 | 1 | 4,2 | 3,57·10 ⁻⁴ | 1,95 |
| 6-7 | 76,75 | 4502 | 1 | 3,2 | 4,69·10 ⁻⁴ | 4,94 |
| 8-9 | 10 | 4495 | 1 | 3,2 | 4,69·10 ⁻⁴ | 2,90 |
| 10-11 | 4,00 | 4467 | 1 | 2,2 | 6,82·10 ⁻⁴ | 3,06 |
| 14-15 | -36,13 | 1155 | 1 | 2,2 | 6,82·10 ⁻⁴ | 2,60 |
| 16-1 | -20,12 | 1147 | 1 | 4,2 | 3,57·10 ⁻⁴ | 3,59 |

Table 14 Pressure drop in pipes in the flake ice refrigeration system at T_{cond}=5°C

| Segment | T _{in,co2} [°C] | P _{in,co2} [kPa] | L _{pipe} [m] | D _{pipe} [cm] | RelRough [-] | ΔP _{pipe} [kPa] |
|---------|--------------------------|---------------------------|-----------------------|------------------------|-----------------------|--------------------------|
| a-b | -30 | 1393 | 1 | 5,2 | 2,88·10 ⁻⁴ | 4,00 |
| b-c | -30,81 | 1389 | 1 | 2,2 | 6,82·10 ⁻⁴ | 1,50 |
| d-e | -30,88 | 1386 | 1 | 2,2 | 6,82·10 ⁻⁴ | 1,50 |
| e-f | -30,91 | 1384 | 1 | 3,2 | 4,69·10 ⁻⁴ | 1,71 |
| g-FID | -30,92 | 1430 | 1 | 3,2 | 4,69·10 ⁻⁴ | 1,71 |

Table 15 Pressure drop in pipes in the FID circuit at T_{cond}=5°C

The dimensions of the pipes in the flake ice machine are based on pipe dimensions presented by Stene (2015).

Pumps

The work of the pumps used in the two systems are calculated using the built-in EES-function “CentrifugalPump1_CL”.

$$\text{CALL CentrifugalPump1_CL}(R\$;0;T_{in};P_{in};m_w;N_{\text{pump}};D_{\text{pump}};D_{\text{hub}} : P_{out};T_{out};W_{\text{pump}};\eta_{\text{pump}})$$

The equation takes the working fluid, temperature, pressure, mass flow, pump speed, pump diameter, pump hub diameter as inputs, and gives the outlet pressure and temperature, work and efficiency as output.

| Pump | T _{in,co2} [°C] | P _{in,co2} [kPa] | \dot{m} [$\frac{kg}{s}$] | N _{pump} [$\frac{1}{s}$] | D _{pump} [m] | D _{pump,hub} [m] | W _{pump} [kW] |
|-----------------|--------------------------|---------------------------|------------------------------|-------------------------------------|-----------------------|---------------------------|------------------------|
| Ice slurry | 0,01 | 0,6117 | 3,86 | 1000 | 0,15 | 0,08 | 0,165 |
| CO ₂ | -30,95 | 1383 | 2 | 1080 | 0,15 | 0,08 | 0,128 |

Table 16 Pump work

⁶ A roughness, ϵ , of $1,5 \cdot 10^{-5}$ is assumed

5.2 Modelling of the Vacuum Ice Maker

The model is based on fundamental thermodynamics including energy and mass balances, and consists of an evacuated chamber, compressors, a condenser, an expansion valve and a vacuum pump.

Three system configurations have been made. Two systems, with one (SVS) or two (TVS) compressor stages, containing only a vacuum system with heat exchange to the ambient air, and a cascade system with the vacuum system running at constant condensing temperature, and a CO₂ system with a condensing temperature which adjusts according to the ambient temperature. The system configuration of the latter is shown in Figure 4-8. A schematic of the vacuum system with two compressor stages is shown in Figure 5-2.

The following simplifications are made:

- Heat losses to the ambient are negligible.
- Power consumption of vacuum pump is not included.
- Water cooling in separate system is not included.
- Constant enthalpy through pipes
- All the inlet water is turned into snow

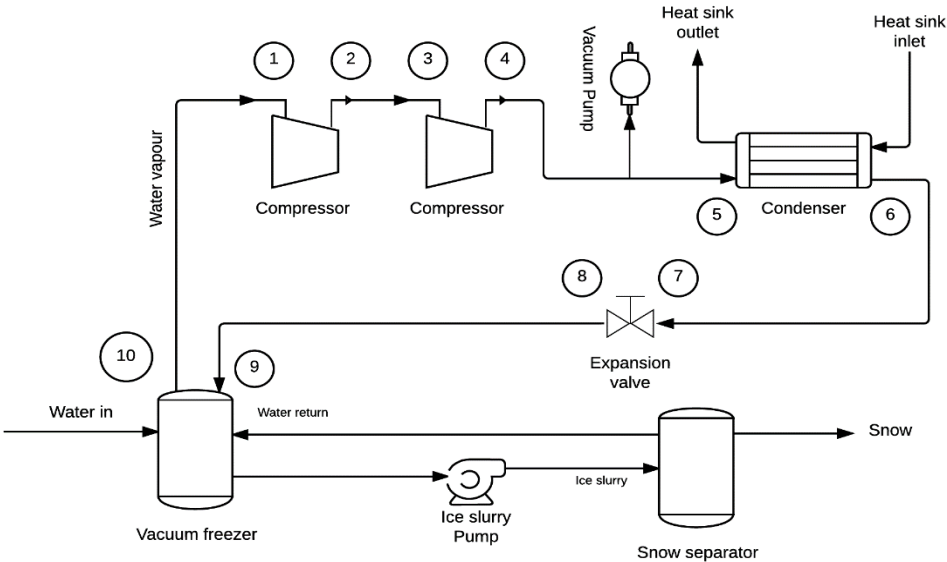


Figure 5-2 Schematic of the model of a vacuum ice maker

The thermodynamic properties of point 1-10 are presented in appendix B.

The total energy that needs to be removed from the water is shown in (5.19), where the first term describes the energy needed to cool the water to 0°C, and the second term describes the energy to freeze the water. The rate at which vapour will leave the vacuum freezer is expressed in (5.20).

$$Q_{tot} = Q_{freezing} + Q_{cooling} = \dot{m}_w C_{p,w} \Delta T + \dot{m}_w C_{p,fusion} \quad (5.19)$$

$$\dot{m}_g = \frac{Q_{tot}}{h_{10} - h_9} \quad (5.20)$$

As seen in Figure 5-3, the vapour leaving the vacuum freezer is fed back after being condensed. There is a mass balance between the snow separator and freezer, leading to constant water levels in both. The mass balance of the freezer and snow separator, (5.21), reduces to (5.22).

$$\dot{m}_{w,in} + \dot{m}_{g,cond} = \dot{m}_g + \dot{m}_{snow\ out} \quad (5.21)$$

$$\dot{m}_{w,in} = \dot{m}_{snow,out} \quad (5.22)$$

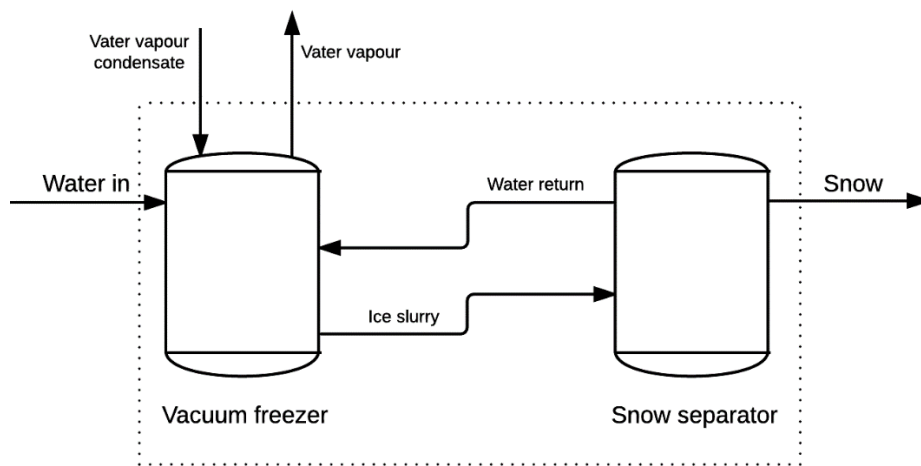


Figure 5-3 Mass balance of the vacuum freezer and snow separator

Surface area of vacuum vessel

The mass flu of vapour in the vacuum vessel is calculated using the Knudsen equation for partial vacuum (Eames et al., 1997),

$$G = f_{ec} \left(\frac{P_l}{\sqrt{T_l}} - \frac{P_g}{\sqrt{T_g}} \right) \sqrt{\frac{M}{2\pi R_g}} \quad (5.23)$$

where G , f and P is the mass flux of vapour, the coefficient of evaporation and pressure of saturated liquid and gas in $\frac{dyne}{cm^2}$, respectively. The pressure in the gas is assumed to be 1 mBar lower than the saturated liquid pressure. Equation (5.24) calculates the required area of the evaporating surface.

$$A_{surface} = \frac{\dot{m}_g}{G} \quad (5.24)$$

Wall thickness of vacuum vessel

Under the condition of partial vacuum, the vessel is subjected to external pressure. Therefore, the thickness of the vessel wall is important. The vessel is assumed to be a pipe with closed ends. Stresses in a cylindrical pressure vessel depend upon the ratio of the inner radius and outer radius $\frac{r_o}{r_i}$, rather than the size of the cylinder (Kaminski, 2005). Based on thick-wall theory three stresses occur, namely hoop, axial and radial stress,

$$\sigma_{hoop} = \frac{\left(P_i r_i^2 - P_o r_o^2 - r_i^2 r_o^2 \frac{P_o - P_i}{r^2} \right)}{r_o^2 - r_i^2} \quad (5.25)$$

$$\sigma_{axial} = \frac{P_i r_i^2 - P_o r_o^2}{r_o^2 - r_i^2} \quad (5.26)$$

$$\sigma_{radial} = \frac{\left(P_i r_i^2 - P_o r_o^2 + r_i^2 r_o^2 \frac{P_o - P_i}{r^2} \right)}{r_o^2 - r_i^2} \quad (5.27)$$

Where r is depending on whether the stresses is calculated by the inner or outer radius. For vessels subjected to external pressure, the inner radius is the critical.

The maximum stress allowed in the wall is calculated for different wall thicknesses (Kaminski, 2005).

$$\sigma_{max} = \frac{E}{3} \left(\frac{r_o - r_i}{2r_i} \right)^2 \quad (5.28)$$

Where E is the Young's modulus of the metal. Stainless steel AISI302, whose properties are built into EES, is used in the calculations. The value of E is 193GPa.

Condenser

The heat transfer coefficient for condensation of steam is calculated based on the following correlation

$$\text{Nu} = \frac{\alpha_f d_e}{k_l} = 0,555 * \left(\frac{\rho_l g (\rho_l - \rho_g) h'_{fg} d_e^3}{\mu_l k_l (T_{cond} + T_{wall})} \right)^{\frac{1}{4}} \quad (5.29)$$

$$h'_{fg} = h_{fg} + 0,375 * c_{p,l} (T_{cond} - T_{wall}) \quad (5.30)$$

where T_{wall} is the wall temperature, $c_{p,l}$ is the specific heat capacity for liquid and h_{fg} is the enthalpy of vaporization (Incropera et al., 2013)

5.2.1 Results

The parameters presented in Table 17 form the basis of the calculations in the vacuum models.

| Parameter | |
|--|----------------------|
| Evaporation temperature, T_{evap} | 0,01 [°C] |
| Evaporation pressure, P_{evap} | 611,7 [Pa] |
| Average ambient temperature, T_{amb} | 5 - 20 [°C] |
| Mass flow water, \dot{m}_w | 0,579 [kg/s] |
| $\Delta T_{cascade,HX}$ | 10 [K] ⁷ |
| $T_{cascade,evap}$ | -5 [°C] |
| $T_{cascade,cond}$ | 5 [°C] |
| ΔT_{cond} | 5 [K] |
| $\eta_{comp,vacuum}$ | 0,5 [-] ⁸ |

Table 17 Input variables vacuum machine

The state points are calculated using built-in thermodynamic data in EES, and the resulting log P-h diagram with $T_{cond}=5^\circ\text{C}$ is shown in Figure A-1. Two-stage compression is included in the diagram. The superheated gas section on the high pressure side is quite small, and the enthalpy difference is limited. This means that little heat can be recovered, and no superheat recovery heat exchanger is applied. The latent heat of evaporation is very large for water, meaning the mass flow of refrigerant is small compared to CO₂. After the condensation the water is saturated, before being throttled. A small amount of gas will be created when throttling, but the expansion losses are rather small.

⁷ $T_{cascade,cond}$ and $\Delta T_{cascade,HX}$ are based on a VIM100 unit for thermal energy storage in Japan. (Ophir, 2008)

⁸ Dependent on pressure ratio and varies from about $\eta_{is} = 0,4$ to $\eta_{is} = 0,6$ (Burandt and Buschmann, 2006). An average $\eta_{is} = 0,5$ is assumed.

The COP for both heating and cooling for the different configurations are shown in Figure 5-4. The TVS has better cooling COP than the SVS throughout the temperature range, while the heating COP is somewhat lower. The cascade system is running with lower COP during the whole temperature. Compared to SVS and TVS, the cascade system has low COP, however a COP of around 4 at $T_{cond}=5^{\circ}\text{C}$ is still quite high. The COP of the SVS and TVS is 26,2% and 26,3% better at $T_{cond}=5^{\circ}\text{C}$, and 31,4% and 33,6% better at $T_{cond}=20^{\circ}\text{C}$, respectively, compared to the cascade system. On the other side, the cascade system is less sensitive to temperature changes and the change of performance is less than for the pure vacuum systems. Systems using water as refrigerant have high COP, but according to equation (4.4) the increased energy saving is less the higher the COP is.

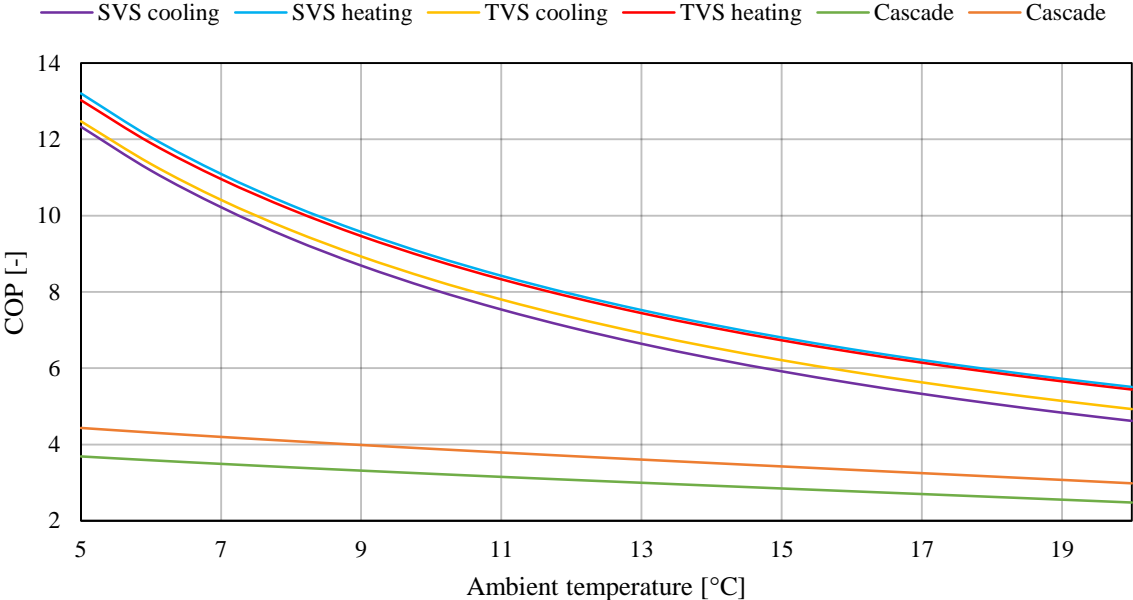


Figure 5-4 Comparison of COP for the different system configurations.

The COP is related to the work of the systems, and one can clearly observe that the cascade system requires a higher power input. The work required in each of the systems are presented in Figure 5-5. At $T=5^{\circ}\text{C}$ the work for the SVS is only 1,1% higher than the TVS, while it increases to 6,7% higher at $T=20^{\circ}\text{C}$. When changing the ambient temperature with 1°C , the work changes in average with 6,8%, 6,4%, and 3% for the SVS, TVS and cascade system, respectively. In average, the power input is 2,7 times higher for the cascade system than the SVS and TVS. The outlet temperature of the compressor, on the other hand, is in favour of the cascade system, as shown in Figure 5-6. The maximum outlet temperature in the ambient

temperature range is 86°C, while it is as high as 242°C and 132°C for the SVS and TVS, respectively. The pressure ratio for the CO₂ part of the cascade is in the same range as the TVS, where the TVS has lowest pressure ratio at T=5°C and the cascade has the lowest at T=20°C. The SVS has 1,4 times higher pressure ratio than the SVS at T=5°C. However, the increase is quite steep and at T=20°C the pressure ratio is 2,3 times higher than the cascade system.

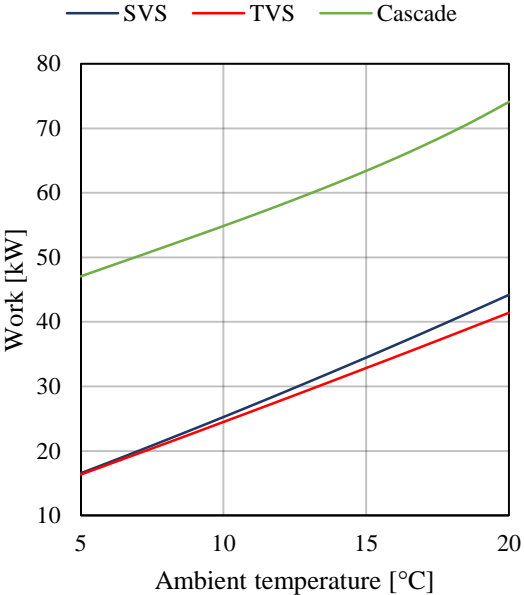


Figure 5-5 Work vs ambient temperature. Vacuum systems

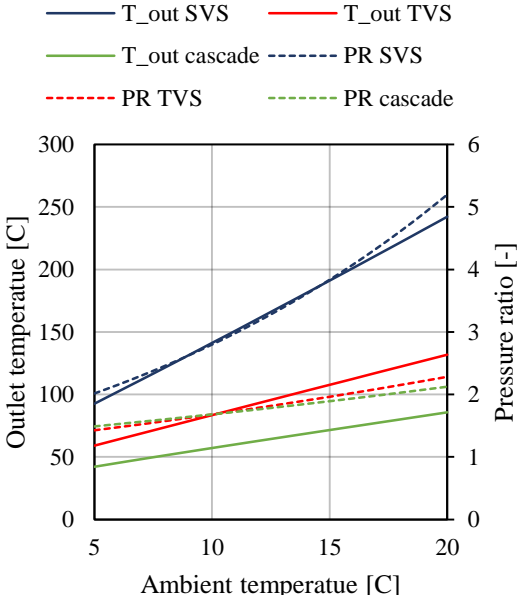


Figure 5-6 Outlet temp and pressure ratios vs ambient temp. Vacuum systems.

In Figure 5-7, the energy consumption during the production period for the different configurations is presented. The energy consumption is per day of production, and 24-hour production is assumed. The difference in energy consumption of the TVS and SVS is small, and at low ambient temperatures the difference is negligible. During a five-day period in September, where the temperatures are highest, the SVS consumes 5% more energy than the TVS. The energy consumption of the cascade system is more than twice the consumption of TVS and SVS most of the time. An interesting observation is that difference in energy consumption is largest at low temperatures, about 4 times higher for the cascade, but at higher ambient temperatures the cascade consumes less than 2 times more energy. The average energy consumption is 5,64 kWh/m³, 5,8 kWh/m³ and 12,8 kWh/m³ for the SVS, TVS and cascade, respectively. All system configurations consume less energy as the ambient temperature decrease, due to lower T_{cond}.

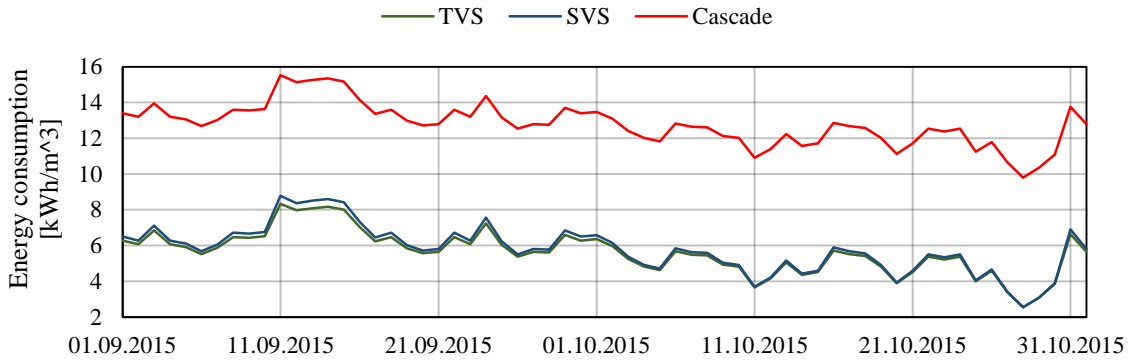


Figure 5-7 Energy consumption during the production period. Vacuum systems

As shown in Figure 5-8, the evaporating coefficient greatly affects the size of the required evaporating surface. To assess the size of the system, the value of f_{ec} is assumed to be 0,2, and the resulting diameter of the evaporating surface is 1,91 m. Figure 5-9 presents the critical wall thickness of the vessel, as the cross-section between the graphs for maximum and critical stress, $\sigma_{critical}$. The stresses are largest for the inner hoop stress. The critical thickness is calculated to be around 1,88% of the inner diameter, and the resulting wall thickness is 3,59 cm.

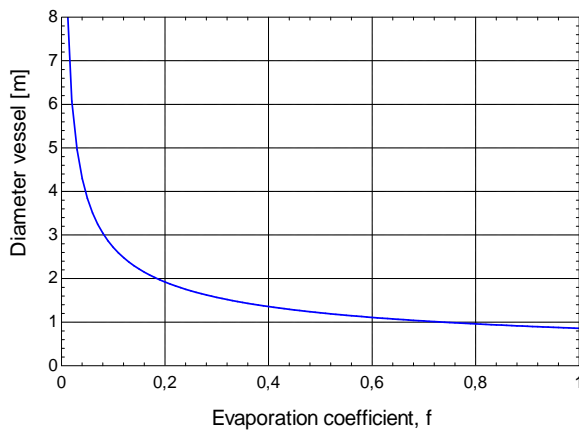


Figure 5-8 Diameter of vacuum vessel with varying evaporation coefficient

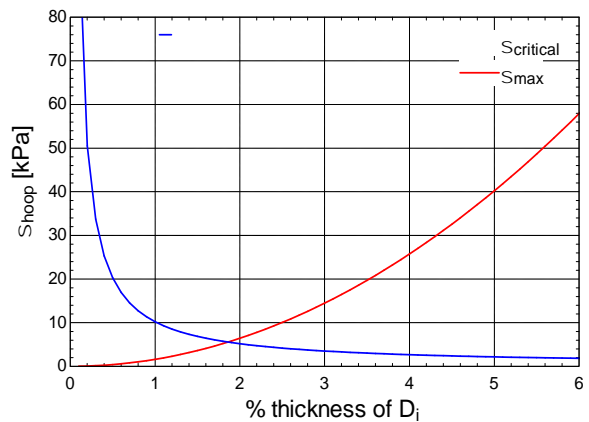


Figure 5-9 Wall thickness of the vacuum vessel

5.2.2 Discussion

Due to the high enthalpy of vaporization in the vacuum system, the refrigerant mass flow is very low compared to the CO₂ unit in the cascade system. This leads to low energy consumption for the compressor, and is the main reason why the vacuum system consumes less energy than the cascade system. In addition, the cascade system has an extra heat exchanger, introducing an extra ΔT , which increases the power consumption. To reduce the energy consumption of the cascade system, it is possible to run the vacuum part at higher $T_{\text{cascade,cond}}$. This will reduce the COP of the vacuum system. However, since the COP is above 20, the reduction in this part is smaller than the gain of COP in the CO₂ unit, and the total COP will increase. If heat recovery is desirable, such modification should be considered. However, the increased $T_{\text{cascade,cond}}$ have to be balanced to avoid too high compressor outlet temperatures.

Comparing the TVS and SVS, the TVS consumes less energy than the SCS throughout the temperature range. However, the investment costs are around 50% higher for a two-stage system than a single-stage system, as reported by Lachner Jr et al. (2007), and the extra investment cost must be compared to the increased efficiency to figure out what is the most profitable. In addition, the operating conditions must be taken into account. The high outlet temperature of the SVS is a result of the high pressure ratio. The ambient temperatures, shown in Figure 5-1, yield a pressure ratio beneath 3 for the SVS most of the time. Assuming that a compressor similar to the one presented in Figure 4-2 is used, the pressure ratio of the compressor is within the operating limits at low ambient temperatures. However, in ambient temperatures above 11°C the required pressure ratio is too high for the compressor to handle, and multi-staging is inevitable. This means that the SVS is not capable of removing the required heat at high temperatures. Therefore, if heat recovery is desirable, thus high operating temperatures, systems running with water as refrigerant is not as suitable as CO₂-systems. The special compressor, both in size and construction, will lead to very large, complex and expensive systems.

Regarding the operating costs of producing the required amount of snow, the TVS are somewhat more reasonable to run than the SVS and much more reasonable than the cascade system. Assuming an average price of 0,8kr/kWh (ssb.no, 2016), including electricity, grid rent and taxes, the costs are 27072 NOK, 27840 NOK and 61440 NOK for the SVS, TVS and cascade respectively. This yields a cost of 4,51 NOK, 4,64 NOK and 10,24 NOK per 1 m³ of snow.

The value of f_{ec} has been discussed extensively in the literature, but it is hard to determine precisely. The coefficient depends on the properties of the gas surrounding the evaporating surface. In a perfect vacuum f_{ec} has a value of 1, meaning that the evaporation rate is maximized, while in ambient pressure the coefficient may just be a fraction of unity (Jones, 1991). Since the operating pressure of the vacuum system is a medium vacuum, the coefficient is assumed to be much lower than for a perfect vacuum and somewhat lower than for ambient pressure. The difficulty of determining the evaporation coefficient, makes the calculations of the required evaporation area rather unreliable. However, the assumed value of f gives a diameter that is plausible when compared to the dimensions of the existing VIM100 machine.

There have to be a pressure difference between the saturated liquid and gas phase for evaporation to happen. If the pressure difference is decreasing, the required area of evaporation is increasing, and when the saturated liquid pressure equals the vapour pressure, the evaporation rate will be zero. Therefore, it is important with a suitable compressor that can handle the water vapour to avoid a reduction in the evaporation coefficient, which in the end will reduce the production capacity of the machine. In a perfect vacuum, $P_g=0$ and $f = 1$, a surface diameter of 0,39 m is required.

The large pressure difference between the ambient and the operating pressure in the vacuum vessel make demands to the thickness of the vessel. Thick-wall theory was utilized to calculate the required thickness, since it is more precise than thin-wall theory. A rule of thumb when utilizing thin-wall theory to calculate the resulting stresses in a cylinder, is that $\frac{t}{d} \leq \frac{1}{40}$ (Shigley et al., 2014). The rule estimates a ratio between the thickness and the diameter that can be related to our case, and a critical thickness of around 2% of the inner diameter is plausible. According to the European standard EN 13458-2:2002 for static vacuum vessels, the safety factor for external pressure against buckling is 3. This means the real thickness will be 10,77 cm.

To compare the energy consumption of the different configurations assessed in this section with existing vacuum systems is difficult, due to the fact that the system design of the commercially available systems is not available to the public. Therefore, the figures of energy consumption in datasheets provided by the manufacturers are only a guideline. Even though the production capacity of the models is increased to match the VIM100, the energy consumption is substantially lower and the comparison may not give the true picture.

5.3 Modelling of the Flake Ice Maker

The model is based on fundamental thermodynamics including energy and mass balances. This system is an indirect CO₂ system containing compressors, an intercooler between the compressor stages, a condenser and superheat condenser, a suction gas heat exchanger(SGHX), an expansion valve, an evaporator/condenser, CO₂ liquid drum, a liquid pump, and the FID. A schematic is presented in Figure 5-10.

The following simplifications are made:

- Heat losses to the ambient are negligible.
- Constant enthalpy through pipes
- All the inlet water is turned into snow
- Separate water cooling system is not included

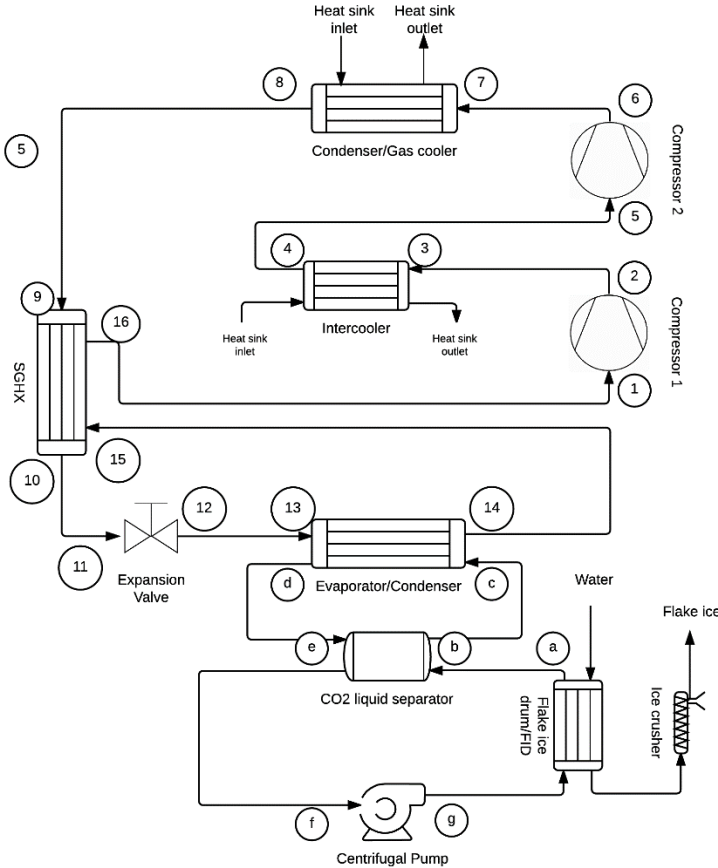


Figure 5-10 Schematic of flake ice machine

The thermodynamic properties of point 1-16 are presented in appendix B.

5.3.1 Modelling of the Flake Ice Drum (FID)

The FID is designed as shown in Figure 5-11. The figure is a section of the FID. It is a sandwich construction, composed of two steel layers, and an extruded aluminium profile with CO₂ pipes. The idea is that the steel will strengthen the structure, and that it will degrade less than aluminium when the ice is scraped off. To compare the heat transfer to other metals, the aluminium section is substituted with carbon and stainless steel. The inner diameter of the FID is 2,5m, while the height is 2,6m. These dimensions are based on the size of commercially available flake ice makers (GEA.com, 2016). In order to avoid the rotating seals, the FID is designed to be scraped on the inside. The number of CO₂-pipes is assumed to be 300, which yields a distance of 26 mm between each pipe. The thickness of the steel layer is set to 3mm, the aluminium layer is set to 15 mm, and the CO₂-pipes are 5 mm in diameter. The light blue area in Figure 5-11 indicates the freezing surface. The pipe dimension is in the same region as pipes used in publications about CO₂ vaporization (Zhao and Bansal, 2007, Yoon et al., 2004, Hassan and Shedid, 2015). It is assumed that there are no limitations of the size of the FID, since the machine will be stationary in Granåsen.

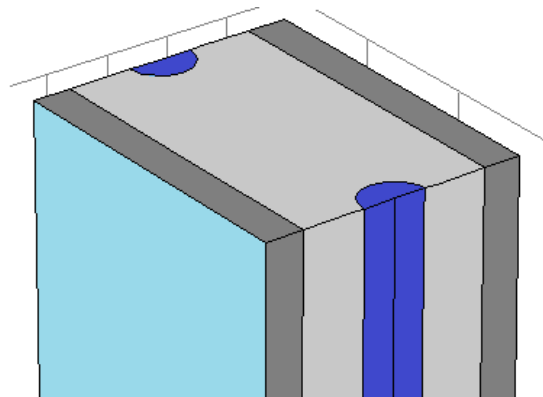


Figure 5-11 Geometry of FID

To be able to produce 50 tons/day flake ice with a density of $\rho_{flake,ice} = 500 \text{ kg/m}^3$, 54,54 m^3 ice with density of 916,7 kg/m^3 must be produced. The desirable ice thickness is 3mm, which connected with the dimensions of the FID, yields that the drum has to be scraped every 48,5s.

$$\rho_{ice} V_{ice} = \rho_{flake,ice} V_{flake,ice} \rightarrow V_{ice} = \frac{\rho_{flake,ice}}{\rho_{ice}} * V_{flake,ice} = \frac{500 \frac{\text{kg}}{\text{m}^3}}{916,7 \frac{\text{kg}}{\text{m}^3}} * 100 \text{ m}^3 = 54,54 \text{ m}^3$$

The heat needed to be transported away from the water is calculated in equation (5.19). The energy needed to sub-cool the water has to be included, $Q_{sc} = m_w c_{p,ice} \Delta T_{sc}$.

Evaporation of CO₂

The two-phase heat transfer coefficient correlation for evaporation of CO₂ was given under the condition of forced flow (Choi et al., 2007).

$$\alpha_{evap,CO_2} = S * \alpha_{nb} + F * \alpha_f \quad (5.31)$$

where S is a nucleate boiling suppression factor, and F is a factor developed by (Choi et al., 2007) to account for the increase in the convective turbulence due to the presence of the vapour phase.

$$F = 0,05 * (\phi_f^2) + 0,95 \quad (5.32)$$

$$S = 7,2694 * (\phi_f^2)^{0,0094} * Bo^{0,2814} \quad (5.33)$$

where ϕ_f^2 is a two-phase frictional multiplier which is a function of the Lockhart Martinelli parameter X_{tt} , and Bo is the boiling number. The boiling number is a dimensionless number that represents the ratio of generated vapour in the evaporator.

$$\phi_f^2 = 1 + \frac{C}{X_{tt}} + \frac{1}{X_{tt}^2} \quad (5.34)$$

C is the Chisholm parameter which depends on whether the flows is turbulent or laminar. In this case both the water flow and refrigerant flow are turbulent, and the value of C is 20.

$$X_{tt} = \left(\frac{\mu_f}{\mu_g}\right)^{\frac{1}{8}} + \left(\frac{1-z}{z}\right)^{\frac{7}{8}} + \left(\frac{\rho_g}{\rho_f}\right)^{\frac{1}{2}} \quad (5.35)$$

Where μ_f and μ_g are the kinematic viscosity of the liquid and gas phase, respectively, z is the gas quality, and ρ_f and ρ_g is the density of the liquid and gas phase.

$$Bo = \frac{\frac{Q_{water}}{A_{ht}}}{G * h_{fg}} \quad (5.36)$$

where A_{ht} represents the total heat transfer area within the FID, G is the mass flux of refrigerant and h_{fg} is the enthalpy of vaporization of CO₂.

The liquid heat transfer coefficient, α_f , is defined by the Dittus-Boelter correlation in (5.37).

$$Nu = 0,023 * \left(\frac{G * (1-z) * d_h}{\mu_f}\right)^{0,8} * Pr_f^{0,4} \quad (5.37)$$

where $d_h, k_{ref}, G, \mu_f,$ and Pr_f are the hydraulic diameter, heat conductivity coefficient, mass flux, kinematic viscosity and Prandtl number of CO₂, respectively.

The heat transfer by nucleate boiling (Choi et al., 2007) is presented in equation (5.38).

$$\alpha_{nb} = 55 * P_r^{0,12} * (-0,4343 * \ln(P_r))^{-0,55} * M^{-0,5} * q^{0,67} \quad (5.38)$$

where P_r, M and q are the reduced pressure, molecular weight of CO₂ and heat flux in $\frac{W}{m^2}$, respectively.

The friction pressure drop is calculated by (5.11), substituting f with f_{tp} calculated in (5.39).

The two-phase Fanning friction factor for evaporation is given by the correlation proposed in (Amalfi et al., 2016). This correlation is found by a best fit from a large experimental databank

$$f_{tp} = C * 15,698 \left(\frac{G^2 d_e}{\rho_m \sigma}\right)^{-0,475} \left(\frac{(\rho_f - \rho_g) g d_e^2}{\sigma}\right)^{0,255} \left(\frac{\rho_f}{\rho_g}\right)^{-0,571} \quad (5.39)$$

where C is given by

$$C = 2,125 \left(\frac{\beta}{\beta_{max}}\right)^{9,993} + 0,955 \quad (5.40)$$

β_{max} is 70° and the mean density is

Heat transfer coefficient along vertical plate

The water flows on the subcooled surface of the FID, where the physical properties can be regarded as constant. The heat transfer coefficient on the water side is determined by equation (5.41) (Incropera et al., 2013)

$$\alpha_w = 0,037 * \frac{k_w}{h} * \left(\frac{u_w * h}{\nu_w} - B \right)^{\frac{4}{5}} * Pr_w^{\frac{1}{3}} \quad (5.41)$$

where h , k_w , u_w , ν_w , and Pr_w are the is the height of the FID, heat conductivity coefficient, velocity, kinematic viscosity and Prandtl number of water, respectively. The constant B is determined by the value of the critical Reynolds number, $Re_{x,c} = 5 * 10^5$. That is,

$$B = 0,037 * Re_{x,c}^{\frac{4}{5}} - 0,644 * Re_{x,c}^{\frac{1}{2}} \quad (5.42)$$

Dynamic model of the ice growth process on the flake ice drum

The overall heat transfer coefficient of the whole process is determined by the resistances of the refrigerant side, the aluminium and steel wall, the ice layer and the water side.

$$U = \frac{1}{\frac{1}{\alpha_{evap,co2}} + \frac{\delta_{al}}{k_{wall,al}} + \frac{\delta_{sst}}{k_{wall,sst}} + \frac{x}{k_{ice}} + \frac{1}{\alpha_w}} \quad (5.43)$$

Where δ and x are the thickness of the wall and ice layer and k_{wall} and k_{ice} are the thermal conductivity of the wall and ice layer.

It is desirable to simulate the change in ice thickness with time. This determines how fast the ice layer grows, dictating how much ice is produced, and it influence the heat transfer as the ice layer thickness increase. The model is developed by applying heat and mass conservation to the control volume in Figure 4-10. There are two boundary conditions; temperature continuity at the liquid and solid phase boundary, (5.44), and energy conservation, (5.45) (Cao et al., 2015, Zhao et al., 2008).

$$T_b = T_w \quad (5.44)$$

$$q_{ice} - q_w = \rho_{ice} v_{ice} h_{ice} - \rho_w v_w h_w = 0 \quad (5.45)$$

Mass conservation yields, $\rho_{ice}v_{ice} = \rho_wv_w$, and (5.45) reduces to

$$q_{ice} - q_w = \rho_wv_w(h_w - h_{ice}) = \rho_wv_wL \quad (5.46)$$

where L is the latent heat of fusion.

The conduction and convection equation are introduced into (5.46) to get,

$$\alpha_{ice} \frac{\partial T_{ice}}{\partial x} - \alpha_w(T_w - T_{ice}) = \rho_wL \frac{\partial x}{\partial t} \quad (5.47)$$

The conduction part of equation (5.47) may be written as

$$\alpha_{ice} \frac{\partial T_{ice}}{\partial x} = \frac{T_{ice} - T_{wall}}{\frac{x}{\alpha_{ice}}} = \frac{T_{ice} - T_{ref}}{\frac{1}{\alpha_{evap,co2}} + \frac{\delta_{al}}{k_{wall}} + \frac{\delta_{sst}}{k_{wall}} + \frac{x}{\alpha_{ice}}} \quad (5.48)$$

Equation (5.48) reduces to

$$\frac{T_{ice} - T_{ref}}{\frac{1}{\alpha_{evap,co2}} + \frac{\delta_{al}}{k_{wall}} + \frac{\delta_{sst}}{k_{wall}} + \frac{x}{\alpha_{ice}}} dt = \rho_wL dx + \alpha_w(T_w - T_{ice})dt \quad (5.49)$$

which from the ice thickness, x, and ice growth rate, $\frac{dx}{dt}$, can be calculated.

5.3.2 Heat Exchangers

Condenser and evaporator/condenser

Equation (5.31) is used to calculate the evaporation heat transfer coefficient of the evaporator/condenser. The hydraulic diameter, d_h , used for the FID, is changed to the equivalent diameter, d_e .

The condensation heat transfer coefficient for condensing CO₂ in the condenser and evaporator/condenser is calculated using a correlation developed by Park and Hrnjak (2009). The condensation is divided in two parts, cooling of gas and phase change. The duty became too high if all the heat was rejected in a single heat exchanger of the type used.

$$\alpha_{cond,co2} = \frac{k_f^{\frac{2}{3}} * C_{p,f}^{\frac{1}{3}}}{\mu_f^{\frac{15}{7}}} * \left(\frac{1-z}{z} * \left(\frac{\rho_f}{\rho_g} \right)^{0,5} + 1 \right) \quad (5.50)$$

The two-phase friction pressure drop in the condenser is calculated by (5.51)(Longo, 2010). The correlation was originally made for hydrocarbons. Therefore, the calculated pressure drop will not represent the actual pressure drop, but it will provide an estimation of the value.

$$\Delta P_{f,cond} = \frac{1,9G^2}{2\rho_m} \quad (5.51)$$

Intercooler

To cool the refrigerant between the compressor stages an intercooler is utilized. If heat recovery is desirable the heat from this stage can be utilized. Equation (5.2) is used to calculate the heat transfer coefficient on both the refrigerant and water side. The intercooler cools the refrigerant, such that the superheat of the gas is 10K.

SGHX

A SGHX does not necessarily improve the COP of subcritical systems (Llopis et al., 2015), due to increased compressor work as a result of pressure drop in the SGHX and increased specific volume of the gas. The main purpose of the SGHX in this system is to provide a superheat to the suction gas, which protects the low stage compressor. In addition, the SGHX provide sub-cooling of the CO₂ on the high pressure side, and the extra compressor work related to the superheat is somewhat compensated.

The SGHX was modelled using the built-in function “HeatExchanger2_CL” in EES.

$$\text{CALL HeatExchanger2_CL}(H\$;0;m_{\text{warm}}; h_{\text{warm,in}}; P_{\text{warm,in}}; C\$; 0; m_{\text{cold}}; h_{\text{cold,in}}; P_{\text{cold,in}}; T_{\text{diff}}; \Delta P_{\text{warm}}; \Delta P_{\text{cold}}; h_{\text{warm,out}}; P_{\text{warm,out}}; h_{\text{cold,out}}; P_{\text{cold,out}}; Q_{\text{SGHX}}; \eta_{\text{SGHX}}) \quad (5.52)$$

The equation takes the working fluid, mass flow, inlet enthalpy, inlet pressure, temperature difference between warm inlet and cold outlet, and pressure drop in % as inputs, and gives the outlet enthalpies, pressure, heat transferred and efficiency as output. ΔP was set to 0,5% of the inlet pressure, and $T_{\text{diff}}=30\text{K}$.

5.3.3 Compressor

To calculate the isentropic efficiency and volumetric efficiency, correlations made by Eikevik (2016a) were utilized. The correlations are based on measurements of one type of compressor, and might not calculate the correct efficiencies for the compressors suitable for the flake ice system.

$$\eta_{is} = -0,00000461\text{PR}^6 + 0,00027131\text{PR}^5 - 0,00628605\text{PR}^4 + 0,07370258\text{PR}^3 - 0,46054399\text{PR}^2 + 1,40653347\text{PR} - 0,87811477 \quad (5.53)$$

$$\lambda_{is} = 0,0011\text{PR}^2 - 0,0487\text{PR} + 0,9979 \quad (5.54)$$

where PR is the pressure ratio of each compressor.

The compressors in this system run on full speed all the time, and an advanced regulation system is therefore not necessary. To prevent too high compressor outlet temperatures at high ambient temperatures, a two stage system was designed. The volume flow through the compressors is 139,9 m³/h and 75,35 m³/h in the low and high stage at an ambient temperature of T_{amb}=5°C, respectively. Commercially available compressors with the required volume flow is limited. GEA has a model series named Grasso 5HP, which is capable of handle volume flows up to 202 m³/h (GEA.com, 2016), but the high stage design pressure is limited to 50 bars. One such compressor may be used in the low stage in combination with a compressor designed for trans-critical operation. Another solution is a combination of compressors designed for subcritical, HXG4, and trans-critical, HXG2, operation. The cycle operates within the limits shown in Figure 5-12 and Figure 5-13. Choosing the right low stage compressor is therefore a question of investment and maintenance costs.

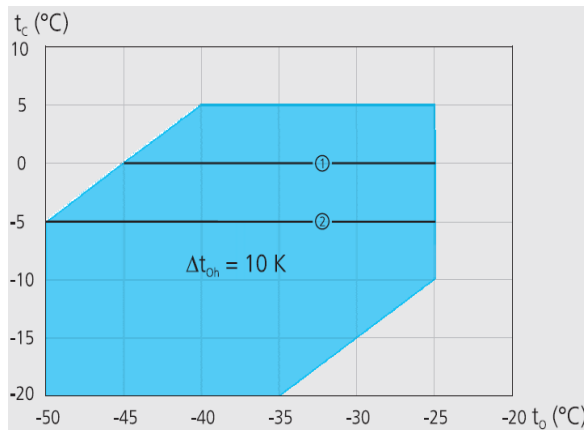


Figure 5-12 Operating limits low stage compressor, model HGX4. T_c is condensing temperature. T₀ is evaporating temperature. (GEA.com, 2016)

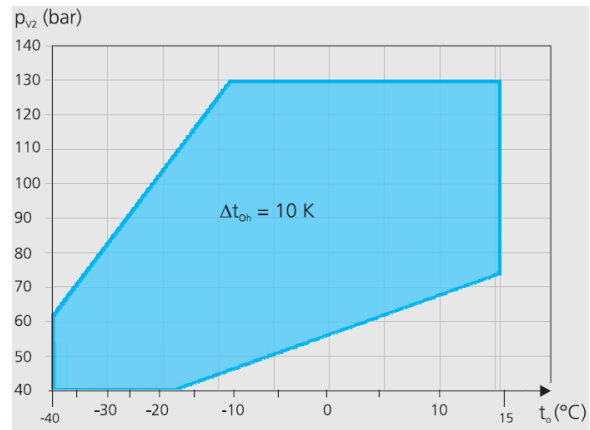


Figure 5-13 Operating limits high stage compressors, model HGX2. P_{v2} is condensing pressure. T₀ is evaporating temperature. (GEA.com, 2016)

The HXG4 compressor is limited to a volume flow of 48,2 m³/h, and three such compressors are needed. In the upper stage, the limit is 38,2 m³/h, and two compressors are needed. The difference in volume flow is due to different density of the gas.

| | Model | \dot{V}_{lim} [m ³ /h] | \dot{V} [m ³ /h] | # comp | \dot{V}_{comp} [m ³ /h] |
|-------------------|-------------|-------------------------------------|-------------------------------|--------|--------------------------------------|
| Low stage | Grasso 55HP | 168 | 139,9 | 1 | 139,9 |
| Low stage | HGX4 | 48,2 | 139,9 | 3 | 46,63 |
| High stage | HGX2 | 38,2 | 75,35 | 2 | 37,68 |

Table 18 Volume flow compressors

5.3.4 Results

The parameters presented in Table 19 form the basis of the calculations in the flake ice model.

| Flake ice drum(FID) | | Refrigeration system | |
|--|------------|---|---------------|
| Evaporation temperature, T_{evap} | -30 [°C] | Evaporation temperature, T_{evap} | -35 [°C] |
| Evaporation pressure, P_{evap} | 1428 [kPa] | Evaporation pressure, P_{evap} | 1381 [kPa] |
| Mass flow CO_2 , \dot{m}_{FID} | 2 [kg/s] | Average ambient temperature, T_{amb} | 5 - 20 [°C] |
| T_{water} | 5 [°C] | Mass flow CO_2 , \dot{m}_{CO_2} | 0,9425 [kg/s] |
| $X_{\text{out,FID}}$ | 0,35 [-] | ΔT_{cond} | 5 [K] |
| | | $T_{\text{water,cond}}$ | 5 [°C] |

Table 19 Input variables vacuum machine

The state points are calculated using built-in thermodynamic data in EES, and the resulting log P-h diagram with $T_{\text{amb}}=5^\circ\text{C}$ is shown in Figure A-2. Two-stage compression is included in the diagram.

The COP for both heating and cooling for both single (SCS) and two-stage (TCS) compression are shown in Figure 5-14. The SCS is running with higher COP in ambient temperatures below 14°C , while the TCS is running more efficiently at high condensing temperatures. The cooling COP of the SCS is 22% better at $T_{\text{cond}}=5^\circ\text{C}$, but 12,3% poorer at $T_{\text{cond}}=20^\circ\text{C}$, compared to the TCS. The heating COP for SCS is better throughout the whole temperature range, but if increasing the condensing temperature, and the trend continues, the COP will sink below the COP of the TCS.

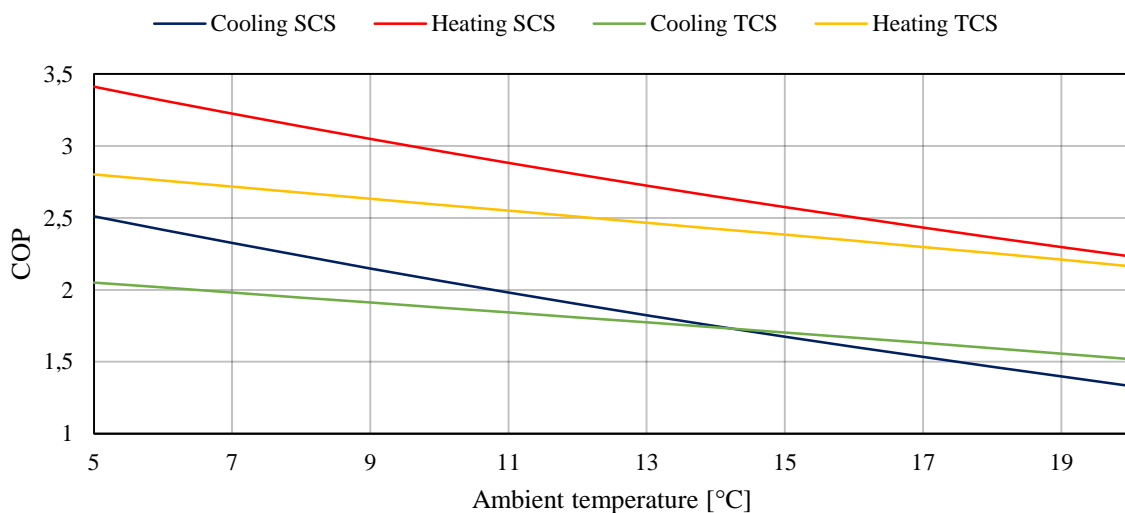


Figure 5-14 Comparison of COP for one- and two stage systems. Flake ice

The work required in each of the systems are presented in Figure 5-15. One can clearly observe that around 14°C, the work of the two systems is equal, similar to the COP. The increase of required power input is rather steep, and for every 1°C increase of T_{amb} , the work increase in average by 4,3% and 2% for SCS and TCS, respectively. The outlet temperature of the compressors, on the other hand, shows a different pattern. In Figure 5-16, the compressor outlet temperature is always higher for SCS than TCS. The maximum outlet temperature in the ambient temperature range is 156,8°C and 87,9°C for the SCS and TCS, respectively. The maximum compressor outlet temperatures for CO₂ systems is 150°C (Eikevik, 2016b). This means that the outlet temperature for SCS is too high at high ambient temperatures above 18,7°C. In addition, the pressure ratio for the SCS is twice the pressure ratio for the TCS at $T_{amb}=5^{\circ}\text{C}$, and at higher T_{amb} the difference is even larger.

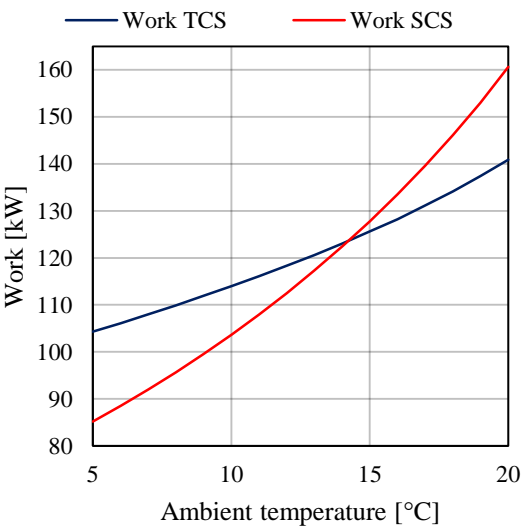


Figure 5-15 Comparison of work for one- and two stage systems. Flake ice

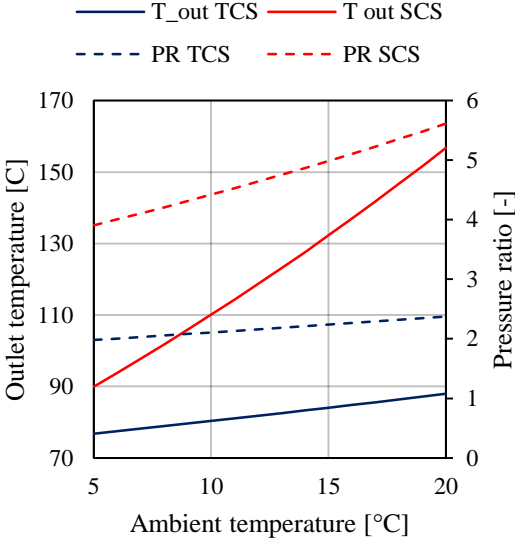


Figure 5-16 Comparison of outlet temperature and pressure ratios. Flake ice.

In Figure 5-17, the energy consumption during the production period for the different configurations is presented. The energy consumption is per day of production, and 24-hour production is assumed. During the production period, the SCS consumes less energy than the TCS most of the time. Its only in a small period of 5 days in the middle of September where the TCS consumes less than the SCS. One can observe that the difference between the two configurations becomes quite large at the low temperatures, and at the lowest temperature in October the difference in energy consumption is 31,6% lower, in favour of the SCS.

In addition, the energy consumption of the SCS is more sensitive to temperature changes than the TCS, and the difference between the warmest and coldest day is 14,3 kWh/m³, compared to 7,3 kWh/m³ for the TCS. The average energy consumption is 24,47 kWh/m³ and 27,1 kWh/m³ for the SCS and TCS, respectively.

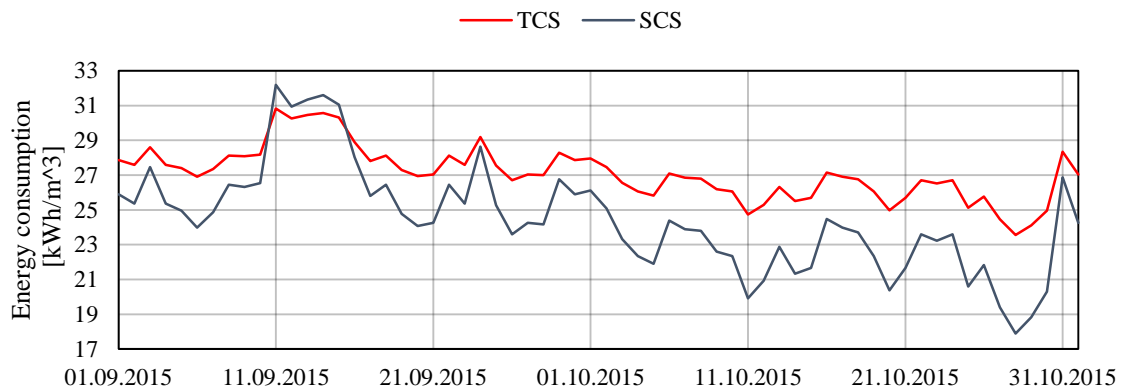


Figure 5-17 Energy consumption at T=-30°C. Flake ice machine.

As seen in Figure 5-18, construction using aluminium(Al) in the core has higher overall heat transfer coefficient than with carbon steel(CS) or stainless steel(SST) initially. After a few seconds, constructions with CS equalize the Al-constructions, and the U-values remains nearly equal as the ice production proceed. SST-constructions have lower U-value all along, but from 30 seconds the U-value is under 1% less than Al. In average, the U-values reduce with 53,6% for CS, 54,8% for Al, and 47,5% for SST, from t=0s to t=80s. Figure 5-19 shows the ice growth rate using different metals in the core of the structure. Initially, the growth rate for Al is highest, before the growth rate of CS-constructions become larger after just 1 second. From 5s, they are nearly the same. The growth rate decreases quite dramatically for CS and Al the first 5s, and from 20s the growth rate is nearly the same for all three metals. Between t=0s and t=30s, the reduction of the growth rate is 89,2% and 92,1% for CS and Al, respectively. The decline of the growth rate is not as dramatic for SST, and the reduction between t=0s and t=30s is 74,4%. At t=30s, the growth rate is only 2,4% less than Al. Comparison between the ice growth rate and U-value reveals that the ice growth rate decreases more rapidly than U-values.

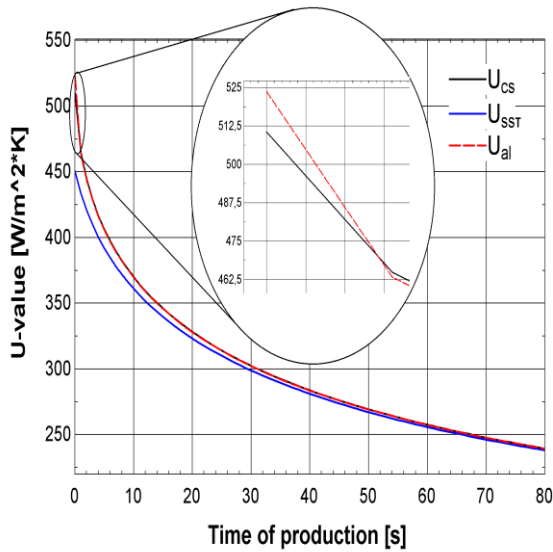


Figure 5-18 Variation of the overall heat transfer coefficient for different materials at $T=-30^{\circ}\text{C}$

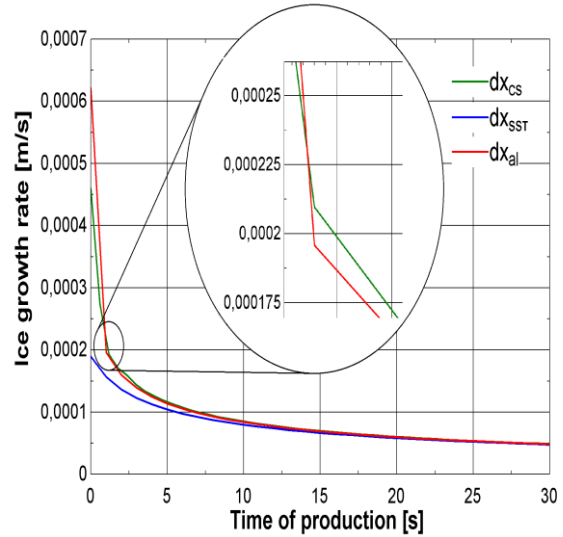


Figure 5-19 Ice growth rate [m/s] vs ice thickness [m] at $T=-30^{\circ}\text{C}$

Figure 5-20 presents the ice thickness as function of time. The trend is that the increase in ice thickness is largest in the early stages of the freezing process, while it is slowly decreasing as the production continues. To produce an ice layer with thickness of 3mm, Al-constructions need 32s, CS-constructions need 34s and SST need 45s, which is within the time limit of $t=48,5\text{s}$ to produce 50 tons/day.

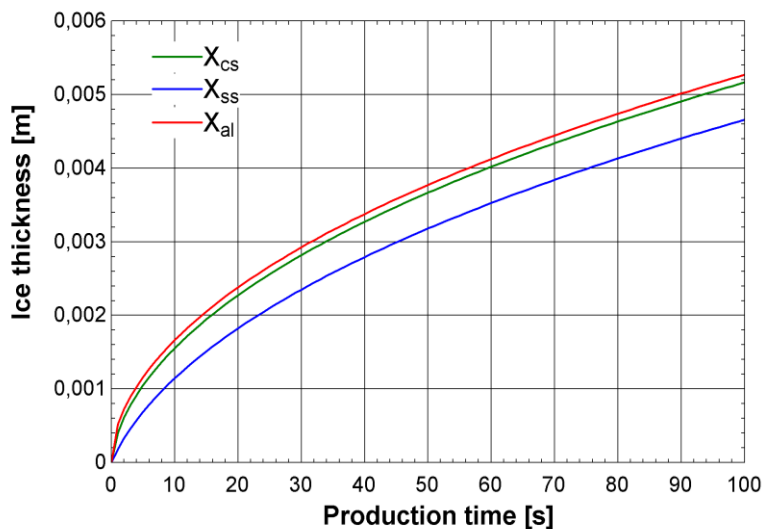


Figure 5-20 Variation of ice thickness with time at $T=-30^{\circ}\text{C}$

As shown in Figure 5-21, the refrigeration temperature is important for the propagation of the ice layer. It can be observed that the ice growth rate is significantly reduced as the refrigerant temperature increases. At a refrigeration temperature of $T=-40^{\circ}\text{C}$ it takes 23s to grow a 3mm thick ice layer, while at $T=-15^{\circ}\text{C}$ it takes 76s. The ice layer thickness is almost halved for $T=-15^{\circ}\text{C}$ compared to $T=-40^{\circ}\text{C}$ throughout the temperature range. Figure 5-22 shows the ice production capacity at various refrigerant temperatures. The production capacity is highly dependent of the refrigerant temperature, and a 1°C change, changes the production capacity with $1102\frac{\text{kg}}{\text{day}}$, $1115\frac{\text{kg}}{\text{day}}$ and $1087\frac{\text{kg}}{\text{day}}$ in average for CS, SST and Al, respectively. The capacity of the CS and Al constructions are nearly the same, while the capacity for SST is 1,1% less than CS at $T=-40^{\circ}\text{C}$ and 2,8% lower at $T=-15^{\circ}\text{C}$. At $T=-40^{\circ}\text{C}$, CS-constructions have slightly higher production capacity than Al. The opposite is the case at $T=-15^{\circ}\text{C}$, where Al has slightly higher capacity.

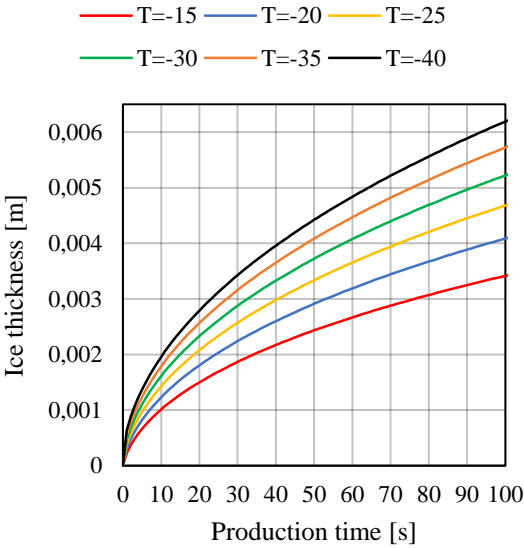


Figure 5-21 Ice layer thickness for carbon steel constructions vs time at different refrigeration temperatures

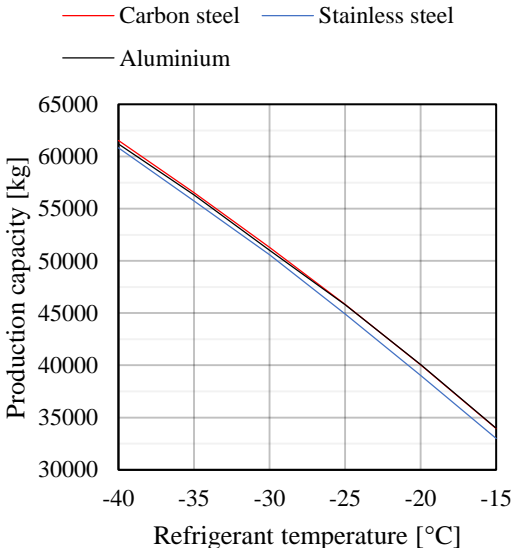


Figure 5-22 Capacity as function of refrigerant temperature

5.3.5 Discussion

As seen in the Figure A-2, the temperature and enthalpy difference between the outlet of compressors and the saturation line is quite large, means that a significantly amount of heat can be recovered. Therefore, a heat exchanger is applied, both in the middle- and high-pressure part. The high pressure heat rejection is split into two heat exchangers, because the duty became too large using only one heat exchanger, and the U-value calculations did not converge. The latent heat of evaporation for CO₂ is moderate, meaning the mass flow of CO₂ also becomes moderate. Compared to systems using ammonia, e.g. SF220, the mass flow in the CO₂ system is high, but it is smaller than the mass flow for systems running with HFK, e.g SF100. After the condensation the CO₂ is saturated, before being throttled. A significant amount of gas will be created when throttling, which means a large expansion loss. However, the SGHX has somewhat reduced the throttling loss. It is possible to further reduce the throttling losses with a SGHX, but this will be on the expense of increased compressor work. An ejector or expander may be utilized to increase the efficiency.

During the production period, the SCS consumes less energy than a TCS most of the time. The enthalpy difference across the two pressure stages is larger than for the SCS, and this leads to the different energy consumption. Therefore, the system with one compressor stage is more efficient and it is the desired system configuration when operated sub-critically and the ambient temperatures is rather low. However, at an ambient temperature of 18,7°C the outlet temperatures are above the maximum temperatures for CO₂ compressor outlet temperatures, and it may be shut down in order to protect the system. It is mainly problems related to the compressor lubrication oil which is limiting the system. If heat recovery is desirable, systems with two compressor stages is inevitable.

A SCS is simpler, and the number of compressors are reduced from 5 to 4. In addition, the intercooler heat exchanger is not necessary. This will reduce the investment costs. Regarding the costs of operating the two systems, SCS are more reasonable to run. The costs of running the SCS from September 1. to November 1. is 117500 NOK, while it is 130150 NOK for the TCS. This yields a cost of 19,6 NOK and 21,7 NOK per m³ snow, which means that TCS is 10,7% more expensive to run.

In principle, constructions using Al have higher overall heat transfer coefficient than CS-constructions, since its thermal conductivity is higher. However, the analysis of the FID shows that most of the time the average U-value is larger for CS-constructions. Since CO₂ have very high heat transfer coefficient, the thermal resistance is very low and almost negligible. Compared to the resistance for the metals and CO₂, the thermal resistance of ice is high due to low heat conduction through the ice layer. The ice growth rate is initially high for aluminium construction, leading to a rapid increase of the ice thickness. Due to a thicker ice layer on the Al-construction, the U-value is smaller than for CS. Therefore, it is the thickness of the ice layer rather than the properties of chosen material that decides the U-value and heat transfer. Since the initial ice growth rate of aluminium constructions is highest, the ice thickness is largest for aluminium throughout out production period, although the growth rate is slightly less than for carbon steel constructions.

By changing the refrigerant temperature, capacity and the ice growth rate can be changed. At low temperatures CS-constructions have higher capacity, due to higher average U-value. However, at lower refrigerant temperatures the Al-constructions have slightly higher average U-value than CS-constructions, leading to higher capacity. Hence, the total heat transfer resistance is lower for Al than CS at low refrigeration temperatures. When increasing the temperature, the CO₂ heat transfer coefficient decrease. This means that the thermal resistance increase, but the it is still low. At lower temperature the ice growth rate is lower. This results in a thinner ice layer, which reduces the heat transfer resistance of the ice. Therefore, the material conductivity contributes more to the total resistance. Since Al has higher thermal conductivity, the resistance is lower and the resulting U-value is higher. Still, the difference in production capacity is limited.

By lowering the refrigerant temperature, the energy consumption increases due to lower evaporation temperature and increased pressure ratios. In addition, the properties of the compressor lubrication oil have to be taken into account. The chosen GEA compressors can handle condensation temperatures down to -50°C, and the oil is fully miscible at such low temperatures. An alternative to increase capacity, is to include more FID's. This way the refrigerant temperature can be kept relatively high and the pressure ratios are moderate.

The power consumption for the SF100 and the model is evaluated at an ambient temperature of 15°C. Furthermore, the full system design of the machine is not available to the public, and the

figures of power consumption in the datasheets provided by the manufacturers, which states a power consumption of 130kW for the SF100, are only a guideline. The power consumption for the TCS CO₂ system is 125,6kW, which is 3,4% lower than the SF100, while the power consumption for the SCS system is 127,7kW, which is 1,8% lower than the SF100. Thus, the results from the model shows that the CO₂ system is more energy efficient than the existing solution. However, the model does not include all necessary components, and therefore the real power consumption may be different.

5.4 Comparison between the Vacuum and Flake Ice Model

The comparison is based on the results from the models developed in this section. Regarding the energy consumption, the results reveal that the vacuum systems consume less energy than the flake ice systems. Comparing the average energy consumption, the most efficient vacuum system consumes just 20,8% of the energy required by the least efficient flake ice system. The COP reflects this, where the vacuum system has a COP-value of 13,2, while the COP-value of the flake ice system is 2,1 at $T_{amb}=5^{\circ}\text{C}$. The evaporation temperature is much higher for the vacuum systems, and thus the temperature lift is small compared to the flake ice systems. In terms of operation costs, the snow from the flake ice system is 4,8 times more expensive than from the vacuum systems. The saving of operation costs is around 100000 NOK per production period. However, the investment costs are much higher for the vacuum system, mostly because of the special compressors. Therefore, the life-cycle cost is more important than the investment or operational costs alone.

The results show that at higher ambient temperatures, the outlet temperature is a limiting factor for the vacuum systems. Thus, if heat recovery is desired the investment cost will be very high for vacuum systems due to multiple compressors. Such system will also be large. The flake ice refrigeration system is more compact, mainly because of the size of the compressors. The vacuum vessel and FID are about the same size, but the vacuum system needs the large snow separator in addition. Hence, the vacuum system is more space demanding.

6 Calculations of the Flake Ice Drum using COMSOL

6.1 General

COMSOL Multiphysics is a general-purpose software platform, based on advanced numerical methods, for modelling and simulating physics-based problems. COMSOL is used to analyse the temperature distribution between the refrigerant pipes and on the freezing surface, and to determine the required thickness of the sandwich construction. The results obtained in the COMSOL model is not implemented into the EES model. However, the results from COMSOL are used to evaluate if the EES calculations and design assumptions are plausible.

The model is drawn in COMSOL and is based on the assumed dimensions in the EES-model, as explained in section 5.3. The following physics were utilized:

- Heat transfer in solids
- Heat transfer in fluids
- Turbulent flow
- Solid mechanics

The Multiphysics nodes Temperature coupling, Flow coupling and Fluid-structure interaction were used to couple the solid and liquid domains of the model.

COMSOL has a built-in library of materials, but liquid CO₂ is not included and had to be made. To simplify the problem, the average properties of CO₂ liquid and gas at an outlet gas quality of 0,35, as calculated in EES, was assumed and only one-phase flow is encountered. The density, viscosity and thermal conductivity are calculated with equation (5.13) (Levy, 1999). In addition, a heat flux corresponding to the required heat removal from the water is used, instead of modelling the phase change of water. The water heat transfer coefficient calculated in the EES model is used. This was done due to problems using the two-phase heat transfer model in COMSOL. Changes in the velocity of the refrigerant is neglected, due to little contribution from the changed CO₂ heat transfer coefficient to the average overall heat transfer coefficient. Therefore, the model is not exact, but will provide an estimation of the temperature distribution between the pipes and on the freezing surface. Input variables are shown in appendix C.

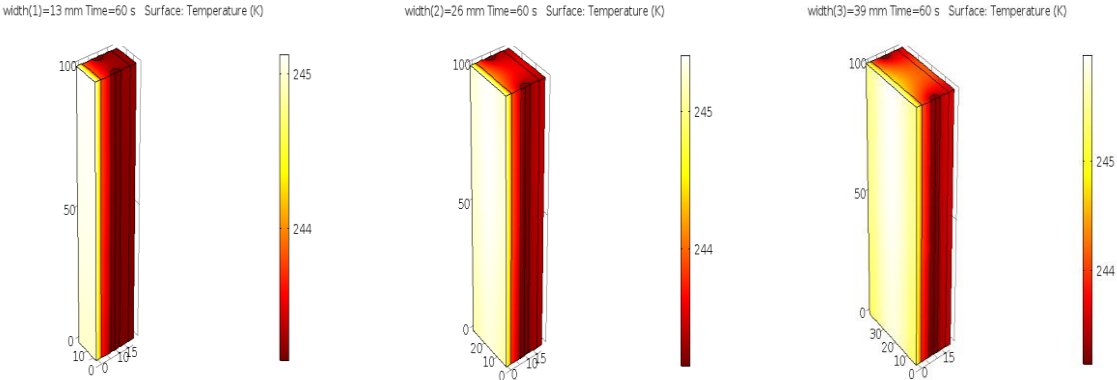
6.1.1 Results

The results are obtained by a stationary and time dependent solver. The displacement is calculated with the stationary solver, while the temperature distribution is calculated with the time dependent time solver to see when the temperature distribution stabilizes. To compare the results for different parameters, parametric sweeps are used. Both width and depth of the model are included in the parametric sweep. By increasing the width, the number of refrigerant pipes change. However, the number of pipes do not influence the heat transfer that much, since the CO₂ heat transfer coefficient are very high and contributes little to the average overall heat transfer coefficient.

| | | | | | | |
|----------------|------|------|------|------|------|------|
| Width | 13mm | 26mm | 39mm | 52mm | 65mm | 78mm |
| # pipes | 600 | 300 | 200 | 150 | 120 | 100 |

Temperature distribution

The calculations are done over a 60s period, and they show that the temperature distribution stabilizes within this time range. Figure 6-1 shows the temperature distribution between the pipes and on the freezing surface at different refrigerant pipe spacing. Observations reveal that the temperature span between the pipes increase as the distance between the pipes increases. The temperature span is 2°C, 2,3°C, 2,8°C, 3,6°C, 4,3°C and 5,1°C, for 13mm, 26mm, 39mm, 52mm, 65mm and 78mm, respectively. The variation in the three first distances is not very large, while it increases with about 1°C per 13mm increased width above 52mm.



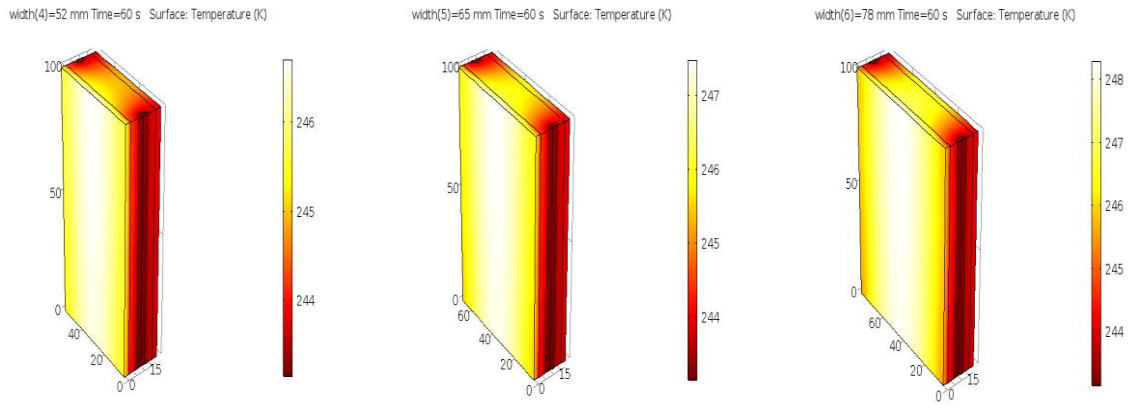


Figure 6-1 Temperature distribution between the refrigerant pipes with different width

Figure 6-2 shows the temperature distribution between the pipes and on the freezing surface with varying depth of the model. The steel layer thickness is set to 20% of the depth of the aluminium part, to have the same ratio between aluminium and steel. The figure reveals that the thickness of the wall does not affect the temperature distribution that much, and the difference in surface temperature between depth=5mm and depth=20mm is about 1°C. The highest freezing surface temperature is 244,8K, 244,9K, 245,4K and 245,9K for 5mm, 10mm, 15mm and 20mm, respectively.

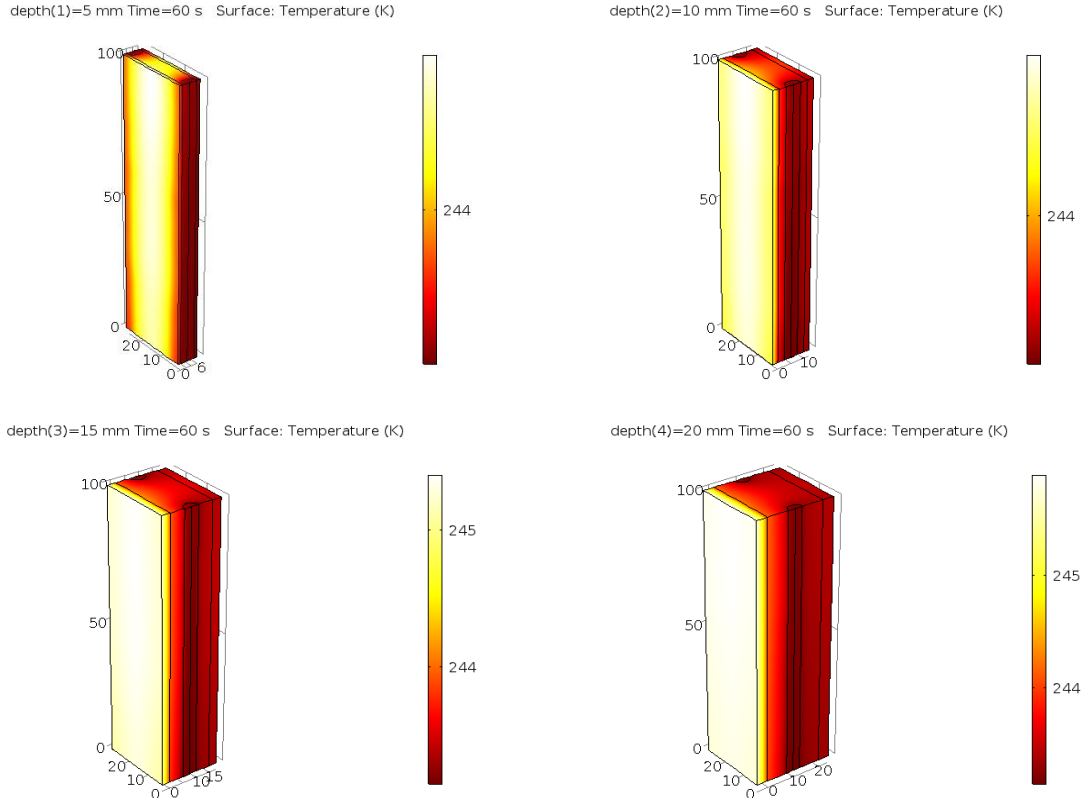


Figure 6-2 Temperature distribution at varying depth of model. Width=26mm

Displacement and structural integrity

The displacement in Figure 6-3 is greatly exaggerated, but the colour legend shows the right displacement. The FID wall facing away from the freezing surface and in dark blue colour, is a fixed constraint in the COMSOL model, and will not displace. As shown, the greatest displacement is in the area around the refrigerant pipe, and in the direction of the freezing surface. This may lead to an uneven surface, which may cause damage to the scraping device. However, the displacement is rather small, and according to Figure 6-4 it varies from 0,00047mm to 0,000124mm. The figure reveals that the displacement is dependent on the depth of the model. Particularly from 5mm to 10mm the change in displacement is quite dramatic. The minimum displacement is when the model is 15mm thick, and when increasing the thickness, the displacement increases slightly. The results are equal when the height of the model is increased.

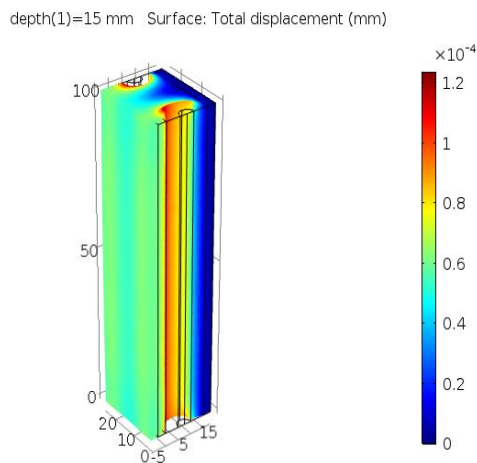


Figure 6-3 Total displacement at depth=15mm

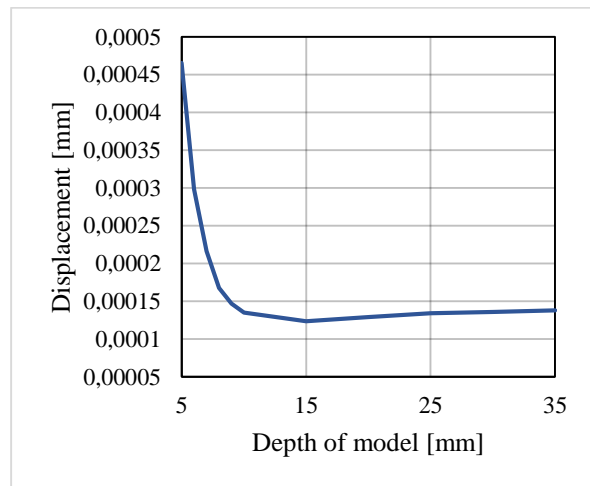


Figure 6-4 Displacement at different model thickness

In the same way as the displacement, the stress is largest around the pipe, as seen in Figure 6-5. The stress concentration is in direction of the centre of the model. The minimum stress is 2,67 MPa at a depth of 15mm. Figure 6-6 illustrates the dependency between stresses and thickness of the model. High stresses may lead to failure of the structure. However, the maximum stresses are rather small, and as the thickness increases the stresses decrease. The figure reveals that the stresses are almost halved when increasing the thickness from 5mm to 15mm. Like the displacement, further increase of the thickness increases the stresses slightly.

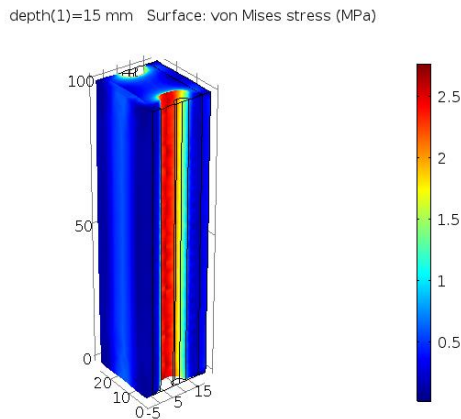


Figure 6-5 Von Mises stress at depth=15mm

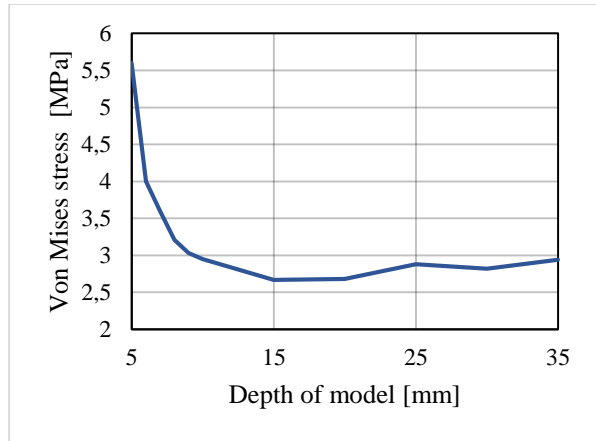


Figure 6-6 Von Mises stress at different model thickness

6.1.2 Discussion

It is desirable with low temperature variation at the freezing surface to avoid an uneven ice layer, which influence the production capacity. The temperature distribution changes only 0,8°C for distances up to 39mm. This means that constructions with 200 refrigerant pipes or more, have more or less the same temperature distribution. For constructions with less than 200 pipes, the temperature distribution changes more, and larger temperature variations are seen. Thus, it is desirable with a distance less than 39mm to have an even temperature distribution across the freezing surface. Changing the thickness of the model will only result in a small reduction of the surface temperature, and production capacity will not suffer too much. Hence, it is more a question of strength, material cost and production methods to decide what thickness to choose.

The freezing surface may become uneven due to displacements of the construction. This can lead to wear of the ice scraper, and in worst case failure. In addition, the freezing surface itself may be harmed. However, the displacement in this case is rather small and the scraper will most likely not be affected by this. The pressure in the pipes induces stresses in the metal. These stresses are also quite small, and compared to the ultimate strength of the materials presented in Table 10, the stresses are well within the limits. The thickness has to be 5 mm and the pressure must increase tenfold to exceed the ultimate tensile strength of the aluminium.

Based on the evaluation of the results from the COMSOL model, the assumed dimensions in the EES model gives satisfactory temperature profile on the freezing surface, and the strength and displacement is within the limits of the metals.

7 Conclusions and Suggestions for Further Work

7.1 Conclusions

The main results from the flake ice maker simulations models are:

- SCS consumes less energy than the TCS during most of the production period. It is only at temperatures above 14°C that the TCS is more efficient. The average energy consumption during the production period is 24,47 kWh/m³ and 27,1 kWh/m³ for the SCS and TCS, respectively. The compressor outlet temperature limits the operation of the SCS at 18,7°C, and more compressors stages must be applied above this ambient temperature.
- The U-value and ice growth rate are highly dependent on the ice thickness. The ice layer has higher thermal resistance than the metals and refrigerants, and influence the heat transfer the most. At low refrigerant temperatures the CS-constructions have highest production capacity, while at higher refrigerant temperatures Al-constructions produce more.
- The material used in the ice drum, the refrigerant temperature and ice layer thickness decides the ice layer growth rate, and the ice layer thickness will reach 3mm after t=32s, t=34s and t=45s for Al, CS, SST-constructions at T_{ref}=-30°C, respectively.
- Since the differences between the materials are small, it is more a question of production cost and production method when choosing the appropriate metal. Based on the cost of the metal, CS is the most reasonable. However, aluminium is easier to shape to the desired design. If the flake ice drum is produced for other purposes than flake ice making, e.g. food processing, stainless steel must be utilized on the freezing surface to fulfil the EU-regulations, on the expense of the production capacity.
- Based on the calculations, both the SCS and TCS is more energy efficient than the SF100. The energy consumption is 3,4% and 1,8% lower for the SCS and TCS, respectively.

The main results from the vacuum ice maker simulations are

- TVS consumes less energy than SVS during the production period. The average energy consumption during the production period is 5,64 kWh/m³ and 5,8 kWh/m³ for the TVS and SVS, respectively. A cascade system with CO₂ consumes in average 12,8 kWh/m³. The pressure ratio limits the SVS at 11°C, and more compressors stages must be applied in higher ambient temperature.
- The vacuum vessel is calculated to be 1,91m in diameter, assuming an evaporating coefficient of 0,2, and have 10,77 cm thick walls.
- The calculated energy consumption is much less than the existing solution. A comparison is difficult, since the configuration of the existing machine is not available to the public.
- Vacuum ice makers are expensive to build, due to the special compressor. Although it is more energy efficient to run, the high investment costs may be disqualifying.

The main results from the COMSOL simulations are:

- The maximum distance between the pipes should be 39mm. The temperature variations on the freezing surface changes more when decreasing the number of refrigerant pipes to below 200. This results in an uneven ice layer, and reduced production capacity.
- The thickness of the construction does not affect the heat transfer too much. Therefore, the thickness can be optimized regarding the structural strength, rather than the heat transfer.
- The suggested model dimensions are within the limits, with small displacement, stresses and a satisfying temperature distribution.

General results from all simulations

- Comparison between the vacuum and flake ice makers, reveal that vacuum machines are more energy efficient than flake ice machines. The cost per m³ produced snow is significantly lower for vacuum systems. However, the investment costs will be higher for the vacuum systems, and the life-cycle cost should be taken into consideration when choosing the right system.
- The snow produced by the different machines is expensive, and heat recovery should be included to make the machines more reasonable.

7.2 Suggestions for Further Work

Based on the work carried out in this thesis, the following aspects are suggested to be investigated in future work:

- Improve the EES-models, by including more accurate heat exchanger models. More detailed information about the applied heat exchangers can be included. In addition, more equipment, such as valves, can be included.
- Adapt the models to trans-critical operation for CO₂, which is necessary for heat recovery.
- Include more FIDs to increase the production capacity of the flake ice system, to match to existing TIS.
- Include an ejector or expander to the CO₂ refrigeration system to increase the efficiency
- A FID with a spiral tubing, instead of straight refrigerant pipes, can be investigated
- Improve the model in COMSOL, by including two-phase refrigerant flow and simulating the phase transition for the water.
- Investigate the investment costs and operation costs of the different solutions in detail.
- Look into the operation strategy of the machines to minimize the energy consumption and maximize the snow production.
- Build a prototype of the systems suitable for the lab.

Bibliography

- AGA. 24./02-2016 2016. *RE: Liquid Nitrogen price*.
- AMALFI, R. L., VAKILI-FARAHANI, F. & THOME, J. R. 2016. Flow boiling and frictional pressure gradients in plate heat exchangers. Part 2: Comparison of literature methods to database and new prediction methods. *International Journal of Refrigeration*, 61, 185-203.
- ANON 2008. Phase diagram for water. *google.no*. carleton.edu.
- ANON 2015. Global Warming. *Wikipedia, the free encyclopedia*.
- ANON. 2016. *Vacuum* [Online]. [Accessed].
- AQUATROLS.COM. 2016. *DRIFT Snowmaking additive* [Online]. [Accessed].
- ARIAS, J. & LUNDQVIST, P. 2006. Heat recovery and floating condensing in supermarkets. *Energy and Buildings*, 38, 73-81.
- ASAOKA, T., SAITO, A., OKAWA, S., ITO, T. & IZUMI, N. 2009. Vacuum freezing type ice slurry production using ethanol solution 1st report: Measurement of vapor-liquid equilibrium data of ethanol solution at 20 °C and at the freezing temperature. *International Journal of Refrigeration*, 32, 387-393.
- AUSTIN, B. T. & SUMATHY, K. 2011. Transcritical carbon dioxide heat pump systems: A review. *Renewable and Sustainable Energy Reviews*, 15, 4013-4029.
- BAIL, A. L. & HAVET, M. Ice slurry production in a tubular heat exchanger. The 24th IIR International Congress of Refrigeration, 2015 Yokohama, Japan.
- BANSAL, P. 2012. A review – Status of CO₂ as a low temperature refrigerant: Fundamentals and R&D opportunities. *Applied Thermal Engineering*, 41, 18-29.
- BÉDÉCARRATS, J.-P., DAVID, T. & CASTAING-LASVIGNOTTES, J. 2010. Ice slurry production using supercooling phenomenon. *International Journal of Refrigeration*, 33, 196-204.
- BELLAS, I. & TASSOU, S. A. 2005. Present and future applications of ice slurries. *International Journal of Refrigeration*, 28, 115-121.
- BURANDT, B. & BUSCHMANN, M. H. New Centrifugal Compressor for Water Steam. In: ASME, ed. ASME Turbo Expo 2006: Power for Land, Sea, and Air, 2006 Barcelona, Spain.
- CAO, W., BEGGS, C. & MUJTABA, I. M. 2015. Theoretical approach of freeze seawater desalination on flake ice maker utilizing LNG cold energy. *Desalination*, 355, 22-32.
- CARPENTER, W. H. 1995. *Flake ice-making apparatus*.
- CHAMOUN, M., RULLIERE, R., HABERSCHILL, P. & BERAIL, J. F. 2012a. Dynamic model of an industrial heat pump using water as refrigerant. *International Journal of Refrigeration*, 35, 1080-1091.
- CHAMOUN, M., RULLIERE, R., HABERSCHILL, P. & JEAN-LOUIS, P. 2012b. Experimental investigation of a new high temperature heat pump using water as refrigerant for industrial heat recovery. *International Refrigeration and Air Conditioning Conference*. Purdue.
- CHOI, K.-I., PAMITRAN, A. S. & OH, J.-T. 2007. Two-phase flow heat transfer of CO₂ vaporization in smooth horizontal minichannels. *International Journal of Refrigeration*, 30, 767-777.
- EAMES, I. W., MARR, N. J. & SABIR, H. 1997. The evaporation coefficient of water: a review. *International Journal of Heat and Mass Transfer*, 40, 2963-2973.
- EGOLF, P. W. & KAUFFELD, M. 2005. From physical properties of ice slurries to industrial ice slurry applications. *International Journal of Refrigeration*, 28, 4-12.
- EIKEVIK, T. M. 2015. Forelesningsmateriale i TEP4255.
- EIKEVIK, T. M. 2016a. 11.1 Compressors.
- EIKEVIK, T. M. 2016b. *RE: Personal communication*. Type to DIESETH, J.-B. R.
- EU. 2014. *Regulation (EU) No 517/2014 of the European Parliament and of the Council of 16 April 2014 on fluorinated greenhouse gases and repealing Regulation (EC) No 842/2006 Text with EEA relevance* [Online]. Available: http://eur-lex.europa.eu/legal-content/EN/TXT/?uri=uriserv:OJ.L_.2014.150.01.0195.01.ENG [Accessed 09/12-15].
- FUJIWARA, T. 2003. Artificial snow producing and releasing apparatus and method thereof. Google Patents.
- FUMOTO, K., T., K. & T., I. Study on generator for ice slurry using the pressure shift freezing method. The 24th IIR International Congress of Refrigeration, 2015 Yokohama, Japan.

- GARCÍA-CASCALES, J. R., VERA-GARCÍA, F., CORBERÁN-SALVADOR, J. M. & GONZÁLVEZ-MACIÁ, J. 2007. Assessment of boiling and condensation heat transfer correlations in the modelling of plate heat exchangers. *International Journal of Refrigeration*, 30, 1029-1041.
- GEA.COM. 2016. *GEA.com* [Online]. [Accessed].
- GJERLAND, M. & OLSEN, G. Ø. 2014. Snøproduksjon og snøpreparering. In: KULTURDEPARTEMENTET (ed.).
- GRAHAM, J., JOHNSTON, W. A. & NICHOLSON, F. J. 1993. *Ice in Fisheries*, Food and Agriculture Organization of the United Nations.
- HASSAN, M. A. M. & SHEDID, M. H. 2015. Experimental investigation of two phases evaporative heat transfer coefficient of carbon dioxide as a pure refrigerant and oil contaminated under forced flow conditions in small and large tube. *International Journal of Refrigeration*, 56, 28-36.
- HAUGSVÆR, N. 2016. *Slik fikk Tøyen 1100 kubikkmeter snø på to dager* [Online]. aftenposten.no. Available: <http://www.osloby.no/nyheter/Slik-fikk-Toyen-1100-kubikkmeter-sno-pa-to-dager-8367841.html> [Accessed 24/02-2016].
- HÄGG, C., LUNDQVIST, P. & STRÖMBLAD, M. 2005. Ice Slurry as Secondary Fluid in Refrigeration Systems: Fundamentals and Applications in Supermarkets. Stockholm: KTH.
- IDE-SNOWMAKER.COM. 2015. *VIM Technology* [Online]. Available: <http://www.ide-snowmaker.com/vacuum-ice-maker-vim/files/32/vacuum-ice-maker-vim.html> [Accessed].
- IDE TECHNOLOGIES 2015. All Weather Snowmaker - Product Data Sheet. In: TECHNOLOGIES, I. (ed.).
- INCROPERA, F. P., DEWITT, D. P., BERGMANN, T. L. & LAVINE, A. S. 2013. *Principles of Heat and Mass Transfer*.
- INDEXMUNDI.COM 2016. Aluminium price per april 2016.
- JONES, F. E. 1991. *Evaporation of Water With Emphasis on Applications and Measurements*, Taylor & Francis.
- JULLIEN, C., BÉNÉZECH, T., CARPENTIER, B., LEBRET, V. & FAILLE, C. 2003. Identification of surface characteristics relevant to the hygienic status of stainless steel for the food industry. *Journal of Food Engineering*, 56, 77-87.
- KAMINSKI, C. 2005. CET1: Stress Analysis & Pressure Vessels.
- KARSTENSEN, M. 2015. Mail correspondence. In: DIESETH, J.-B. R. (ed.).
- KAUFFELD, M., WANG, M. J., GOLDSTEIN, V. & KASZA, K. E. 2010. Ice slurry applications. *International Journal of Refrigeration*, 33, 1491-1505.
- KILICARSLAN, A. & MÜLLER, N. 2005. A comparative study of water as a refrigerant with some current refrigerants. *International Journal of Energy Research*, 29, 947-959.
- LACHNER JR, B. F., NELLIS, G. F. & REINDL, D. T. 2007. The commercial feasibility of the use of water vapor as a refrigerant. *International Journal of Refrigeration*, 30, 699-708.
- LARSEN, A. H. 2014. Klimaendringer i Norge. In: NATURVERNFORBUNDET (ed.).
- LEVY, S. 1999. *Two-Phase Flow in Complex Systems*, Wiley.
- LI, Q., PIECHNA, J. & MÜLLER, N. 2011a. Design of a novel axial impeller as a part of counter-rotating axial compressor to compress water vapor as refrigerant. *Applied Energy*, 88, 3156-3168.
- LI, Q., PIECHNA, J. & MÜLLER, N. 2011b. Thermodynamic potential of using a counter rotating novel axial impeller to compress water vapor as refrigerant. *International Journal of Refrigeration*, 34, 1286-1295.
- LLOPIS, R., SANZ-KOCK, C., CABELLO, R., SÁNCHEZ, D. & TORRELLA, E. 2015. Experimental evaluation of an internal heat exchanger in a CO2 subcritical refrigeration cycle with gas-cooler. *Applied Thermal Engineering*, 80, 31-41.
- LONGO, G. A. 2010. Heat transfer and pressure drop during hydrocarbon refrigerant condensation inside a brazed plate heat exchanger. *International Journal of Refrigeration*, 33, 944-953.
- LORENTZEN, G. 1994. Revival of carbon dioxide as a refrigerant. *International Journal of Refrigeration*, 17, 292-301.

- MADSBOELL, H., WEEL, M. & KOLSTRUP, A. 2015. Development of a water vapor compressor for high temperature heat pump applications. *ICR 2015*. Yokohama, Japan.
- MARTÍNEZ, D. S., SOLANO, J. P., ILLÁN, F. & VIEDMA, A. 2014. Analysis of heat transfer phenomena during ice slurry production in scraped surface plate heat exchangers. *International Journal of Refrigeration*, 48, 221-232.
- MCLINDEN, M. O., KAZAKOV, A. F., STEVEN BROWN, J. & DOMANSKI, P. A. 2014. A thermodynamic analysis of refrigerants: Possibilities and tradeoffs for Low-GWP refrigerants. *International Journal of Refrigeration*, 38, 80-92.
- MEPS.CO.UK 2016. Stainless and carbon steel prices per january 2016.
- MOORE, E. B. & MOLINERO, V. 2011. Structural transformation in supercooled water controls the crystallization rate of ice.
- MOUNEER, T. A., EL-MORSI, M. S., NOSIER, M. A. & MAHMOUD, N. A. 2010. Heat transfer performance of a newly developed ice slurry generator: A comparative study. *Ain Shams Engineering Journal*, 1, 147-157.
- NEKSÅ, P. 2002. CO₂ heat pump systems. *International Journal of Refrigeration*, 25, 421-427.
- NORTHSTAR.COM. 2015. *Carbon steel features* [Online]. [Accessed].
- O'DONOVAN, A. & GRIMES, R. 2015. Pressure drop analysis of steam condensation in air-cooled circular tube bundles. *Applied Thermal Engineering*, 87, 106-116.
- OPHIR, A. 2007. *Energy Efficient Vacuum Ice-Maker Using Water as Refrigerant For Thermal Energy Storage And Heat Pumps* [Online]. Available: <http://www.districtenergy.org/assets/pdfs/07CampConference/Ophir.pdf> [Accessed 01.09.15 2015].
- OPHIR, A. 2008. Mechanical Heat Pumps Using Water as Refrigerant for Ice Production and Air Conditioning. *IDEA 99th Annual Convention*. Orlando, Florida.
- ORSHOVEN, D. V., KLEIN, S. A. & BECKMAN, W. A. 1993. An Investigation of Water as a Refrigerant. *Journal of Energy Resources Technology*, 115, 257-263.
- PACHTER, M. & BARAK, A. 1967. The vacuum freezing vapor compression (Zarchin) process Present status and future trends. *Desalination*, 2, 358-367.
- PALM, B. 2014. Köldmedier med låg GWP (HFO). In: KTH (ed.).
- PARK, C. Y. & HRNJAK, P. 2009. CO₂ flow condensation heat transfer and pressure drop in multi-port microchannels at low temperatures. *International Journal of Refrigeration*, 32, 1129-1139.
- PAUL, J. 2002. Innovative Applications of Pumpable Ice Slurry. *The proceedings of The Institute of Refrigeration*, 98, 62-77.
- PAUL, J. Concept of operating indoor skiing halls with "binary snow" as a snow substitute. 21st IIR International Congress of Refrigeration: Serving the Needs of Mankind., 2003 2007a Washington DC, United States. IIF-IIR.
- PAUL, J. State-of-the-art cooling with "water as refrigerant". The 22nd IIR International Congress of Refrigeration., 2007 2007b Beijing, China. IIF-IIR.
- PEARSON, A. 2008. Refrigeration with ammonia. *International Journal of Refrigeration*, 31, 545-551.
- REULENS, W. 2009. *Natural Refrigerant CO₂*, KHLim vzw.
- SAMUELSEN, P. 2015. Mail correspondence. In: DIESETH, J.-B. R. (ed.).
- SAREVSKI, V. N. & SAREVSKI, M. N. 2016. *Water (R718) Turbo Compressor and Ejector Refrigeration / Heat Pump Technology*, Butterworth-Heinemann.
- SAWALHA, S. 2013. Investigation of heat recovery in CO₂ trans-critical solution for supermarket refrigeration. *International Journal of Refrigeration*, 36, 145-156.
- SAWALHA, S. & CHEN, Y. 2010. Investigations of Heat Recovery in Different Refrigeration System Solutions in Supermarkets: Effsys2 project final report.: KTH, Applied Thermodynamics and Refrigeration.
- SHAH, R. K. & SEKULIĆ, D. P. 2007. Fundamentals of Heat Exchanger Design. *Fundamentals of Heat Exchanger Design*. John Wiley & Sons, Inc.
- SHIGLEY, MISCHKE & BUDYNAS 2014. *Machine Design Tutorial 4–15: Pressure Vessel Design*.
- SINGH, R. & KACHHWAHA, S. S. 2015. Heat Transfer and Pressure Drop Analysis of Chilled Water and Ice Slurry in a Plate Heat Exchanger. *Journal of Thermal Science and Engineering Applications*, 8, 011020-011020.

- SNOMAX.COM. 2015. *Effects of Snomax* [Online]. Available: <http://www.snomax.com/> [Accessed].
- SNOWMAGIC.COM. 2015. *snowmagic.com* [Online]. Available: snowmagic.com [Accessed].
- SSB.NO. 2016. *Lavere strømpriser i 2015* [Online]. Available: <https://www.ssb.no/energi-og-industri/statistikker/elkraftpris/kvartal/2016-02-25> [Accessed].
- STAMATIOU, E., MEEWISSE, J. W. & KAWAJI, M. 2005. Ice slurry generation involving moving parts. *International Journal of Refrigeration*, 28, 60-72.
- STENE, J. 2015. Lecture notes, TEP16 Heat pump technology.
- TECHNOALPIN.COM. 2015. *technoalpin.com* [Online]. Available: <http://www.technoalpin.com/en/engineering.html> [Accessed].
- TUCKER, E. 2014. *Meet the Canadians making snow for Sochi's melting mountains* [Online]. Available: <http://globalnews.ca/news/1154579/meet-the-canadians-making-snow-for-sochis-melting-mountains/> [Accessed].
- WANG, H., FENG, R., DUAN, H. & CHEN, A. 2016. Investigation into the ice generator with double supercooled heat exchangers. *Applied Thermal Engineering*, 98, 380-386.
- WOBST, E., KALITZIN, N. & APLEY, R. 2004. Turbo Water Chiller with Water as Refrigerant. *International Compressor Engineering Conference*.
- YOON, S. H., CHO, E. S., HWANG, Y. W., KIM, M. S., MIN, K. & KIM, Y. 2004. Characteristics of evaporative heat transfer and pressure drop of carbon dioxide and correlation development. *International Journal of Refrigeration*, 27, 111-119.
- YR.NO. 2016. *Klimastatistikk* [Online]. [Accessed].
- ZHAO, J. D., LIU, N. & KANG, Y. M. 2008. Optimization of ice making period for ice storage system with flake ice maker. *Energy and Buildings*, 40, 1623-1627.
- ZHAO, X. & BANSAL, P. K. 2007. Flow boiling heat transfer characteristics of CO₂ at low temperatures. *International Journal of Refrigeration*, 30, 937-945.
- ZSEBIK, A., BALIKÓ, S. & CSATA, Z. 2014. Heat Recovery from CO₂ Refrigeration Systems. *Energy Engineering*, 111, 41-56.

Appendix

A. Log p-h diagram

Vacuum ice machine

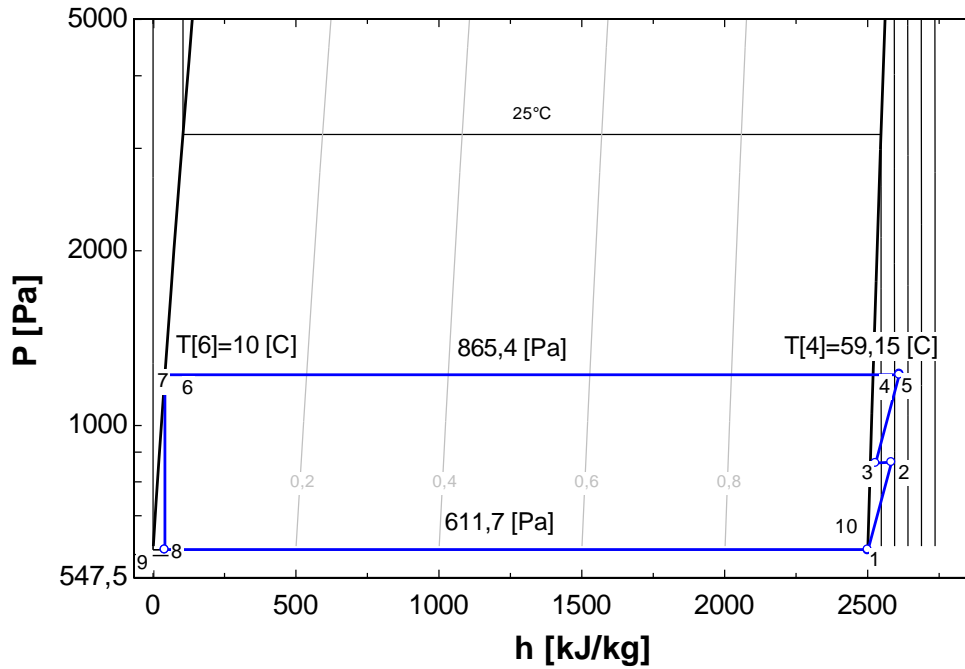


Figure A-1 Log P-h diagram of the vacuum cycle. $T_{\text{amb}}=5^\circ\text{C}$

Flake ice machine

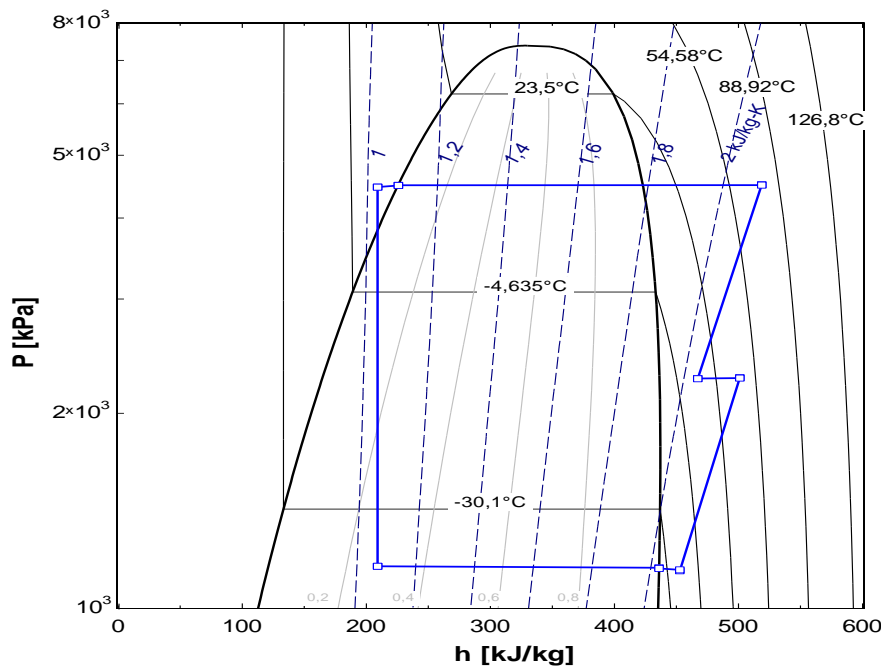


Figure A-2 Log P-h diagram Flake ice system. $T_{\text{amb}}=5^\circ\text{C}$

B. Thermodynamic Data. EES Simulation Models

Vacuum ice maker. Two stage

| State point | Pressure [Pa] | Temperature [°C] | Enthalpy [kJ/kg] | Entropy [kJ/kg·K] | Quality [-] |
|-------------|---------------|------------------|------------------|-------------------|-------------|
| 1 | 609,9 | 0,00961 | 2501 | 9,156 | 1 |
| 2 | 865,4 | 44,42 | 2583 | 9,275 | 100 |
| 3 | 862 | 14,82 | 2528 | 9,094 | 100 |
| 4 | 1228 | 59,15 | 2611 | 9,199 | 100 |
| 5 | 1223 | 59,15 | 2611 | 9,2 | 100 |
| 6 | 1223 | 10 | 41,99 | 0,151 | 0 |
| 7 | 1219 | 9,894 | 41,99 | 0,151 | 0,0001793 |
| 8 | 611,7 | 0,01 | 41,99 | 0,1537 | 0,01679 |
| 9 | 611,7 | 0,01023 | 41,99 | 0,1537 | 0,01679 |
| 10 | 611,7 | 0,01 | 2501 | 9,154 | 1 |

Table 20 At $T_{amb}=5^{\circ}\text{C}$

| State point | Pressure [Pa] | Temperature [°C] | Enthalpy [kJ/kg] | Entropy [kJ/kg·K] | Quality [-] |
|-------------|---------------|------------------|------------------|-------------------|-------------|
| 1 | 609,8 | 0,009587 | 2501 | 9,156 | 1 |
| 2 | 1390 | 110,5 | 2708 | 9,412 | 100 |
| 3 | 1387 | 21,83 | 2541 | 8,919 | 100 |
| 4 | 3169 | 131,9 | 2748 | 9,135 | 100 |
| 5 | 3167 | 131,9 | 2748 | 9,135 | 100 |
| 6 | 3167 | 25 | 104,8 | 0,367 | 0 |
| 7 | 3165 | 24,98 | 104,8 | 0,367 | 0,00003777 |
| 8 | 611,7 | 0,01 | 104,8 | 0,3835 | 0,04189 |
| 9 | 611,7 | 0,01023 | 104,8 | 0,3835 | 0,04189 |
| 10 | 611,7 | 0,01 | 2501 | 9,154 | 1 |

Table 21 At $T_{amb}=20^{\circ}\text{C}$

Vacuum ice maker. Single stage

| State point | Pressure [Pa] | Temperature [°C] | Enthalpy [kJ/kg] | Entropy [kJ/kg·K] | Quality [-] |
|-------------|---------------|------------------|------------------|-------------------|-------------|
| 1 | 609,9 | 0,00961 | 2501 | 9,156 | 1 |
| 2 | 1228 | 92,55 | 2674 | 9,379 | 100 |
| 5 | 1217 | 92,55 | 2674 | 9,383 | 100 |
| 6 | 1217 | 10 | 41,99 | 0,151 | 0 |
| 7 | 1209 | 9,77 | 41,99 | 0,151 | 0,0003892 |
| 8 | 611,7 | 0,01 | 41,99 | 0,1537 | 0,01679 |
| 9 | 611,7 | 0,01023 | 41,99 | 0,1537 | 0,01679 |
| 10 | 611,7 | 0,01 | 2501 | 9,154 | 1 |

Table 22 At $T_{amb}=5^{\circ}\text{C}$

| State point | Pressure [Pa] | Temperature [°C] | Enthalpy [kJ/kg] | Entropy [kJ/kg·K] | Quality [-] |
|-------------|---------------|------------------|------------------|-------------------|-------------|
| 1 | 609,8 | 0,009587 | 2501 | 9,156 | 1 |
| 2 | 3169 | 242,2 | 2962 | 9,601 | 100 |
| 5 | 3162 | 242,2 | 2962 | 9,602 | 100 |
| 6 | 3162 | 25 | 104,8 | 0,367 | 0 |
| 7 | 3159 | 24,95 | 104,8 | 0,367 | 0,00009266 |
| 8 | 611,7 | 0,01 | 104,8 | 0,3835 | 0,04189 |
| 9 | 611,7 | 0,01023 | 104,8 | 0,3835 | 0,04189 |
| 10 | 611,7 | 0,01 | 2501 | 9,154 | 1 |

Table 23 At $T_{amb}=20^{\circ}\text{C}$

Cascade system. Vacuum/single stage CO₂

| State point | Pressure [Pa] | Temperature [°C] | Enthalpy [kJ/kg] | Entropy [kJ/kg·K] | Quality [-] |
|-------------|---------------|------------------|------------------|-------------------|-------------|
| 1 | 609,9 | 0,009618 | 2501 | 9,156 | 1 |
| 2 | 872,6 | 45,51 | 2586 | 9,278 | 100 |
| 5 | 859,9 | 45,51 | 2586 | 9,285 | 100 |
| 6 | 859,9 | 5 | 21,02 | 0,07626 | 0 |
| 7 | 849 | 4,608 | 21,02 | 0,07626 | 0,0006615 |
| 8 | 611,7 | 0,01 | 21,02 | 0,07695 | 0,008406 |
| 9 | 611,7 | 0,01023 | 21,02 | 0,07695 | 0,008406 |
| 10 | 611,7 | 0,01 | 2501 | 9,154 | 1 |

Table 24 Vacuum system. $T_{\text{cond}}=5^{\circ}\text{C}$

| State point | Pressure [kPa] | Temperature [°C] | Enthalpy [kJ/kg] | Entropy [kJ/kg·K] | Quality [-] |
|-------------|----------------|------------------|------------------|-------------------|-------------|
| 1 | 3029 | -0,04172 | 441,5 | 1,903 | 100 |
| 2 | 4502 | 42,17 | 476,7 | 1,966 | 100 |
| 7 | 4501 | 42,16 | 476,7 | 1,966 | 100 |
| 8 | 4501 | 10 | 225,7 | 1,088 | 0 |
| 9 | 4500 | 9,977 | 225,7 | 1,088 | 0,0003181 |
| 10 | 4477 | 7,149 | 217,6 | 1,06 | -100 |
| 11 | 4477 | 7,148 | 217,6 | 1,06 | -100 |
| 12 | 3046 | -5 | 217,6 | 1,068 | 0,1203 |
| 13 | 3046 | -5 | 217,6 | 1,068 | 0,1203 |
| 14 | 3046 | -5 | 433,4 | 1,872 | 1 |
| 15 | 3045 | -5,006 | 433,4 | 1,872 | 1 |
| 16 | 3030 | -0,02294 | 441,5 | 1,903 | 100 |

Table 25 CO₂ system. $T_{\text{evap}}=-5^{\circ}\text{C}$. $T_{\text{cond}}=5^{\circ}\text{C}$

| State point | Pressure [kPa] | Temperature [°C] | Enthalpy [kJ/kg] | Entropy [kJ/kg·K] | Quality [-] |
|-------------|----------------|------------------|------------------|-------------------|-------------|
| 1 | 3028 | 14,96 | 461,9 | 1,976 | 100 |
| 2 | 6434 | 85,65 | 513,6 | 2,021 | 100 |
| 7 | 6433 | 85,65 | 513,6 | 2,021 | 100 |
| 8 | 6433 | 25 | 274,8 | 1,248 | 0 |
| 9 | 6432 | 24,98 | 274,8 | 1,248 | 0,0005562 |
| 10 | 6400 | 18,26 | 246,3 | 1,152 | -100 |
| 11 | 6399 | 18,26 | 246,3 | 1,152 | -100 |
| 12 | 3046 | -5 | 246,3 | 1,175 | 0,2375 |
| 13 | 3046 | -5 | 246,3 | 1,175 | 0,2375 |
| 14 | 3046 | -5 | 433,4 | 1,872 | 1 |
| 15 | 3045 | -5,007 | 433,4 | 1,872 | 1 |
| 16 | 3030 | 14,98 | 461,9 | 1,976 | 100 |

Table 26 CO₂ system. $T_{\text{evap}}=-5^{\circ}\text{C}$. $T_{\text{cond}}=20^{\circ}\text{C}$

Flake ice maker. Two stage

| State point | Pressure [kPa] | Temperature [°C] | Enthalpy [kJ/kg] | Entropy [kJ/kg·K] | Quality [-] |
|-------------|----------------|------------------|------------------|-------------------|-------------|
| 1 | 1144 | -20,18 | 452,6 | 2,098 | 100 |
| 2 | 2270 | 42,07 | 501,1 | 2,153 | 100 |
| 3 | 2267 | 42,05 | 501,1 | 2,153 | 100 |
| 4 | 2264 | 10 | 467,2 | 2,04 | 100 |
| 5 | 2262 | 9,975 | 467,2 | 2,04 | 100 |
| 6 | 4502 | 76,73 | 518,8 | 2,093 | 100 |
| 7 | 4497 | 76,69 | 518,8 | 2,093 | 100 |
| 8 | 4495 | 10 | 225,7 | 1,088 | 0 |
| 9 | 4489 | 9,884 | 225,7 | 1,088 | 0,001609 |
| 10 | 4467 | 4,009 | 209,1 | 1,029 | -100 |
| 11 | 4464 | 4,008 | 209,1 | 1,029 | -100 |
| 12 | 1162 | -35,96 | 209,1 | 1,071 | 0,2796 |
| 13 | 1162 | -35,96 | 209,1 | 1,071 | 0,2796 |
| 14 | 1156 | -36,11 | 436 | 2,029 | 1 |
| 15 | 1154 | -36,16 | 436 | 2,029 | 100 |
| 16 | 1148 | -20,12 | 452,6 | 2,098 | 100 |

Table 27 At $T_{amb}=5^{\circ}\text{C}$

| State point | Pressure [kPa] | Temperature [°C] | Enthalpy [kJ/kg] | Entropy [kJ/kg·K] | Quality [-] |
|-------------|----------------|------------------|------------------|-------------------|-------------|
| 1 | 1139 | -5,15 | 467,3 | 2,16 | 100 |
| 2 | 2707 | 70,41 | 526,4 | 2,20 | 100 |
| 3 | 2705 | 70,38 | 526,4 | 2,20 | 100 |
| 4 | 2701 | 10,00 | 460,8 | 1,99 | 100 |
| 5 | 2698 | 9,97 | 460,8 | 1,99 | 100 |
| 6 | 6434 | 87,85 | 516,4 | 2,03 | 100 |
| 7 | 6430 | 87,82 | 516,4 | 2,03 | 100 |
| 8 | 6428 | 25,00 | 274,8 | 1,25 | 0 |
| 9 | 6423 | 24,93 | 274,8 | 1,25 | 0,00263 |
| 10 | 6391 | 17,40 | 243,5 | 1,14 | -100 |
| 11 | 6387 | 17,39 | 243,5 | 1,14 | -100 |
| 12 | 1162 | -35,96 | 243,5 | 1,22 | 0,389 |
| 13 | 1162 | -35,96 | 243,5 | 1,22 | 0,389 |
| 14 | 1154 | -36,16 | 436,0 | 2,03 | 1 |
| 15 | 1150 | -36,24 | 436,0 | 2,03 | 100 |
| 16 | 1145 | -5,07 | 467,3 | 2,15 | 100 |

Table 28 At $T_{amb}=20^{\circ}\text{C}$

Flake ice maker. Single stage

| State point | Pressure [kPa] | Temperature [°C] | Enthalpy [kJ/kg] | Entropy [kJ/kg·K] | Quality [-] |
|-------------|----------------|------------------|------------------|-------------------|-------------|
| 1 | 1153 | -20,18 | 452,5 | 2,096 | 100 |
| 2 | 4502 | 89,97 | 533,8 | 2,135 | 100 |
| 7 | 4501 | 89,96 | 533,8 | 2,135 | 100 |
| 8 | 4495 | 10 | 225,7 | 1,088 | 0 |
| 9 | 4489 | 9,886 | 225,7 | 1,088 | 0,001582 |
| 10 | 4467 | 4,075 | 209,3 | 1,03 | -100 |
| 11 | 4464 | 4,074 | 209,3 | 1,03 | -100 |
| 12 | 1170 | -35,77 | 209,3 | 1,071 | 0,2792 |
| 13 | 1170 | -35,77 | 209,3 | 1,071 | 0,2792 |
| 14 | 1165 | -35,91 | 436,1 | 2,028 | 1 |
| 15 | 1162 | -35,96 | 436,1 | 2,028 | 100 |
| 16 | 1156 | -20,11 | 452,5 | 2,096 | 100 |

Table 29 At $T_{amb}=5^{\circ}\text{C}$

| State point | Pressure [kPa] | Temperature [°C] | Enthalpy [kJ/kg] | Entropy [kJ/kg·K] | Quality [-] |
|-------------|----------------|------------------|------------------|-------------------|-------------|
| 1 | 1146 | -5,15 | 467,2 | 2,154 | 100 |
| 2 | 6434 | 156,8 | 597,2 | 2,234 | 100 |
| 7 | 6433 | 156,7 | 597,2 | 2,234 | 100 |
| 8 | 6428 | 25 | 274,8 | 1,248 | 0 |
| 9 | 6424 | 24,93 | 274,8 | 1,249 | 0,002552 |
| 10 | 6392 | 17,44 | 243,6 | 1,143 | -100 |
| 11 | 6387 | 17,43 | 243,6 | 1,143 | -100 |
| 12 | 1170 | -35,77 | 243,6 | 1,216 | 0,3883 |
| 13 | 1170 | -35,77 | 243,6 | 1,216 | 0,3883 |
| 14 | 1161 | -35,99 | 436,1 | 2,028 | 1 |
| 15 | 1157 | -36,07 | 436,1 | 2,028 | 100 |
| 16 | 1152 | -5,071 | 467,2 | 2,153 | 100 |

Table 30 At $T_{amb}=20^{\circ}\text{C}$

C. Input Variables COMSOL Model

| Parameter | Value | Unit | Description |
|-----------------|---|---------------------|--|
| μ_g | 0.00001246 | kg/(m·s) | dynamic viscosity gas |
| μ_l | 0.0001642 | kg/(m·s) | Dynamic viscosity liquid |
| μ_m | $1/((x_m/\mu_g)+((1-x_m)/\mu_l))$ | kg/(m·s) | Average dynamic viscosity |
| ρ_{g,CO_2} | 37.1 | kg/m ³ | Gas density of CO ₂ |
| ρ_{l,CO_2} | 1076 | kg/m ³ | Liquid density of CO ₂ |
| ρ_m | $1/((x_m/\rho_{g,CO_2})+((1-x_m)/\rho_{l,CO_2}))$ | kg/m ³ | Mean density |
| C_{p,g,CO_2} | 1141 | J/(kg·K) | Specific heat capacity gas |
| C_{p,l,CO_2} | 2073 | J/(kg·K) | Specific heat capacity liquid CO ₂ |
| $C_{p,m}$ | $(c_{p,l,CO_2}+c_{p,g,CO_2})/2$ | J/(kg·K) | Average specific heat capacity |
| Depth | 5-20 | mm | Depth of the aluminium part of the model |
| h_{water} | 575 | W/m ² ·K | Water heat transfer coefficient |
| Height | 100 | mm | Height of model |
| k_{g,CO_2} | 0.01342 | W/(m·K) | Thermal conductivity gas CO ₂ |
| k_{l,CO_2} | 0.1463 | W/(m·K) | Thermal conductivity liquid CO ₂ |
| k_m | $1/((x_m/k_{g,CO_2})+((1-x_m)/k_{l,CO_2}))$ | W/(m·K) | Average thermal conductivity |
| L_{CO_2} | 303.5 | kJ/kg | Enthalpy of vaporization |
| P_{CO_2} | 1428 | kPa | Evaporation pressure |
| Q_{water} | 9500 | W/m ² | Heat transferred from ice |
| T_{CO_2} | 243.15 | K | Evaporation temperature |
| u_{in} | 0.244 | m/s | Inlet velocity pipes |
| Width | 26-78 | mm | Width of model, from centre to centre of pipes |
| x_m | 0,175 | [-] | Average gas quality |
| ΔP | 30 | kPa | Pressure loss pipes |

Table 31 COMSOL input variables

D. Heat Transfer Coefficients for Heat Exchangers

| Heat exchanger | α_{warm} [W/m ² ·K] | α_{cold} [W/m ² ·K] |
|-------------------------|---------------------------------------|---------------------------------------|
| Condenser/evap | 6733 | 6832 |
| Intercooler | 693,3 | 3219 |
| Superheat HX | 426,8 | 5155 |
| Condenser | 3638 | 2265 |
| SGHX warm | 1549 | 636,1 |
| FID | 9998 | 575 |
| Condenser Vacuum | 8407 | 22862 |

E. EES Code. Vacuum Ice Maker

```
$UnitSystem SI C Pa kJ mass
```

```
-----
To better understand the code, it is recommended to go the state-point
calculations. The procedures are calculated in sequence from top to bottom.
This is not the case for the main body, where EES decides what to calculate
first. See Computational Flow. This is recommended since the procedures are
put in the start of the script due to syntax reasons.
```

```
When simulation the cascade system, T_cond=5 [C]
```

```
-----"
```

```
"-----"
```

```
"Calculation of the size of the vacuum vessel"
```

```
"-----"
```

```
PROCEDURE areavessel(R$m_dot_gas;T_amb;V_dot:D_vessel[1])
```

```
$ARRAY ON
```

```
T_1= 0,01 [C] "Operating temperature Vacuum vessel"
```

```
T_1_k=ConvertTemp(C;K;T_1)
```

```
P_1=P_sat(R$;T=T_1)*convert(Pa;dyne/cm^2) "Operating pressure [dyne/cm^2]"
```

```
DELTAP=100 [Pa]*convert(Pa;dyne/cm^2) "Guessed pressure difference"
```

```
P_g=P_1-DELTAP "Pressure in gas"
```

```
T_g=T_sat(R$;P=P_g) "Temperature gas"
```

```
T_g_k=ConvertTemp(C;K;T_g)
```

```
R=8,31447*10^7 [kJ/K*kmol] "Universal gas constant"
```

```
M=MolarMass(R$) "Molar mass water"
```

```
f[1]=1 "Evaporation coefficient 0,1<f<1"
```

```
df=0,01
```

```
i=0
```

```
perc[1]=0,001
```

```
dperc=0,001
```

```
percent[1]=perc[1]*100
```

```
REPEAT
```

```
i=i+1
```

```
!"Area and diameter"
```

```
A_vessel[i]=(m_dot_gas*1000)/(f[i]*(P_1/sqrt(T_1_k)-
P_g/sqrt(T_g_k))*sqrt((M/(2*pi*R))))*convert(cm^2;m^2) "Evaporation rate of
water, Knudsen eq-n"
```

```
D_vessel[i]=sqrt(4*A_vessel[i]/pi) "Diameter vacuum vessel"
```

```
f[i+1]=f[i]-df
```

```
r_i=D_vessel[i]/2*convert(m;mm) "Inner radius of vessel"
```

```
r_o=r_i+r_i*perc[i] "Outer radius of vessel"
```

```
perc[i+1]=(perc[i]+dperc)
```

```
percent[i+1]=perc[i+1]*100
```

```
!"Strength of pressure vessel"
```

```
p_i=611 [Pa] "Inner pressure"
```

```
p_o=101325 [Pa] "Ambient pressure"
```

```
"Outer radius"
```

```
sigma_t_o[i]=(p_i*r_i^2-p_o*r_o^2-r_i^2*r_o^2*(p_o-p_i)/r_o^2)/(r_o^2-
r_i^2)*convert(Pa;MPa) "Tangential Stress"
```

```

sigma_r_o[i]=(p_i*r_i^2-p_o*r_o^2+r_i^2*r_o^2*(p_o-p_i)/r_o^2)/(r_o^2-
r_i^2)*convert(Pa;MPa) "Radial Stress"
sigma_l[i]=(p_i*r_i^2-p_o*r_o^2)/(r_o^2-r_i^2)*convert(Pa;MPa) "Longitudinal
Stress"

"Inner radius"
sigma_t_i[i]=abs((p_i*r_i^2-p_o*r_o^2-r_i^2*r_o^2*(p_o-p_i)/r_i^2)/(r_o^2-
r_i^2)*convert(Pa;MPa)) "Tangential Stress, Kritisk radius"
sigma_r_i[i]=(p_i*r_i^2-p_o*r_o^2+r_i^2*r_o^2*(p_o-p_i)/r_i^2)/(r_o^2-
r_i^2)*convert(Pa;MPa) "Radial Stress"

E=YoungsModulus(Stainless_AISI302; T=T_amb)*convert(GPa;MPa) "Youngs
Modulus"
t[i]=r_o-r_i "Thickness of vacuum vessel"
sigma_max[i]=(E/3)*(t[i]/(2*r_i))^2 "Maximum stress"
p_max[i]=(2*E/3)*(t[i]/(2*r_i))^3 "Maximum pressure"

UNTIL (i>99)

END
"-----"

PROCEDURE
heattransfercond(m_dot_gas;m_dot_water;T_water_outlet;T_cond;T_w_avg;T[5];T
[6];w_plate_cond;x_plate_cond:U_cond)
"!Overall heat transfer coefficient for condenser."
W$='Water'
R$='Water'

delta_wall_cond=1 [mm]*convert(mm;m) "Wall thickness stainless steel"
k_ss=Conductivity(Stainless_AISI302; T=17) "Thermal conductivity stainless
steel"
d_e=7 [mm]*convert(mm;m) "Equivalent diameter"

"Cold side"
P_cold=101,325 [kPa] "Ambient Pressure"
k_cold=Conductivity(W$;T=T_water_outlet;P=P_cold) "Thermal conductivity
water"
mu_cold=Viscosity(W$;T=T_water_outlet;P=P_cold) "Dynamic viscosity"
mu_wall_water=viscosity(W$;T=(T_cond+T_w_avg)/2;P=P_cold+0,01)
A=(d_e)*w_plate_cond*0,5*x_plate_cond "Flow area"
G=m_dot_water/A "Mass flux"
Pr_cold=Prandtl(W$;T=T_water_outlet;P=P_cold) "Prandtl number"
Re_cold=(G*d_e)/mu_cold "Reynolds number"

"Martin correlation for one-phase flow water"
beta_cold=45 "Chevron angle"
f0_martin_cold = (1,8*log10(Re_cold)-1,5)^(-
2) "parameter for friction factor calculation"
f1_martin_cold= 39/(Re_cold^0,289) "parameter for friction factor
calculation"
f_martin_cold=(1 /
(cos(beta_cold)/sqrt(0,18*tan(beta_cold)+0,36*sin(beta_cold)+(f0_martin_col
d/cos(beta_cold))) + ((1-cos(beta_cold))/(sqrt(3,8*f1_martin_cold)))) )^2
"friction factor"
Nusselt_cold=0,122*(Pr_cold^(1/3))*(mu_cold/mu_wall_water)^(1/6)*(f_marti
n_cold*( (Re_cold^2)*sin(2*beta_cold)))^0,374 "Nusselt number"
alpha_cold = (Nusselt_cold*k_cold)/d_e "heat transfer coefficient water"

"Warm side"
P_warm=P_sat(R$;T=T_cond)

```



```

k_warm_o=Conductivity(R$;P=P_warm+0,01;T=T[6])
mu_warm_o=Viscosity(R$;P=P_warm+0,01;T=T[6])
mu_warm_i=Viscosity(R$;P=P_warm+0,01;T=T[5])
mu_wall_ref=viscosity(R$;T=(T_cond+T_w_avg)/2;P=P_warm+0,01)
rho_warm_o=Density(R$;P=P_warm+0,01;T=T[6])
rho_warm_i=Density(R$;P=P_warm+0,01;T=T[5])
cp_l=cp(R$;T=T_cond+0,001;P=P_warm)
G_warm=(m_dot_gas)/A
T_sh_out=Temperature(R$;P=P_warm;x=1)
Pr_warm=Prandtl(R$;T=(T[5]+T[6])/2;P=P_warm)

"Dobson and Chato correlation V&M boka"
h_fg=Enthalpy_vaporization(R$;T=T_cond)
h_fg_f=h_fg+0,375*cp_l*(T_cond-(T_cond+T_w_avg)/2)
alpha_warm=(k_warm_o/d_e)*0,555*((rho_warm_o*g*(rho_warm_o-
rho_warm_i)*h_fg_f*d_e^3)/(mu_warm_o*k_warm_o*(T_cond-
(T_cond+T_w_avg)/2)))^(1/4)
"heat transfer coefficient vapor"

U_cond=1/((1/alpha_cold)+(delta_wall_cond/k_ss)+(1/alpha_warm)) "Overall
heat transfer coefficient"

END "Procedure"

"-----
  General information and calculations of the system
-----"

R$='water'

"!Model specifications"
m_snow=50000 [kg/day] "Production capacity of system"

"!From mass balance of vacuum freezer and snow separator"
m_dot_w=m_snow*convert(kg/day;kg/s) "Mass flow of water"

"!Water inlet temperature"
T_water_outlet=4,5 [C] "Water outlet temperature from
chiller"

"!Ambient temperature"
$ifNot Parametric table
T_amb=5 [C] "Ambient temperature 5-20 degC"
$Endif

DELTAT_cond=5 [K] "DeltaT in condenser"
T_cond=T_amb+DELTAT_cond "Condensation temperature"

"!Vacuum freezer"
P_vacuum=611,7 [Pa] "Pressure inside the freezer"
T_vacuum=0,01 [C] "Temperature inside the freezer"
T_vac_liq=0,009 [C]
h_evap=enthalpy_vaporization(R$;T=T_vacuum)
"Latent heat of vapourization"
h_fusion=enthalpy_fusion(R$) "Latent heat of fusion"
P$=phase$(R$;T=T_vac_liq;P=P_vacuum) "Phase of water"
C_p_liq_LP=specheat(R$;T=T_vac_liq;P=P_vacuum) "Specific heat of the liquid
phase"

"!Heat to be removed"

```

```

Q_1=m_dot_w*C_p_liq_LP*(T_water_outlet-T_vacuum) "Energy to change the
temperature of the inlet water"
Q_2=m_dot_w*h_fusion "Energy to freeze the inlet water"
Q_tot=Q_1+Q_2 "Energy to be removed by evaporation/Cooling capacity"
Q_evap=(h[10]-h[9]) "Cooling capacity [kJ/kg] of cycle"

```

```

"!Mass flow of water vapour"

```

```

m_dot_gas=Q_tot/Q_evap "Mass flow of vapour"
v_g=Volume(R$;T=T_vacuum;P=P_vacuum) "Specific volume of vapour"
V_dot=(m_dot_gas*v_g*convert(m^3/s;m^3/h))
"Volumetric flow vapour"

```

```

"-----"
"-----"
" System Solution by control volume
"-----"
"-----"

```

```

{State 1 to state 2}
{Control volume: Compressor}
"!State points 1: Compressor inlet"
h[1]=h[10] "Enthalpy of vapour inlet"
x[1]=1 "Gas quality"
T[1]=temperature(R$;P=P[1];h=h[1]) "Temperature "
s[1]=entropy(R$;P=P[1];h=h[1]) "Entropy"
eta_IS=0,5 [-] "Compressor efficiency"
HL=0,1 [-] "Relative heat loss i compressor, % of input power"
lambda=0,7 "Volumetric efficiency"
v_g_1=Volume(R$;T=T_vacuum;P=P_vacuum) "Specific volume of vapour"
V_dot_1=(m_dot_gas*v_g_1*convert(m^3/s;m^3/h)) "Volumetric flow vapour"

```

```

"!State points 2: Compressor outlet"

```

```

P[2]=sqrt(P[1]*P[4]) "Pressure"
h[2]=h[1]+DELTA_W*(1-HL) "Energy balance on real compressor-assumed
adiabatic"
s[2]=entropy(R$;h=h[2];P=P[2]) "Entropy of state 3"
T[2]=temperature(R$;h=h[2];P=P[2]) "Discharge gas temperature"
h_2_IS=enthalpy(R$;P=P[2];s=s[1]) "Isentropic enthalpy"
w_IS=(h_2_IS-h[1]) "Energy balance on isentropic compressor"
DELTA_W=w_IS/eta_IS "Real compressor entalphy difference"
T_discharge=T[2] "Discharge gas temperatur"
x[2]=quality(R$;h=h[2];T=T[2]) "Gas quality"
Q_loss=((h[2]+DELTA_W)-(h[2]+DELTA_W*(1-HL)))*m_dot_gas "Heat loss in
compression"

```

```

"-----"

```

```

{State 2 to state 3}
{Control Volume : Connecting Pipe}

```

```

"!Pipe Information"

```

```

e_23=0,000015[m] {Roughness, Drawn Tubing}
D_23=40[cm]*convert(cm;m) {Pipe Diameter}
RR_23=e_23/D_23 {Relative Roughness}
L_23=1 [m] {Length of pipe}

```

```

"!Pressure drop"

```

```

call PipeFlow(R$;T[2];P[2];m_dot_gas;D_23;L_23;RR_23:{h_T_23}; {h_H_23}
;DELTA_P_23; {Nusselt_T_23}; f_34; Re_23)

```

```

P[3]=P[2]-DELTA_P_23

```

```

"-----"

```

```

{State 3 to state 4}
{Controll volume: Compressor}
"!State points 3: Compressor inlet"
T[3]=T_sat(R$;P=P[3])+10
h[3]=enthalpy(R$;P=P[3];T=T[3])
s[3]=entropy(R$;P=P[3];h=h[3])

"!State points 4: Compressor outlet"
P[4]=P_sat(R$;T=T_cond)
h[4]=h[3]+DELTAW*(1-HL) "Energy balance on real compressor-assumed
adiabatic"
s[4]=entropy(R$;h=h[4];P=P[4]) "Entropy of state 3"
T[4]=temperature(R$;h=h[4];P=P[4]) "Discharge gas temperature"
h_4_IS=enthalpy(R$;P=P[4];s=s[3]) "Isentropic enthalpy"
w_IS_4=(h_4_IS-h[3]) "Energy balance on isentropic compressor"
DELTAW_2=w_IS_4/eta_IS "Real compressor entalphy
difference"
T_discharge_2=T[4] "Discharge gas temperatur"
x[4]=quality(R$;h=h[4];T=T[4]) "Gas quality"
Q_loss_2=((h[2]+DELTAW_2)-(h[4]+DELTAW_2*(1-HL)))*m_dot_gas "Heat loss in
compression"
v_g_2=Volume(R$;T=T[4];P=P[4]) "Specific volume of vapour"
V_dot_2=(m_dot_gas*v_g_2*convert(m^3/s;m^3/h)) "Volumetric flow vapour"
"-----"
{State 4 to state 5}
{Control Volume : Connecting Pipe}

"!Pipe Information"
e_45=0,000015[m] {Roughness, Drawn Tubing}
D_45=35[cm]*convert(cm;m) {Pipe Diameter}
RR_45=e_45/D_45 {Relative Roughness}
L_45=1 [m] {Length of pipe}

"!Pressure drop"
call PipeFlow(R$;T[4];P[4];m_dot_gas;D_45;L_45;RR_45:{h_T_45}; {h_H_45}
;DELTAP_45; {Nusselt_T_45}; f_45; Re_45)

P[5]=P[4]-DELTAP_45

"-----"
{State 5 to state 6}
{Controll volume: Condenser}
"!State 5 : Condenser inlet"

h[5]=h[4]
T[5]=temperature(R$;P=P[5];h=h[5])
x[5]=quality(R$;h=h[5];T=T[5])
s[5]=entropy(R$;T=T[5];h=h[5])
v[5]=Volume(R$;T=T[5];P=P[5])
rho[5]=density(R$;P=P[5];x=1)
mu[5]=viscosity(R$;T=T[5];P=P[5])
V_dot[5]=(m_dot_gas*v[5]*convert(m^3/s;m^3/h))

"!Size and Pressure drop in condenser"
CALL
heattransfercond(m_dot_gas;m_dot_water;T_water_outlet;T_cond;T_w_avg;T[5];T
[6];w_plate_cond;x_plate_cond:U_cond)

P_amb=101325 [Pa]
C_p_w=Cp(R$;P=P_amb;T=T_water_outlet)
m_dot_water=10 [kg/s]

```

```

T_out_cond=T_water_outlet+Q_cond/(m_dot_water*C_p_w)
T_w_avg=(T_water_outlet+T_out_cond)/2

dt_1=T[6]-T_out_cond
dt_2=T[5]-T_water_outlet
DELTA_T_cond_lmtd=((dt_1)-(dt_2))/ln((dt_1)/(dt_2)) "LMTD in Condenser"

U_cond_1=3243 [W/m^2*K]
UA_cond=Q_cond/DELTA_T_cond_lmtd
A_cond=(UA_cond*1000)/U_cond_1
w_plate_cond=500 [mm]*convert(mm;m) "Alfa Laval AXP112"
h_plate_cond=1658 [mm]*convert(mm;m) "Alfa Laval AXP112"
x_plate_cond=CEIL(A_cond/(2*h_plate_cond*w_plate_cond))

"Pressure drop condenser"
rho_cond=(rho[5]+rho[6])/2 "Average density"
mu_l=viscosity(R$;T=T[6];x=0)
mu_g=viscosity(R$;T=T[6];x=1)
d_e=7 [mm]*convert(mm;m)
D_p=0,4 [m]
g=9,81
G_p_cond=(m_dot_gas)/((pi/4)*D_p^2) "Mass velocity through the port"
A_o_cond=0,5*x_plate_cond*w_plate_cond*d_e
"Flow area"
G_cond=(m_dot_gas)/A_o_cond "Mass velocity through the core"

DELTA_T_cond_g = rho_cond*g*h_plate_cond "gravity driven acceleration"
DELTA_T_cond_acc = (G_cond^2)*1*( (1/rho[5]) - (1/rho[6])) "acceleration
pressure, quality change is 1"
DELTA_T_cond_p = 0,75*(G_p_cond^2)/rho_cond "inlet/outlet pressure loss"
DELTA_T_cond_fr = (1,9*G_cond^2)/(2*rho_cond) "kinetic model from Longo
2010"
DELTA_T_cond_test = (DELTA_T_cond_fr+DELTA_T_cond_p - DELTA_T_cond_acc -
DELTA_T_cond_g)
"The pressure drop is very high, and AlfaLaval is asked for advice. No
feedback was given"

P[6]=P[5]{-DELTA_T_cond}

"!State 6: Condenser Outlet"
T[6]=T_cond
x[6]=0
h[6]=enthalpy(R$;T=T[6];x=x[6])
s[6]=entropy(R$;T=T[6];x=x[6])
rho[6]=density(R$;P=P[6];x=x[6])
mu[6]=viscosity(R$;T=T[6];P=P[6])
"-----"

{State 6 to state 7}
{Control Volume : Connecting Pipe}
"!Pipe Information"
e_67=0,000015 [m] {Roughness, Drawn Tubing}
D_67=35 [cm]*convert(cm;m) {Pipe Diameter}
RR_67=e_67/D_67 {Relative Roughness}
L_67=1 [m] {Length of pipe}

"!Pressure drop"
call PipeFlow(R$;T[6];P[6];m_dot_gas;D_67;L_67;RR_67:{h_T_67}; {h_H_67}
;DELTA_T_67; {Nusselt_T_67}; f_67; Re_67)

P[7]=P[6]-DELTA_T_67

```

```

"-----"

{State 7 to state 8}
{Control volume: Expansion valve}
"!State 7 : Expansion Valve Inlet"
h[7]=h[6]
T[7]=temperature(R$;P=P[7];h=h[7])
x[7]=quality(R$;h=h[7];T=T[7])
s[7]=entropy(R$;T=T[7];h=h[7])

"!State 8 : Expansion Valve Outlet"
h[8]=h[7]
T[8]=T_vacuum
P[8]=P_sat(R$;T=T[8])+0,01
s[8]=entropy(R$;T=T[8];h=h[8])
x[8]=quality(R$;T=T[8];s=s[8])
"-----"

{State 8 to state 9}
{Control Volume : Connecting Pipe}

"Assume no pressure drop"
P[9]=P[8]
"-----"

{State 9 to state 10}
{Control volume: Vacuum freezer}
"!State points 9: Freezer inlet"
h[9]=h[8]
T[9]=temperature(R$;P=P[9];h=h[9])
x[9]=quality(R$;T=T[9];h=h[9])
s[9]=entropy(R$;T=T[9];h=h[9])
"Entropy of vapour inlet"
"Temperature in point 7"

"!State points 10: Freezer outlet"
T[10]=T_vacuum
P[10]=P[9]
x[10]=1
h[10]=enthalpy(R$;P=P[10];x=x[10])
s[10]=entropy(R$;P=P[10];x=x[10])
"Enthalpy of vapour inlet"
"-----"

{State 10 to state 1}
{Control Volume : Connecting Pipe}
"!Pipe Information"
e_101=0,000015[m]
D_101=5[cm]*convert(cm;m)
RR_101=e_101/D_101
L_101=1 [m]
{Roughness, stainless steel}
{Pipe Diameter}
{Relative Roughness}
{Length of pipe}

"!Pressure drop"
call PipeFlow(R$;T[10];P[10];m_dot_gas;D_101;L_101;RR_101:{h_T_101};
{h_H_101} ;DELTA_T_101; {Nusselt_T_101}; f_101; Re_101)

P[1]=P[10]-DELTA_T_101
"-----"

"!Pressure ratio"
PR_1=P[2]/P[1]
PR_2=P[4]/P[3]
"Pressure ratio, comp 1"
"Pressure ratio, comp 2"

"!Compressor"
W_comp_1=m_dot_gas*(DELTA_W)
"Compressor work, comp 1"

```

```

W_comp_2=m_dot_gas*(DELTAW_2)           "Compressor work, comp 2"
W_tot=W_comp_1+W_comp_2+P_ag_tot+W_pump_iceslurry+W_snowsep "Total work"
V_dot_s_1=v_dot_1/lambda                "Suction volume of compressor"
V_dot_s_2=v_dot_2/lambda                "Suction volume of compressor"

"!Condenser"
Q_cond=m_dot_gas*(h[5]-h[6])            "Condensation heat"

"!Evaporator"
Q_cooling=m_dot_gas*(h[10]-h[9])        "Cooling capacity"

"!COP"
COP=Q_cooling/W_tot                     "COP for cooling"
COP_c=Q_cond/W_tot                      "COP for cooling"
"-----"

"!Size of vessel"

CALL areavessel(R$;m_dot_gas;T_amb;V_dot:D_vessel[1])

"!Volume"
V_vessel=1 [m^3]                        "Assumed volume of ice slurry in
vessel"
"-----"

"!Ice slurry pump"
x=0,15                                  "Fraction of ice to water"
m_iceslurry=m_dot_w/x                   "Mass flow of ice slurry"

"At ice fractions below 15% the pump power is not affected"
T_iceslurry=0,01
P_iceslurry=P_vacuum+0,1
N_iceslurry=1000
[1/min]*convert(1/min;1/s)             "RPM pump"
D_iceslurry=0,15 [m]                   "Diameter pump"
D_iceslurry_hub= 0,08 [m]              "Diameter pump hub"

Call CentrifugalPump1_CL( R$; 0; T_iceslurry; P_iceslurry; m_iceslurry ;
N_iceslurry; D_iceslurry; D_iceslurry_hub: P_out_pump_iceslurry;
T_out_pump_iceslurry; W_pump_iceslurry; eta_pump_iceslurry)

"!Agitation power"
"See The control of ice slurry systems: an overview"
P_ag=25 [W/m^3]                         "Recommended power to have
homogeneity"
P_ag_tot=P_ag*V_vessel*convert(W;kW)

"!Snow separator"
"Size is around 30 m^3"
"Motor to operate snow separator. From BUUS-tech-data, same as motor in
flake ice drum"
W_snowsep=370 [W]*convert(W;kW)

```

F. EES Code. Flake Ice Maker

```
$UnitSystem SI C kPa kJ mass  
$Reference R744 IIR
```

```
"-----  
To better understand the code, it is recommended to go the state-point  
calculations. The procedures are calculated in sequence from top to bottom.  
This is not the case for the main body, where EES decides what to calculate  
first. See Computational Flow. This is recommended since the procedures are  
put in the start of the script due to syntax reasons.  
  
To calculate a single stage system. The points from [2] to [7] is commented  
out. P[7]=P[3]. In addition, the outlet pressure of compressor 1, must to  
the condensation pressure. The pipe dimensions may be changed for the  
program to converge.  
  
When simulation the cascade system, T_evap=-5 [C]  
-----"
```

```
"-----  
PROCEDURES  
-----"
```

```
PROCEDURE  
flakeicedrum(T_evap_flake;m_co2_fl_real;T_water_in;m_w;x_pipe;Q_water:U1[1]  
;U1_avg)
```

```
{Calculation of propagation of the ice layer and overall heat transfer  
coefficient for the flake ice drum  
for carbon and stainless steel vessel.}
```

```
$ARRAYS ON
```

```
"!Forced flow refrigerant side"
```

```
R$='R744'
```

```
h_flake=2,6 [m] "Height of flake ice  
drum"
```

```
d_flake=2,5 [m] "Diameter of flake ice drum"
```

```
u_w=0,5 [m/s] "Water speed along drum"
```

```
A_flake=pi*d_flake*h_flake "Area flake ice drum"
```

```
P_ref=P_sat(R$;T=T_evap_flake) "Pressure"
```

```
k_ref=Conductivity(R$;T=T_evap_flake;P=P_ref+0,01)
```

```
"Thermal conductivity. CO2"
```

```
d=5 [mm]*convert(mm;m) "Diameter of pipe"
```

```
d_hyd=d "Hydraulic diameter"
```

```
"CO2 evaporation correlation"
```

```
mu_f=Viscosity(R$;T=T_evap_flake;x=0) "Dynamic viscosity. Liquid"
```

```
mu_g=Viscosity(R$;T=T_evap_flake;x=1) "Dynamic viscosity. Gas"
```

```
rho_f=Density(CarbonDioxide;T=T_evap_flake;x=0)
```

```
"Density. Liquid"
```

```
rho_g=Density(CarbonDioxide;T=T_evap_flake;x=1)
```

```
"Density. Gas"
```

```
h_fg=Enthalpy_vaporization(R$;T=T_evap_flake)
```

```
"Enthalpy of vaporization"
```

```
M=MolarMass(R$) "Molar mass"
```

```
k_f=Conductivity(R$;T=T_evap_flake;x=0) "Thermal conductivity. Liquid"
```

```

k_g=Conductivity(R$;T=T_evap_flake;x=1) "Thermal conductivity. Gas"
cp_f=Cp(R$;T=T_evap_flake;x=0) "Specific heat capacity. Liquid"
cp_g=Cp(R$;T=T_evap_flake;x=1) "Specific heat capacity. Gas"
C=20 "Turbulent Chisholm factor"
PC=P_crit(R$) "Critical pressure"
P_r=P_ref/PC "Reduced pressure"
G=m_co2_fl_real/(x_pipe*PI*d_hyd^2/4) "Mass flux"
q=Q_water*1000/(pi*d*h_flake*x_pipe) "Heat per m2"
Bo=(Q_water/(pi*d*h_flake*x_pipe))/(G*h_fg)
"Boiling number"
Pr_f=Prandtl(R$;P=P_ref+0,01;x=0) "Prandtl number"

x[1]=0,1
dx=0,1
N=10

DUPLICATE i=2;N
x_ma[i-1]=(mu_f/mu_g)^(1/8)*((1-x[i-1])/x[i-1])^(7/8)*(rho_g/rho_f)^0,5
"Lockhart Martinelli parameter"
phi_f[i-1]=(1+C/x_ma[i-1]+1/(x_ma[i-1]^2)) "Two-phase frictional multiplier"
F[i-1]=0,05*(phi_f[i-1])+0,95 "Correlation factor"
S[i-1]=7,2694*(phi_f[i-1])^0,0094*Bo^0,2814 "Nucleate boiling suppression
factor\"
h_nbc[i-1]=55*P_r^0,12*(-0,4343*ln(P_r))^(-0,55)*M^(-0,5)*q^0,67 "Nucleate
boiling heat transfer"
h_lo[i-1]=0,023*(k_f/d)*((G*(1-x[i-1])*d)/mu_f)^0,8*(Pr_f^0,4) "Dittus-
Boelter correlation"
alpha_ref[i-1]=S[i-1]*h_nbc[i-1]+F[i-1]*h_lo[i-1] "Heat transfer correlation"

x[i]=x[i-1]+dx

END

alpha_ref=1/9*SUM(alpha_ref[i];i=1;9) "Average heat transfer
correlation"

"!Free flow on water side"
W$='water'
P_w=101,325 [kPa] "Pressure"
k_w=Conductivity(W$;T=T_water_in;P=P_w+0,01[kPa])
"Thermal conductivity"
rho_w=density(W$;T=T_water_in;P=P_w+0,01) "Density"
nu_w=KinematicViscosity(W$;T=T_water_in;P=P_w+0,01) "Kinematic viscosity"
c_p_w=specheat(W$;T=T_water_in;P=P_w+0,01)
"Specific heat capacity"
Pr_w=Prandtl(W$;T=T_water_in;P=P_w+0,01) "Prandtl number"
Re_w=(u_w*h_flake)/nu_w "Reynolds number"

Re_x_c=5*10^5 "Critical Reynolds number"
B=0,037*Re_x_c^(4/5)-0,664*Re_x_c^(1/2) "Correlation factor"
alpha_w=(k_w/h_flake)*(0,037*Re_w^(4/5)-B)*(Pr_w^(1/3)) "Correlation for
turbulent flow over flat plate. Incropera (2013)"

"!Carbon steel drum"
delta_wall=0,5 [cm]*convert(cm;m) "Thickness of drum wall"
delta_wall_2=0,3 [cm]*convert(cm;m) "Thickness of second drum wall"
k_al=Conductivity(Aluminum; T=-30) "Heat conductivity aluminum"
S_u_al=UltimateStress(Aluminum; T=-30) "UTS aluminium"

```



```

k_ice=Conductivity(Ice;T=0;P=101,325)           "Thermal conductivity ice"
k_cs=Conductivity(Carbon_steel; T=-15)         "Heat conductivity carbon steel"
S_u_ss=UltimateStress(Stainless_AISI302;
T=17)                                           "UTS. Stainless steel"

T_i=0 [C]
DELTAh_fusion=enthalpy_fusion(W$)*convert(kJ/kg;J/kg)

X1[1]=0
dt=1
t[1]=0
Time=120

DUPLICATE i=2;time

"Overall heat transfer coefficient"
U1[i-1]=1/((1/alpha_ref)+(delta_wall_2/k_cs)+(delta_wall/k_al)+(x1[i-1]/k_ice)+(1/alpha_w))

"Ice thickness as function of time"
dx1[i-1]=((((T_i-
T_evap_flake)/((1/alpha_ref)+(delta_wall_2/k_cs)+(delta_wall/k_al)+(X1[i-1]/k_ice)))-alpha_w*(T_water_in-T_i))))*dt)/(rho_w*DELTAh_fusion)

X1[i]=X1[i-1]+dx1[i-1]
t[i]=t[i-1]+dt

"The Ice growth rate [m/s]"
ds\dt1[i-1]=((((T_i-
T_evap_flake)/((1/alpha_ref)+(delta_wall_2/k_cs)+(delta_wall/k_al)+(X1[i-1]/k_ice)))-alpha_w*(T_water_in-T_i)))/(rho_w*DELTAh_fusion)

END

U1_avg=sum(U1[i];i=1;70-1)/70                  "Average U-value. Carbon steel"
Q_cs=U1_avg*h_flake*pi*d_flake*(T_water_in-T_evap_flake) "Heat transfer with carbon steel"

"!Stainless steel drum"
{k_ss=16 [W/m*k]                               "Heat conductivity stainless steel"}
k_ss=Conductivity(Stainless_AISI302;
T=17)                                           "Heat conductivity stainless steel"
X2[1]=0

DUPLICATE i=2;time

"Overall heat transfer coefficient"
U2[i-1]=1/((1/alpha_ref)+(delta_wall_2/k_ss)+(delta_wall/k_al)+(X2[i-1]/k_ice)+(1/alpha_w))

"Ice thickness as function of time"
dx2[i-1]=((((T_i-
T_evap_flake)/((1/alpha_ref)+(delta_wall_2/k_ss)+(delta_wall/k_al)+(X2[i-1]/k_ice)))-alpha_w*(T_water_in-T_i))))*dt)/(rho_w*DELTAh_fusion)

X2[i]=X2[i-1]+dx2[i-1]

"The Ice growth rate [m/s]"

```

```

ds\dt2[i-1]=((((T_i-
T_evap_flake)/((1/alpha_ref)+(delta_wall_2/k_ss)+(delta_wall/k_al)+(X2[i-
1]/k_ice)))-alpha_w*(T_water_in-T_i)))/(rho_w*DELTAh_fusion)

```

END

```

U2_avg=sum(U2[i];i=1;70-1)/70 "Average U-value. Stainless
steel"

```

```

Q_ss=U2_avg*h_flake*pi*d_flake*(T_water_in-T_evap_flake) "Heat transfer
with of stainless steel"

```

!"Aluminium drum"

```
X3[1]=0
```

```
DUPLICATE i=2;time
```

"Overall heat transfer coefficient"

```

U3[i-1]=1/((1/alpha_ref)+(delta_wall_2/k_al)+(X3[i-
1]/k_ice)+(delta_wall/k_al)+(1/alpha_w))

```

"Ice thickness as function of time"

```

dx3[i-1]=((((((T_i-
T_evap_flake)/((1/alpha_ref)+(delta_wall_2/k_al)+(delta_wall/k_al)+(X3[i-
1]/k_ice)))-alpha_w*(T_water_in-T_i))))*dt)/(rho_w*DELTAh_fusion)

```

```
X3[i]=X3[i-1]+dx3[i-1]
```

"The Ice growth rate [m/s]"

```

ds\dt3[i-1]=((((T_i-
T_evap_flake)/((1/alpha_ref)+(delta_wall_2/k_al)+(delta_wall/k_al)+(X3[i-
1]/k_ice)))-alpha_w*(T_water_in-T_i)))/(rho_w*DELTAh_fusion)

```

END

```

U3_avg=sum(U3[i];i=1;70-1)/70 "Average U-value. Aluminium"

```

```

Q_al=U3_avg*h_flake*pi*d_flake*(T_water_in-T_evap_flake) "Heat transfer
with of stainless steel"

```

END

"-----"

```

PROCEDURE heattransfercondevap(m_dot_co2;m_co2_fl_real;T_evap;
T_evap_flake;x[13];w_plate;h_plate;x_plate;b_plate:U_cond_evap;G_2)

```

!"Overall heat transfer coefficient for condenser evaporator. Forced flow on both sides"

{Calculates the heat transfer coefficients and U-value for the for condenser/evaporator}

\$ARRAY ON

```
R$='R744' "Refrigerant string. CO2"
```

```
delta_wall_condevap=1 [mm]*convert(mm;m) "Thickness HX plates"
```

```
k_ss=Conductivity(Stainless_AISI302; "Thermal conductivity. Stainless
T=17) steel"
```

```
d_e=7 [mm]*convert(mm;m) "Equivalent diameter"
```

"Cold side"

```
P_cold=P_sat(R$;T=T_evap) "Pressure"
```

```

mu_f=Viscosity(R$;T=T_evap;x=0)           "Dynamic viscosity. Liquid"
mu_g=Viscosity(R$;T=T_evap;x=1)           "Dynamic viscosity. Gas"
rho_f=Density(CarbonDioxide;T=T_evap;x=0) "Density. Liquid"
rho_g=Density(CarbonDioxide;T=T_evap;x=1) "Density. Gas"
h_fg=Enthalpy_vaporization(R$;T=T_evap)   "Enthalpy of vaporization"
M=MolarMass(R$)                            "Molar mass"
k_f=Conductivity(R$;T=T_evap;x=0)         "Thermal conductivity
CO2"
cp_f=Cp(R$;T=T_evap;x=0)                  "Specific heat capacity"
C=20                                        "Turbulent Chisholm factor"
PC=P_crit(R$)                              "Critical pressure"
P_r=P_cold/PC                              "Reduced pressure"
A=(d_e)*w_plate*0,5*x_plate               "Total Flow area"
G_2=m_dot_co2/A                            "Mass flux"
q=213,9*1000/(2*w_plate*h_plate*x_plate)  "Heat per m2"
Bo=(213,9/(2*w_plate*h_plate*x_plate))/(G_2*h_fg)
      "Boiling number"
Pr_f=Prandtl(R$;P=P_cold+0,01;x=0)         "Prandtl number"
g=9,81                                     "Gravitational constant"

x[1]=0,1
dx=0,1
N=10

DUPLICATE i=2;N
x_ma[i-1]=(mu_f/mu_g)^(1/8)*((1-x[i-1])/x[i-1])^(7/8)*(rho_g/rho_f)^0,5
"Lockhart Martinelli factor"
phi_f[i-1]=(1+C/x_ma[i-1]+1/(x_ma[i-1]^2)) "Two-phase frictional multiplier"
F[i-1]=0,05*(phi_f[i-1])+0,95              "Correlation factor"
S[i-1]=7,2694*(phi_f[i-1]^0,0094*Bo^0,2814 "Nucleate boiling suppression
factor"
h_nbc[i-1]=55*P_r^0,12*(-0,4343*ln(P_r))^(0,55)*M^(0,5)*q^0,67 "Nucleate
boiling heat transfer coefficient"
h_lo[i-1]=0,023*(k_f/(1,2*d_e))*((G_2*(1-x[i-1])*(1,2*d_e))/mu_f)^0,8*((Pr_f)^0,4) "Dittus-Boelter correlation"
alpha_ref[i-1]=S[i-1]*h_nbc[i-1]+F[i-1]*h_lo[i-1] "Heat transfer coefficient"

x[i]=x[i-1]+dx

END

alpha_cold=1/9*SUM(alpha_ref[i];i=1;9)      "Average heat transfer
coefficient"

"Warm side"
P_warm=P_sat(R$;T=T_evap_flake)
k_warm_o=Conductivity(R$;P=P_warm+0,01;x=0)

mu_warm_o=KinematicViscosity(R$;P=P_warm+0,01;x=0)
rho_warm_o=density(R$;P=P_warm+0,01;x=0)
rho_warm_i=density(R$;P=P_warm+0,01;x=1)
Cp_l=Cp(R$;P=P_warm+0,01;x=0)

DUPLICATE i=2;N
alpha_warm[i-1]=(k_warm_o^(2/3)*Cp_l^(1/3))/mu_warm_o^(7/15)*((x[i-1]/(1-x[i-1]))*(rho_warm_o/rho_warm_i)^0,5+1) "Condensation correlation CO2"
x[i]=x[i-1]+dx
END

```

```

alpha_warm=1/9*SUM(alpha_warm[i];i=1;9)    "Average heat transfer
coefficient"
U_cond_evap=1/((1/alpha_cold)+(delta_wall_condevap/k_ss)+(1/alpha_warm))
"U-value condenser/evaporator"
END "Procedure"
"-----"

PROCEDURE
heattransfercond(m_dot_co2;m_dot_water;T_water_in;T_cond;T_w_cond_avg;w_pla
te_cond;x_plate_cond:U_cond)
"!Overall heat transfer coefficient for condenser/gas cooler . Forced flow
on both sides"

$ARRAY ON
W$='Water'
R$='R744'
delta_wall_cond=1 [mm]*convert(mm;m)
k_ss=Conductivity(Stainless_AISI302; T=17)
d_e=7 [mm]*convert(mm;m)    "Equivalent diameter plate HX"

"Cold side"
P_cold=101,325 [kPa]
k_cold=Conductivity(W$;T=T_water_in;P=P_cold)
mu_cold=Viscosity(W$;T=T_water_in;P=P_cold)
mu_wall_water=viscosity(W$;T=(T_cond+T_w_cond_avg)/2;P=P_cold+0,01)
A=(d_e)*w_plate_cond*0,5*x_plate_cond
G=m_dot_water/A
Pr_cold=Prandtl(W$;T=T_water_in;P=P_cold)
Re_cold=(G*d_e)/mu_cold

"Martin correlation for one-phase flow water"
beta_cold=45    "Chevron angle plate HX"
f0_martin_cold = 64/Re_cold    "parameter for friction factor
calculation"
f1_martin_cold= 597/Re_cold+3,85    "parameter for friction factor
calculation"
f_martin_cold=(1 /
(cos(beta_cold)/sqrt(0,18*tan(beta_cold)+0,36*sin(beta_cold)+(f0_martin_col
d/cos(beta_cold))) + ((1-cos(beta_cold))/(sqrt(3,8*f1_martin_cold)))) )^2
"friction factor"
Nusselt_cold=0,122*(Pr_cold^(1/3))*((mu_cold/mu_wall_water)^(1/6))*(f_marti
n_cold*( (Re_cold^2)*sin(2*beta_cold))^0,374 "Nusselt number"
alpha_cold= (Nusselt_cold*k_cold)/d_e    "heat transfer coefficient water"

"Warm side"
P_warm=P_sat(R$;T=T_cond)
k_warm_o=Conductivity(R$;P=P_warm+0,01;x=0)
mu_warm_o=KinematicViscosity(R$;P=P_warm+0,01;x=0)
rho_warm_o=density(R$;P=P_warm+0,01;x=0)
rho_warm_i=density(R$;P=P_warm+0,01;x=1)
Cp_l=Cp(R$;P=P_warm+0,01;x=0)

N=10
x[1]=0,1
dx=0,1

DUPLICATE i=2;N
alpha_warm[i-1]=(k_warm_o^(2/3)*Cp_l^(1/3))/mu_warm_o^(7/15)*((x[i-1]/(1-
x[i-1]))*(rho_warm_o/rho_warm_i)^0,5+1)
x[i]=x[i-1]+dx

```

END

```
alpha_warm=1/9*SUM(alpha_warm[i];i=1;9)
U_cond=1/((1/alpha_cold)+(delta_wall_cond/k_ss)+(1/alpha_warm))
END "Procedure"
```

-----"

PROCEDURE

```
heattransfersh(m_dot_co2;m_dot_water_sh;T_water_in;T_cond;T[7];T_out_suh_1;
T_ref_avg;T_w_avg;w_plate_sh;x_plate_sh;U_sh)
"!Overall heat transfer coefficient for condenser/gas cooler . Forced flow
on both sides"
```

\$ARRAY ON

```
W$='Water'
R$='R744'
delta_wall_cond=1 [mm]*convert(mm;m)
k_ss=Conductivity(Stainless_AISI302; T=17)
d_e=7 [mm]*convert(mm;m)
```

"Cold side"

```
P_cold=101,325 [kPa]
k_cold=Conductivity(W$;T=T_water_in;P=P_cold)
mu_cold=Viscosity(W$;T=T_water_in;P=P_cold)
mu_wall_water=viscosity(W$;T=(T_ref_avg+T_w_avg)/2;P=P_cold+0,01)
A=(d_e)*w_plate_sh*0,5*x_plate_sh
G=m_dot_water_sh/A
Pr_cold=Prandtl(W$;T=T_water_in;P=P_cold)
Re_cold=(G*d_e)/mu_cold
```

"Martin correlation for one-phase water"

```
beta_cold=45 "Chevron angle"
f0_martin_cold = 64/Re_cold "parameter for friction factor
calculation"
f1_martin_cold= 597/Re_cold+3,85 "parameter for friction factor
calculation"
f_martin_cold=(1 /
(cos(beta_cold)/sqrt(0,18*tan(beta_cold)+0,36*sin(beta_cold)+(f0_martin_col
d/cos(beta_cold))) + ((1-cos(beta_cold))/(sqrt(3,8*f1_martin_cold)))) )^2
"friction factor"
Nusselt_cold=0,122*(Pr_cold^(1/3))*((mu_cold/mu_wall_water)^(1/6))*(f_marti
n_cold*( (Re_cold^2)*sin(2*beta_cold)))^0,374 "Nusselt number"
alpha_cold = (Nusselt_cold*k_cold)/d_e "heat transfer coefficient water"
```

"Warm side"

```
P_warm=P_sat(R$;T=T_cond)
k_warm_o=Conductivity(R$;P=P_warm+0,01;x=1)
k_warm_i=Conductivity(R$;P=P_warm+0,01;T=T[7])
k_avg=(k_warm_o+k_warm_i)/2
mu_warm_o=Viscosity(R$;P=P_warm+0,01;x=1)
mu_warm_i=Viscosity(R$;P=P_warm+0,01;T=T[7])
mu_avg=(mu_warm_o+mu_warm_i)/2
mu_wall_ref=viscosity(R$;T=(T_ref_avg+T_w_avg)/2;P=P_warm+0,01)
```

```
G_warm=(m_dot_co2)/A
T_sh_out=Temperature(R$;P=P_warm;x=1)
Pr_warm=Prandtl(R$;T=(T[7]+T_sh_out)/2;P=P_warm)
Re_warm=(G_warm*d_e)/mu_avg
```

"Martin correlation for one-phase co2 flow"

```
beta_warm=45 "Chevron angle"
```

```

f0_martin = (1,8*log10(Re_warm)-1,5)^(-2) "parameter for friction factor
calculation"
f1_martin= 39/(Re_warm^0,289) "parameter for friction factor
calculation"
f_martin=(1 /
(cos(beta_warm)/sqrt(0,18*tan(beta_warm)+0,36*sin(beta_warm)+(f0_martin/cos
(beta_warm))) + ((1-cos(beta_warm))/(sqrt(3,8*f1_martin)))) )^2
"friction factor"
Nusselt_w=0,122*(Pr_warm^(1/3))*((mu_avg/mu_wall_ref)^(1/6))*(f_martin*(
(Re_warm^2)*sin(2*beta_warm)))^0,374 "Nusselt number"
alpha_warm= (Nusselt_w*k_avg)/d_e "heat transfer coefficient water"

U_sh=1/((1/alpha_cold)+(delta_wall_cond/k_ss)+(1/alpha_warm))
END "Procedure"
"-----"

PROCEDURE
heattransferSGHX(m_dot_co2;P[9];T[9];P[10];T[10];P[15];T[15];P[16];T[16];T
avg_warm_sghx;T_avg_cold_sghx;w_plate_sghx;x_plate_sghx;U_sghx)
"!Overall heat transfer coefficient for condenser evaporator. Forced flow
on both sides"

R$='R744'
delta_wall_condevap=1 [mm]*convert(mm;m)
k_al=Conductivity(Aluminum; T=17)
d_e=0,007 [m] "Equivalent diameter"

"Cold side"
k_c1=Conductivity(R$;T=T[15];P=P[15]+0,01)
k_c2=Conductivity(R$;T=T[16];P=P[16]+0,01)
k_c_avg=(k_c1+k_c2)/2
mu_cold_i=Viscosity(R$;T=T[15];P=P[15]+0,01)
mu_cold_o=Viscosity(R$;T=T[16];P=P[16]+0,01)
mu_cold_avg=Viscosity(R$;T=(T[15]+T[16])/2;P=((P[15]+0,01)+(P[16]+0,01))/2)
mu_wall_cold=viscosity(R$;T=(T_avg_warm_sghx+T_avg_cold_sghx)/2;P=P[15]+0,0
1)
A=(d_e)*w_plate_sghx*0,5*x_plate_sghx
G=m_dot_co2/A
Pr_cold=Prandtl(R$;T=(T[15]+T[16])/2;P=(P[15]+P[16])/2)
Re_cold=(G*d_e)/mu_cold_avg

"Martin correlation for one-phase flow water"
beta_cold=45
f0_martin_cold = (1,8*log10(Re_cold)-1,5)^(-
2) "parameter for friction factor calculation"
f1_martin_cold= 39/(Re_cold^0,289) "parameter for friction factor
calculation"
f_martin_cold=(1 /
(cos(beta_cold)/sqrt(0,18*tan(beta_cold)+0,36*sin(beta_cold)+(f0_martin_col
d/cos(beta_cold))) + ((1-cos(beta_cold))/(sqrt(3,8*f1_martin_cold)))) )^2
"friction factor"
Nusselt_cold=0,122*(Pr_cold^(1/3))*((mu_cold_avg/mu_wall_cold)^(1/6))*(f_ma
rtin_cold*( (Re_cold^2)*sin(2*beta_cold)))^0,374 "Nusselt number"
alpha_cold = (Nusselt_cold*k_c_avg)/d_e "heat transfer coefficient water"

"Warm side"
k_h1=Conductivity(R$;T=T[9];P=P[9]+0,1)
k_h2=Conductivity(R$;T=T[10];P=P[10]+0,1)
k_h_avg=(k_h1+k_h2)/2 "Average thermal conductivity"
mu_warm_i=Viscosity(R$;T=T[9];P=P[9]+0,01)
mu_warm_o=Viscosity(R$;T=T[10];P=P[10]+0,01)

```

```

mu_warm_avg=Viscosity(R$;T=(T[9]+T[10])/2;P=((P[9]+0,01)+(P[10]+0,01))/2)
"Average dynamic viscosity"
mu_wall_ref=viscosity(R$;T=(T_avg_warm_sghx+T_avg_cold_sghx)/2;P=P[9]+0,01)
rho_avg=density(R$;T=T[9];P=P[9]+0,1) "Average density"
Pr_hot=Prandtl(R$;T=(T[9]+T[10])/2;P=(P[9]+0,1+P[10])/2)
Re_hot=(G*d_e)/mu_warm_avg

"Martin correlation for one-phase co2 liquid flow"
beta_warm=45 "Chevron angle"
f0_martin = (1,8*log10(Re_hot)-1,5)^(-2) "parameter for friction factor
calculation"
f1_martin= 39/(Re_hot^0,289) "parameter for friction factor
calculation"
f_martin=(1 /
(cos(beta_warm)/sqrt(0,18*tan(beta_warm)+0,36*sin(beta_warm)+(f0_martin/cos
(beta_warm))) + ((1-cos(beta_warm))/(sqrt(3,8*f1_martin)))) )^2
"friction factor"
Nusselt_w=0,122*(Pr_hot^(1/3))*((mu_warm_avg/mu_wall_ref)^(1/6))*(f_martin*
(Re_hot^2)*sin(2*beta_warm))^0,374 "Nusselt number"
alpha_warm= (Nusselt_w*k_h_avg)/d_e "heat transfer coefficient water"
U_sghx=1/((1/alpha_cold)+(delta_wall_condevap/k_al)+(1/alpha_warm))

END "Procedure"
"-----"

PROCEDURE
heattransferic(m_dot_co2;m_dot_water_ic;T_water_in;P[3];T[3];P[4];T[4];T_re
f_avg_ic;T_w_avg_ic;w_plate_ic;x_plate_ic:U_ic)
"!Overall heat transfer coefficient for condenser/gas cooler . Forced flow
on both sides"

$ARRAY ON
W$='Water'
R$='R744'
delta_wall_ic=1 [mm]*convert(mm;m)
k_ss=Conductivity(Stainless_AISI302; T=17)
d_e=7 [mm]*convert(mm;m)

"Cold side"
P_cold=101,325 [kPa]
k_cold=Conductivity(W$;T=T_water_in;P=P_cold)
mu_cold=Viscosity(W$;T=T_water_in;P=P_cold)
mu_wall_water=viscosity(W$;T=(T_ref_avg_ic+T_w_avg_ic)/2;P=P_cold+0,01)
A=(d_e)*w_plate_ic*0,5*x_plate_ic
G=m_dot_water_ic/A
Pr_cold=Prandtl(W$;T=T_water_in;P=P_cold)
Re_cold=(G*d_e)/mu_cold

"Martin correlation for one-phase flow water"
beta_cold=45
f0_martin_cold = 64/Re_cold{(1,8*log10(Re_cold)-1,5)^(-2)}"parameter for
friction factor calculation"
f1_martin_cold=
597/Re_cold+3,85{39/(Re_cold^0,289)} "parameter for friction factor
calculation"
f_martin_cold=(1 /
(cos(beta_cold)/sqrt(0,18*tan(beta_cold)+0,36*sin(beta_cold)+(f0_martin_col
d/cos(beta_cold))) + ((1-cos(beta_cold))/(sqrt(3,8*f1_martin_cold)))) )^2
"friction factor"
Nusselt_cold=0,122*(Pr_cold^(1/3))*((mu_cold/mu_wall_water)^(1/6))*(f_marti
n_cold*(Re_cold^2)*sin(2*beta_cold))^0,374 "Nusselt number"

```

```

alpha_cold = (Nusselt_cold*k_cold)/d_e      "heat transfer coefficient water"

"Warm side"
k_warm_i=Conductivity(R$;P=P[3];T=T[3])
k_warm_o=Conductivity(R$;P=P[4];T=T[4])
k_avg=(k_warm_i+k_warm_o)/2
mu_warm_i=Viscosity(R$;P=P[3];T=T[3])
mu_warm_o=Viscosity(R$;P=P[4];T=T[4])
mu_avg=(mu_warm_i+mu_warm_o)/2
mu_wall_ref=viscosity(R$;T=(T_ref_avg_ic+T_w_avg_ic)/2;P=P_cold+0,01)
G_warm=m_dot_co2/A
Pr_warm=Prandtl(R$;T=(T[3]+T[4])/2;P=P[3])
Re_warm=(G_warm*d_e)/mu_avg

"Martin correlation for one-phase co2 flow"
beta_warm=45
f0_martin = (1,8*log10(Re_warm)-1,5)^(-2) "parameter for friction factor
calculation"
f1_martin= 39/(Re_warm^0,289)           "parameter for friction factor
calculation"
f_martin=(1 /
(cos(beta_warm)/sqrt(0,18*tan(beta_warm)+0,36*sin(beta_warm)+(f0_martin/cos
(beta_warm))) + ((1-cos(beta_warm))/(sqrt(3,8*f1_martin)))) )^2
"friction factor"
Nusselt_w=0,122*(Pr_warm^(1/3))*((mu_avg/mu_wall_ref)^(1/6))*(f_martin*(
(Re_warm^2)*sin(2*beta_warm)))^0,374 "Nusselt number"
alpha_warm= (Nusselt_w*k_avg)/d_e      "heat transfer coefficient water"
U_ic=1/((1/alpha_cold)+(delta_wall_ic/k_ss)+(1/alpha_warm))

END "Procedure"
"-----"

"-----"
"!Calling procedures to get arrays"

CALL
flakeicedrum(T_evap_flake;m_co2_fl_real;T_water_in;m_w;x_pipe;Q_water:U1[1]
;U1_avg)

"-----"
General information
"-----"

R$='R744'           "Refrigerant string"
W$='water'         "Water string"

"!Ambient temperature"
$ifNot Parametric table
T_amb=20 [C]       "Ambient temperature 5-20 degC"
$Endif

DELTAT_cond=5 [K] "DeltaT in condenser"
T_cond=T_amb+DELTAT_cond "Condenser temperature"

"-----"
Flake ice machine and lower part of the system. Solution by control
volume
"-----"
{Controll volume: Flake ice maker}

m_ice=50000 [kg]   "Production capacity"

```



```

rho_ice=density(Ice;T=0;P=101,325)           "Density ice"
V_ice=m_ice/rho_ice
V_dot_ice=V_ice/(3600*24)
m_w=V_dot_ice*rho_ice                       "Water consumption"
T_water_in= 5 [C]                           "Temperature of inlet water"
DELTAT_sc_w=7 [C]                           "Subcooling of ice"
c_P_w_lq=specheat(W$;T=T_water_in;x=0)      "Specific heat liquid water"
h_fusion_w=enthalpy_fusion(W$)             "Enthalpy of fusion"
c_P_w_s=specheat(W$;T=-1;x=0)              "Specific heat vapour water"

"!Heat transfered from water to CO2"
Q_water = m_w*(c_P_w_lq*(T_water_in) + h_fusion_w + c_P_w_s*(DELTAT_sc_w))
"Heat removed from water"

"!CO2 flake ice machine"
T_evap_flake=-30 [C]                        "Evaporation temperature Flake
ice drum"
P_evap_flake=P_sat(R$;T=T_evap_flake)      "Evaporation pressure"
m_co2_fl_real=2 [kg/s]                     "Actual flow rate flake ice
drum"
h_fl_co2_in=enthalpy(R$;P=P_evap_flake;x=0)
    "Inlet enthalpy"
h_fl_co2_out=h_fl_co2_in+Q_water/m_co2_fl_real
    "Outlet enthalpy"
x_fl_co2_out=quality(R$;P=P_evap_flake;h=h_fl_co2_out) "Gas quality flake
ice outlet"

"!Pressure drop Flake ice maker"
d_flake=2,5 [m]                             "Diameter flake ice drum"
h_flake=2,6 [m]                             "Height flake ice drum"
mu_fl=Viscosity(R$;T=T_evap_flake;h=h_fl_co2_in)
    "Dynamic viscosity flake ice drum inlet"
rho_fl=Density(R$;T=T_evap_flake;h=h_fl_co2_in)
    "Density flake ice drum inlet"
d_pipe=5 [mm]*convert(mm;m)                 "Refrigerant pipe diameter"
x_pipe=300                                 "Number of refrigerant pipes"
A_o_flake=x_pipe*((d_pipe^2*pi)/4)          "Core flow area"
G_fl=(m_co2_fl_real)/A_o_flake              "Mass flux through the core"
sigma_fl_cold=SurfaceTension(R$;T=T_evap_flake)
    "Surface tension"
rho_fl_f=Density(R$;T=T_evap_flake;x=0)     "Density liquid"
rho_fl_g=Density(R$;T=T_evap_flake;x=1)     "Density gas"
x_m_fl=(x_fl_co2_out+0)/2                   "Average gas quality"
rho_fl_m=(x_m_fl/rho_fl_g+(1-x_m_fl)/rho_fl_f)^(-
1) "Mean density"
We_fl_m=(G_fl^2*d_e)/(rho_fl_m*sigma_fl_cold)
    "Weber number"
Bd_fl_m=((rho_fl_f-
rho_fl_g)*g*d_e^2)/sigma_fl_cold           "Bond number"
rho_fl_ast=(rho_f/rho_fl_g)                 "Density ratio liquid/gas"
beta_fl_ast=45/70                           "ratio beta/beta_max"
C_fl=2,125*beta_fl_ast^9,993+0,955         "Correlation factor"
f_fl=C*15,698*We_fl_m^(-0,475)*Bd_fl_m^0,255*rho_fl_ast^(-0,571)
"Frictional pressure drop factor"

DELTAP_flake_fr=2*f_fl*(h_plate*G_fl^2)/(d_e*rho_fl_m)
    "Pressure drop. Friction"
DELTAP_flake_g=rho_fl_m*g*h_plate           "Pressure drop. Gravitational"
DELTAP_flake_acc=G_fl*(x_fl_co2_out-0)*(1/rho_fl_g-1/rho_fl_f) "Pressure
drop. Acceleration/Deceleration"
DELTAP_flake_p=0,75*((G_p)^2/rho_fl_m)      "Manifold pressure drop"

```

```
DELTAP_flake=(DELTAP_flakep+DELTAP_flakeacc+DELTAP_flakeg+DELTAP_flakef  
r)*convert(Pa;kPa) "Total pressure drop"
```

```
Pa=Pevap_flake-33,5{DELTAP_flake}
```

```
{Controll volume: Pipe flake ice drum to Liquid drum}
```

```
"!Pipe Information"
```

```
eab=0,000015[m] {Roughness, Drawn Tubing}  
Dab=4,2[cm]*convert(cm;m) {Pipe Diameter}  
RRab=eab/Dab {Relative Roughness}  
Lab=1 [m] {Length of pipe}
```

```
"!Pressure drop"
```

```
call
```

```
PipeFlow(R$;Tevap_flake;Pa+0,01;mco2_flreal;Dab;Lab;RRab:{hTab};  
{hHab} ;DELTAPab; {NusseltTab}; fab; Reab)
```

```
Pb1=Pa-DELTAPab
```

```
Tb1=temperature(R$;P=Pb1;h=hflco2out)
```

```
{Controll volume: Liquid drum}
```

```
"Assuming no pressure drop in liquid tank"
```

```
mdotcond=xflco2out*mco2_flreal "Gas mass flow condenser"
```

```
Pliqdrum=Pb1
```

```
Tliqdrum=Tsat(R$;P=Pliqdrum)
```

```
hb=enthalpy(R$;P=Pliqdrum+0,01;x=1)
```

```
{Controll volume: Pipe Liquid drum to cond/evap}
```

```
"!Pipe Information"
```

```
ebc=0,000015[m] {Roughness, Drawn Tubing}  
Dbc=4,2[cm]*convert(cm;m) {Pipe Diameter}  
RRbc=ebc/Dbc {Relative Roughness}  
Lbc=1 [m] {Length of pipe}
```

```
"!Pressure drop"
```

```
call
```

```
PipeFlow(R$;Tliqdrum;Pliqdrum+0,01;mdotcond;Dbc;Lbc;RRbc:{hTbc};  
{hHbc} ;DELTAPbc; {NusseltTbc}; fbc; Rebc)
```

```
Pc=Pliqdrum-DELTAPbc
```

```
Tc=temperature(R$;P=Pc;h=hflco2out)
```

```
{Controll volume: Evaporator/Condenser}
```

```
DELTATevapcond=5 [K]
```

```
Tevap = Tc-DELTATevapcond
```

```
hc=hb
```

```
"!Pressure drop evap/cond warm side"
```

```
mucd=Viscosity(R$;T=Tc;P=Pc+0,01) "Dynamic viscosity"
```

```
rhocdi=Density(R$;P=Pc+0,01;x=1)
```

```
rhocdo=Density(R$;P=Pc+0,01;x=0)
```

```
rhocd=(rhocdo+rhocdi)/2 "Average density"
```

```
Dpcd=22 [mm]*convert(mm;m) "Port inlet"
```

```
Gpcd=(mdotcond)/((pi/4)*Dpcd2) "Mass velocity through the port"
```

```
Gcd=(mdotcond)/Aoevapcond "Massvelocity through the core"
```

```
DELTAPcdg = rhocd*g*hplate "gravity driven acceleration"
```

```
DELTAPcdacc = (Gcd2)*1*( (1/rhocdi) - (1/rhocdo)) "acceleration  
pressure, quality change is 1"
```

```
DELTAPcdp = 0,75*(Gpcd2)/rhocd "inlet/outlet pressure loss"
```

```

DELTAP_cd_fr = (1,9*G_cd^2)/(2*rho_cd)      "kinetic model from Longo 2010"
DELTAP_cd = (DELTAP_cd_fr+DELTAP_cd_p - DELTAP_cd_acc - DELTAP_cd_g)/1000

P_d=P_c-DELTAP_cd
h_d=h_c-Q_water/m_dot_cond                "Outlet enthalpy"
T_d=temperature(R$;P=P_d;h=h_d)           "Outlet temperature"

{Controll volume: Pipe evaporator/condenser to liquid drum}
"!Pipe Information"
e_de=0,000015[m]                          {Roughness, Drawn Tubing}
D_de=2,2[cm]*convert(cm;m)                {Pipe Diameter}
RR_de=e_de/D_de                           {Relative Roughness}
L_de=1 [m]                                {Length of pipe}

"!Pressure drop"
call PipeFlow(R$;T_d;P_d+0,01;m_dot_cond;D_de;L_de;RR_de:{h_T_de}; {h_H_de}
;DELTAP_de; {Nusselt_T_de}; f_de; Re_de)

P_e=P_d-DELTAP_de
T_e=temperature(R$;P=P_e;h=h_d)

{Controll volume: Pipe liquid drum to pump}
"!Pipe Information"
e_ef=0,000015[m]                          {Roughness, Drawn Tubing}
D_ef=4,2[cm]*convert(cm;m)                {Pipe Diameter}
RR_ef=e_ef/D_ef                           {Relative Roughness}
L_ef=1 [m]                                {Length of pipe}

"!Pressure drop"
call PipeFlow(R$;T_e;P_e+0,01;m_co2_fl_real;D_ef;L_ef;RR_ef:{h_T_ef};
{h_H_ef} ;DELTAP_ef; {Nusselt_T_ef}; f_ef; Re_ef)

P_f=P_e-DELTAP_ef
T_f=temperature(R$;P=P_f;h=h_d)

{Controll volume: CO2-pump}
N_co2_pump=930[1/min]*convert(1/min;1/s)  "RPM pump"
D_co2_pump=0,15 [m]                       "Diameter pump"
D_hub_co2=0,08[m]                         "Diameter pump hub"

Call CentrifugalPump1_CL( R$; 0; T_f; P_f+0,01;m_co2_fl_real; N_co2_pump;
D_co2_pump; D_hub_co2: P_g; T_g; W_co2_pump; eta_co2_pump)

{Controll volume: Pipe pump ot flake ice drum}
"!Pipe Information"
e_g=0,000015[m]                          {Roughness, Drawn Tubing}
D_g=2,2[cm]*convert(cm;m)                {Pipe Diameter}
RR_g=e_g/D_g                             {Relative Roughness}
L_g=1 [m]                                {Length of pipe}

"!Pressure drop"
call PipeFlow(R$;T_g;P_g+0,01;m_co2_fl_real;D_g;L_g;RR_g:{h_T_g}; {h_H_g}
;DELTAP_g; {Nusselt_T_g}; f_g; Re_g)

P_g_fl=P_g-DELTAP_g
T_g_fl=temperature(R$;P=P_g_fl;x=0)
"-----
-----
State points in heat pump. Solution by control volume
-----
-----"

```

```

m_dot_co2=(Q_water)/(h[14]-h[13])           "Mass flow CO2 in Refrigeration
system"

{State 1 to state 2}
{Controll volume: Compressor}
"!State points 1: Compressor inlet"
h[1]=h[16]                                   "Enthalpy"
x[1]=quality(R$;h=h[1];P=P[1])              "Gas quality"
T[1]=temperature(R$;P=P[1];h=h[1])          "Temperature"
s[1]=entropy(R$;h=h[1];P=P[1])              "Entropy"
eta_IS=-0,00000461*PR_12^6+0,00027131*PR_12^5-
0,00628605*PR_12^4+0,07370258*PR_12^3-0,46054399*PR_12^2+1,40653347*PR_12-
0,87811477                                   "Compressor isentropic
efficiency"
lambda=0,0011*PR_12^2-0,0487*PR_12+0,9979 "Compressor volumetric
efficiency"
HL=0,1 [-]                                   "Relative heat loss i compressor,
% of input power"
rho[1]=density(R$;T=T[1];P=P[1])            "Density"
V_s_1=((0,33*m_dot_co2)/(rho[1]*lambda))*3600[s/h]
      "Suction volume of low stage compressor per compressor"
V_s_1_tot=((m_dot_co2)/(rho[1]*lambda))*3600[s/h]
      "Suction volume of low stage compressor"
"!State points 2: Compressor outlet"
P[2]=sqrt(P[1]*P[6])
h[2]=h[1]+DELTAW_12*(1-HL)                   "Energy balance on real
compressor-assumed adiabatic"
s[2]=entropy(R$;h=h[2];P=P[2])              "Entropy"
T[2]=temperature(R$;h=h[2];P=P[2])          "Discharge gas temperature"
T_2_sat=T_sat(R$;P=P[2])                    "Saturation temperature"
h_2_IS=enthalpy(R$;P=P[2];s=s[1])           "Isentropic enthalpy"
w_IS=(h_2_IS-h[1])                           "Energy balance on isentropic
compressor"
DELTAW_12=w_IS/eta_IS                        "Real compressor entalphy
difference"
T_discharge=T[2]                             "Discharge gas temperatur"
x[2]=quality(R$;h=h[2];T=T[2])              "Gas quality"
Q_loss=((h[2]+DELTAW_12)-(h[2]+DELTAW_12*(1-HL)))*m_dot_co2 "Heat loss in
compression"
W_comp_1=0,33*m_dot_co2*(DELTAW_12)         "Compressor work, per compressor"
PR_12=P[2]/P[1]                               "Pressure ratio"
nu[2]=volume(R$;T=T[2];P=P[2])              "Specific volume at low stage
compressor inlet"
"-----"

{State 2 to state 3}
{Control Volume : Connecting Pipe}

"!Pipe Information"
e_23=0,000015[m]                             {Roughness, Drawn Tubing}
D_23=4,2[cm]*convert(cm;m)                   {Pipe Diameter}
RR_23=e_23/D_23                               {Relative Roughness}
L_23=1 [m]                                    {Length of pipe}

"!Pressure drop"
call PipeFlow(R$;T[2];P[2]+0,01;m_dot_co2;D_23;L_23;RR_23:{h_T_23};
{h_H_23} ;DELTAP_23; {Nusselt_T_23}; f_23; Re_23)

P[3]=P[2]-DELTAP_23
"-----"

```

```

{State 3 to state 4}
{Control Volume : Intercooler}
"!State 3 : Intercooler inlet"
h[3]=h[2]
T[3]=temperature(R$;h=h[3];P=P[3])
x[3]=quality(R$;h=h[3];T=T[3])
s[3]=entropy(R$;h=h[3];T=T[3])
mu[3]=viscosity(R$;P=P[3];h=h[3])
rho[3]=density(R$;P=P[3];h=h[3])
"!Pressure drop and size of intercooler"
CALL
heattransferic(m_dot_co2;m_dot_water_ic;T_water_in;P[3];T[3];P[4];T[4];T_ref_avg_ic;T_w_avg_ic;w_plate_ic;x_plate_ic:U_ic)

m_dot_water_ic=2 [kg/s] "Water mass flow"
T_out_ic=T_water_in+Q_ic/(m_dot_water_ic*C_p_w)
    "Water outlet temperature"
T_w_avg_ic=(T_water_in+T_out_ic)/2 "Average water
temperature"
Q_ic=(m_dot_co2/2)*(h[3]-h[4]) "Heat transferred in IC"
T_ref_avg_ic=(T[3]+T[4])/2 "Average CO2 temperature"

dt_1_ic=T[4]-T_water_in
dt_2_ic=T[3]-T_out_ic
DELTAT_ic_lmtd=((dt_1_ic)-(dt_2_ic))/ln((dt_1_ic)/(dt_2_ic)) "LMTD in
Intercooler"

UA_ic=Q_ic/DELTAT_ic_lmtd "Conductance"
U_ic_1=549,3 [W/m^2*K] "Guessed U-value"
A_ic=(UA_ic*1000)/U_ic_1 "Area IC"
w_plate_ic=90 [mm]*convert(mm;m) "Alfa Laval AC120EQ"
h_plate_ic=269 [mm]*convert(mm;m) "Alfa Laval AC120EQ"
x_plate_ic=ROUND(A_ic/(2*w_plate_ic*h_plate_ic))
    "Number of HX plates"

"!Pressure drop"
mu_ic=(mu[3]+mu[4])/2 "Average dynamic viscosity"
rho_ic=(rho[3]+rho[4])/2 "Average density"

G_p_ic=(m_dot_co2)/((pi/4)*D_p^2) "Mass velocity through the port"
A_o_ic=0,5*x_plate_ic*w_plate_ic*d_e "Flow area"
G_ic=(m_dot_co2)/A_o_ic "Mass velocity through the core"
Re_ic=((G_ic*D_e)/mu_ic) "Reynolds number"
f_ic=0,8*Re_ic^(-0,25) "Friction factor"

DELTAP_g_ic = rho_ic*g*h_plate_ic "gravity driven acceleration"
DELTAP_p_ic = 0,75*(G_p_ic^2)/rho_ic "inlet/outlet pressure loss"
DELTAP_fr_ic =
2*f_ic*(h_plate_ic*G_ic^2)/(d_e*rho_ic) "Frictional pressure drop"
DELTAP_ic = (DELTAP_fr_ic+DELTAP_p_ic - DELTAP_g_ic)/1000

P[4]=P[3]-DELTAP_ic

"!State 4: Intercooler outlet"
T[4]=T_water_in+5
h[4]=enthalpy(R$;P=P[4];T=T[4])
s[4]=entropy(R$;P=P[4];h=h[4])
mu[4]=viscosity(R$;P=P[4];h=h[4])
rho[4]=density(R$;P=P[4];h=h[4])
"-----"

```

```

{State 4 to state 5}
{Control Volume : Connecting Pipe}

"!Pipe Information"
e_45=0,000015[m]           {Roughness, Drawn Tubing}
D_45=4,2[cm]*convert(cm;m) {Pipe Diameter}
RR_45=e_45/D_45           {Relative Roughness}
L_45=1 [m]                {Length of pipe}

"!Pressure drop"
call PipeFlow(R$;T[4];P[4]+0,01;m_dot_co2;D_45;L_45;RR_45:{h_T_45};
{h_H_45} ;DELTAP_45; {Nusselt_T_45}; f_45; Re_45)

P[5]=P[4]-DELTAP_45
"-----"

{State 5 to state 6}
{Controll volume: Compressor 2}
"!State points 5: Compressor inlet"
h[5]=h[4]
x[5]=quality(R$;h=h[5];P=P[5])
T[5]=temperature(R$;P=P[5];h=h[5])
s[5]=entropy(R$;h=h[5];P=P[5])

"!State points 6: Compressor outlet"
eta_IS_56=-0,00000461*PR_56^6+0,00027131*PR_56^5-
0,00628605*PR_56^4+0,07370258*PR_56^3-0,46054399*PR_56^2+1,40653347*PR_56-
0,87811477 "Compressor efficiency"
lambda_56=0,0011*PR_12^2-0,0487*PR_12+0,9979
P[6]=P_sat(R$;T=T_cond)+0,01
h[6]=h[5]+DELTAW_56*(1-HL)           "Energy balance on real
compressor-assumed adiabatic"
s[6]=entropy(R$;h=h[6];P=P[6])
T[6]=temperature(R$;h=h[6];P=P[6])   "Discharge gas temperature"
h_6_IS=enthalpy(R$;P=P[6];s=s[5])    "Isentropic enthalpy"
w_6_IS=(h_6_IS-h[5])                 "Energy balance on isentropic
compressor"
DELTAW_56=w_6_IS/eta_IS_56           "Real compressor entalphy
difference"
T_discharge_comp_2=T[6]              "Discharge gas temperatur"
x[6]=quality(R$;h=h[6];T=T[6])       "Gas quality"
Q_loss_56=((h[6]+DELTAW_56)-(h[6]+DELTAW_56*(1-HL)))*m_dot_co2 "Heat loss
in compression"

W_comp_2=0,5*m_dot_co2*(DELTAW_56)    "Compressor work"
PR_56=P[6]/P[5]                      "Pressure ratio"
rho[5]=density(R$;T=T[5];P=P[5])     "Density"
V_s_2=((0,5*m_dot_co2)/(rho[5]*lambda_56))*3600[s/h]
" Suction volume of high stage compressor, per compressor"
V_s_2_tot=((m_dot_co2)/(rho[5]*lambda_56))*3600[s/h]
" Suction volume of high stage
compressor"
nu[5]=volume(R$;T=T[5];P=P[5])       "Specific volume at high stage
compressor inlet"

"-----"

"!Pipe Information"
e_67=0,000015[m]           {Roughness, Drawn Tubing}
D_67=3,2[cm]*convert(cm;m) {Pipe Diameter}
RR_67=e_67/D_67           {Relative Roughness}
L_67=1 [m]                {Length of pipe}

```

```

"!Pressure drop"
call PipeFlow(R$;T[6];P[6];m_dot_co2;D_67;L_67;RR_67:{h_T_67}; {h_H_67}
;DELTAP_67; {Nusselt_T_67}; f_67; Re_67)

P[7]=P[6]-DELTAP_67
"-----"

{State 7 to state 8}
{Controll volume: Condenser}
"!State 7 : Condenser Inlet"
h[7]=h[6]
T[7]=temperature(R$;h=h[7];P=P[7])
x[7]=quality(R$;h=h[4+3];T=T[7])
s[7]=entropy(R$;h=h[7];T=T[7])
rho[7]=Density(R$;T=T[7];P=P[7]+0,01)
mu[7]=Viscosity(R$;T=T[7];P=P[7]+0,01)
h_sat_sh=enthalpy(R$;P=P[7];x=1)
mu_sat_sh=Viscosity(R$;P=P[7];x=1)
rho_sat_sh=density(R$;P=P[7];x=1)

Q_cond=m_dot_co2*(h_sat_sh-h[8])           "Condensation heat"
Q_sh=(m_dot_co2)*(h[7]-h_sat_sh)         "Superheat"

"!Pressure drop and size of Superheat heat exchangers"
"Size superheat HX 1"
CALL
heattransfersh(m_dot_co2;m_dot_water_sh;T_water_in;T_cond;T[7];T_out_suh_1;
T_ref_avg;T_w_avg;w_plate_sh;x_plate_sh:U_sh)

m_dot_water_sh= 10 [kg/s]
T_out_sh_1=T_water_in+Q_sh/(m_dot_water_sh*C_p_w)
T_w_avg=(T_water_in+T_out_sh_1)/2
T_out_suh_1=Temperature(R$;P=P[7];x=1)
T_ref_avg=(T[7]+T_out_suh_1)/2

dt_o_sh=T_out_suh_1-T_water_in
dt_i_sh=T[7]-T_out_sh_1
DELTAT_sh=((dt_o_sh)-(dt_i_sh))/ln((dt_o_sh)/(dt_i_sh)) "LMTD in condenser"

U_sh_1=384 [W/m^2*K]           "Guessed U-value"
UA_sh_1=Q_sh/DELTAT_sh        "Conductance"
A_sh=(UA_sh_1*1000)/U_sh_1     "HX area"
w_plate_sh=150 [mm]*convert(mm;m) "Alfa Laval AXP112"
h_plate_sh= 519 [mm]*convert(mm;m) "Alfa Laval AXP112"
x_plate_sh=ROUND(A_sh/(2*h_plate_sh*w_plate_sh))
      "Number of plates HX"

"!Pressure drop"
mu_sh=(mu_sat_sh+mu[7])/2     "Average dynamic viscosity"
rho_sh=(rho_sat_sh+rho[7])/2  "Average density"

G_p_sh=(m_dot_co2)/((pi/4)*D_p^2) "Mass velocity through the port"
A_o_sh=0,5*x_plate_sh*w_plate_sh*d_e "Flow area"
G_sh=(m_dot_co2)/A_o_sh       "Mass velocity through the core"
Re_sh=((G_sh*D_e)/mu_sh)       "Reynolds number"
f_sh=0,8*Re_sh^(-0,25)        "Friction factor"

DELTAP_sh_g = rho_sh*g*h_plate_sh "gravity driven acceleration"
DELTAP_sh_p= 0,75*(G_p_sh^2)/rho_sh "inlet/outlet pressure loss"

```

```

DELTAp_sh_fr = 2*f_sh*(h_plate_sh*G_sh^2)/(d_e*rho_sh) "Frictional pressure drop"
DELTAp_sh = (DELTAp_sh_fr+DELTAp_sh_p + DELTAp_sh_g)/1000

"!Pressure drop and size of condenser\gas cooler"
C_p_w=Cp('water';P=P_amb;T=T_water_in)
P_amb=101,325 [kPa]
m_dot_water=10 [kg/s]
T_out_cond=T_water_in+Q_cond/(m_dot_water*C_p_w)
T_w_cond_avg=(T_water_in+T_out_cond)/2

"Size"
CALL
heattransfercond(m_dot_co2;m_dot_water;T_water_in;T_cond;T_w_cond_avg;w_plate_cond;x_plate_cond:U_cond)

dt_o=T[8]-T_water_in
dt_i=T_out_suh_1-T_out_cond
DELTAT_cond_lmtd=((dt_o)-(dt_i))/ln((dt_o)/(dt_i)) "LMTD in condenser"

U_cond_1=1277 [W/m^2*K] "Guessed U-value"
UA_cond=Q_cond/DELTAT_cond_lmtd "Conductance"
A_cond=(UA_cond*1000)/U_cond_1 "HX area"
w_plate_cond=150 [mm]*convert(mm;m) "Alfa Laval AXP112"
h_plate_cond=519 [mm]*convert(mm;m) "Alfa Laval AXP112"
x_plate_cond=ROUND(A_cond/(2*h_plate_cond*w_plate_cond)) "Number of HX plates"

"Pressure drop"
mu_cond=(mu_sat_sh+mu[8])/2 "Average dynamic viscosity"
rho_cond=(rho_sat_sh+rho[8])/2 "Average density"

G_p_cond=(m_dot_co2)/((pi/4)*D_p^2) "Mass velocity through the port"
A_o_cond=0,5*x_plate_cond*w_plate_cond*d_e "Flow area"
G_cond=(m_dot_co2)/A_o_cond "Mass velocity through the core"
Re_cond=((G_cond*D_e)/mu_cond) "Reynolds number"
f_cond=0,8*Re_cond^(-0,25) "Friction factor"

DELTAp_cond_g = rho_cond*g*h_plate_cond "gravity driven acceleration"
DELTAp_cond_acc = (G_cond^2)*1*( (1/rho_sat_sh) - (1/rho[8])) "acceleration pressure, quality change is 1"
DELTAp_cond_p = 0,75*(G_p_cond^2)/rho_cond "inlet/outlet pressure loss"
DELTAp_cond_fr = (1,9*G_cond^2)/(2*rho_cond) "kinetic model from Longo 2010"
DELTAp_cond = (DELTAp_cond_fr+DELTAp_cond_p - DELTAp_cond_acc - DELTAp_cond_g)/1000

P[8]=P[7]-(DELTAp_cond+DELTAp_sh)

"!State 8: Condenser Outlet"
x[8]=0
T[8]=T_cond
h[8]=enthalpy(R$;T=T[8];x=x[8])
s[8]=entropy(R$;T=T[8];x=x[8])
rho[8]=Density(R$;T=T[8];P=P[8]+0,01)
mu[8]=Viscosity(R$;T=T[8];P=P[8]+0,01)

"-----"

```



```

{State 8 to state 9}
{Control Volume : Connecting Pipe}

"!Pipe Information"
e_89=0,000015[m]           {Roughness, stainless steel}
D_89=3,2[cm]*convert(cm;m) {Pipe Diameter}
RR_89=e_89/D_89           {Relative Roughness}
L_89=2 [m]                {Length of pipe}

"!Pressure drop"
call PipeFlow(R$;T[8];P[8];m_dot_co2;D_89;L_89;RR_89:{h_T_89}; {h_H_89}
;DELTAP_89; {Nusselt_T_89}; f_89; Re_89)

P[9]=P[8]-DELTAP_89
"-----"

{State 9 to state 10 // State 15 to state 16}
{Controll volume: SGHX}
"!State 9 : SGHX Inlet Hot Side"
h[9]=h[8]
T[9]=temperature(R$;h=h[9];P=P[9])
x[9]=quality(R$;h=h[9];T=T[9])
s[9]=entropy(R$;h=h[9];T=T[9])

"!State 15: SGHX Inlet Cold Side"
h[15]=h[14]
x[15]=quality(R$;P=P[15];h=h[15])
T[15]=temperature(R$;P=P[15];h=h[15])
s[15]=entropy(R$;P=P[15];h=h[15])

Call HeatExchanger2_CL(R$;0; m_dot_co2; h[9]; P[9]; R$; 0; m_dot_co2;
h[15]; P[15]; 30 [C]; 0,005; 0,005: h[10]; P[10]; h[16]; P[16]; Q_dot_SGHX;
eff_SGHX) "30 degrees C difference between hot in and cold out"

DELTAP_sghx_hot=P[9]-P[10]
DELTAP_sghx_cold=P[15]-P[16]

"!Size SGHX"
dt_out=T[10]-T[15]
dt_in=T[9]-T[16]
DELTAT_sghx=((dt_out)-
(dt_in))/ln((dt_out)/(dt_in))           "LMTD in condenser"

T_avg_warm_sghx=(T[10]+T[9])/2
T_avg_cold_sghx=(T[16]+T[15])/2

CALL
heattransferSGHX(m_dot_co2;P[9];T[9];P[10];T[10];P[15];T[15];P[16];T[16];T_
avg_warm_sghx;T_avg_cold_sghx;w_plate_sghx;x_plate_sghx;U_sghx)

UA_sghx=Q_dot_SGHX/DELTAT_sghx           "Conductance"
U_sghx_2=449,7 [W/m^2*K]                 "Guessed U-value"
A_sghx=(UA_sghx*1000)/U_sghx_2          "Area HX"
w_plate_sghx=70 [mm]*convert(mm;m)      "Alfa Laval AXP52"
h_plate_sghx=154 [mm]*convert(mm;m)     "Alfa Laval AXP52"
x_plate_sghx=ROUND(A_sghx/(2*w_plate_sghx*h_plate_sghx)) "number of HX
plates"

"!State 10 : SGHX Outlet Hot Side"
T[10]=temperature(R$;h=h[10];P=P[10])
x[10]=quality(R$;h=h[10];T=T[10])

```

```

s[10]=entropy(R$;h=h[10];T=T[10])

"!State 16 : SGHX Outlet Hot Side"
T[16]=temperature(R$;P=P[16];h=h[16])
x[16]=quality(R$;h=h[16];T=T[16])
s[16]=entropy(R$;h=h[16];T=T[16])

{"Simple SGHX"
h[6]=h[5] - DELTAh_SGHE
P[6]=P[5]

DELTAT_SGHE_SH=10 [C]
P[12]=P[11]
T[12] = T[11] + DELTAT_SGHE_SH           "Temperature in point 12"

DELTah_SGHE = (h[12]-h[11])

DELTah_SGHE2 = h[5]-h[6]                 "Entalphy difference in SGHE"
DELTAT_SGHE_SC=T[5]-T[6]                 "Degree of subcooling"
Q_SGHE = m_dot_co2*(h[5]-h[6])           "Heating capacity of SGHE"
"-----"

{State 10 to state 11}
{Control Volume : Connecting Pipe}

"!Pipe Information"
e_1011=0,000015[m]                       {Roughness, stainless steel}
D_1011=2,2[cm]*convert(cm;m)             {Pipe Diameter}
RR_1011=e_1011/D_1011                    {Relative Roughness}
L_1011=1 [m]                              {Length of pipe}

"!Pressure drop"
call PipeFlow(R$;T[10];P[10];m_dot_co2;D_1011;L_1011;RR_1011:{h_T_1011};
{h_H_1011} ;DELTAP_1011; {Nusselt_T_1011}; f_1011; Re_1011)

P[11]=P[10]-DELTAP_1011

"-----"

{State 11 to state 12}
{Controll volume: Expansion valve}
"!State 11 : Expansion Valve Inlet"
h[11]=h[10]
T[11]=temperature(R$;P=P[11];h=h[11])
s[11]=entropy(R$;T=T[11];h=h[11])
x[11]=quality(R$;h=h[11];T=T[11])

"!State 12 : Expansion Valve Outlet"
h[12]=h[11]
P[12]=P_sat(R$;T=T_evap)
T[12]=temperature(R$;P=P[12];h=h[12])
s[12]=entropy(R$;T=T[12];h=h[12])
x[12]=quality(R$;h=h[12];T=T[12])

"-----"

{State 12 to state 13}
{Control Volume : Connecting Pipe}

"Negliable pressure drop"
P[13]=P[12]

```

```

"-----"
{State 13 to state 14}
{Controll volume: Condenser/evaporator}
"!State 13 : Condenser Inlet"
h[13]=h[12]
T[13]=temperature(R$;h=h[13];P=P[13])
x[13]=quality(R$;h=h[13];s=s[13])
s[13]=entropy(R$;h=h[13];T=T[13])

mu[13]=Viscosity(R$;T=T[13];P=P[13]+0,01)
rho[13]=Density(R$;T=T[13];P=P[13]+0,01)

"!Pressure drop and size of condenser\evaporator"
"Size"
CALL
heattransfercondevap(m_dot_co2;m_co2_fl_real;T_evap;T_evap_flake;x[13];w_pl
ate;h_plate;x_plate;b_plate;U_cond_evap;G_2)

UA_cond_evap=Q_water/DELTAT_evap_cond
U_c_evap=2764 [W/m^2*K]
A_cond_evap=(UA_cond_evap*1000)/U_c_evap
h_plate=519 [mm]*convert(mm;m) "Alfa Laval AC112 plate
dimensions"
w_plate=92 [mm]*convert(mm;m) "Alfa Laval AC112 plate
dimensions"
x_plate=ROUND(A_cond_evap/(2*h_plate*w_plate))
"Number of plates in plate heat exchanger per side"

"!Pressure drop on cold side"
D_p=0,052 [m] "Port diameter"
D_e=0,007 [m] "Equivalent diameter"
b_plate=0,0035 [m] "Channel spacing"
mu_i=(mu[13]+mu[14])/2 "Average dynamic viscosity"
rho_i=(rho[13]+rho[14])/2 "Average density"
g_c=1 "Proportionality factor, 1 when
SI units"
n_p=1 "Number of passes per plate"
g=9,81 [m/s^2] "Gravitational constant"

G_p=(m_dot_co2)/((pi/4)*D_p^2) "Mass velocity through the port"
A_o_evap_cond=0,5*x_plate*w_plate*D_e "Flow area"
sigma_cold=SurfaceTension(R$;T=T_evap) "Surface tension"
rho_f=Density(R$;T=T_evap;x=0) "Density. Liquid"
rho_g=Density(R$;T=T_evap;x=1) "Density. Gas"
x_m=(x[13]+x[14])/2 "Average gas quality"
rho_m=(x_m/rho_g+(1-x_m)/rho_f)^(-1) "Mean density"
We_m=(G_2^2*d_e)/(rho_m*sigma_cold) "Weber number"
Bd_m=((rho_f-rho_g)*g*d_e^2)/sigma_cold "Bond number"
rho_ast=(rho_f/rho_g) "Density ratio. liquid/gas"
beta_ast=45/70 "ratio beta/beta_max"
C=2,125*beta_ast^9,993+0,955 "Correlation factor"
f_tp=C*15,698*We_m^(-0,475)*Bd_m^0,255*rho_ast^(-0,571) "Two-phase friction
factor"

DELTAP_evap_fr=2*f_tp*(h_plate*G_2^2)/(d_e*rho_m)
DELTAP_evap_g=rho_m*g*h_plate
DELTAP_evap_acc=G_2*(x[14]-x[13])*(1/rho_g-1/rho_f)
DELTAP_evap_p=0,75*((G_p)^2/rho_m)
DELTAP_evap_cond=(DELTAP_evap_p+DELTAP_evap_acc+DELTAP_evap_g+DELTAP_evap_fr)
*convert(Pa;kPa)

```

```

P[14]=P[13]-DELTAP_evap_cond

"!State 14: Evaporator Outlet"
x[14]=1
T[14]=temperature(R$;P=P[14];x=x[14])
h[14]=enthalpy(R$;T=T[14];x=x[14])
s[14]=entropy(R$;T=T[14];x=x[14])
mu[14]=Viscosity(R$;T=T[14];P=P[14]+0,01)
rho[14]=Density(R$;T=T[14];P=P[14]+0,01)

Q_cooling=m_dot_co2*(h[14]-h[13])           "Cooling capacity"

"-----"
{State 14 to state 15}
{Control Volume : Connecting Pipe}

"!Pipe Information"
e_1415=0,000015[m]           {Roughness, stainless steel}
D_1415=2,2[cm]*convert(cm;m) {Pipe Diameter}
RR_1415=e_1415/D_1415       {Relative Roughness}
L_1415=1 [m]                 {Length of pipe}

"!Pressure drop"
call
PipeFlow(R$;T[14];P[15]+100;m_dot_co2;D_1415;L_1415;RR_1415:{h_T_1415};
{h_H_1415} ;DELTAP_1415; {Nusselt_T_1415}; f_1415; Re_1415)

P[15]=P[14]-DELTAP_1415
"-----"

{State 15 to state 16}
{Control Volume : SGHX}

"Calculated above"

"-----"
{State 16 to state 1}
{Control Volume : Connecting Pipe}

"!Pipe Information"
e_161=0,000015[m]           {Roughness, stainless steel}
D_161=4,2[cm]*convert(cm;m) {Pipe Diameter}
RR_161=e_161/D_161         {Relative Roughness}
L_161=1 [m]                 {Length of pipe}

"!Pressure drop"
call PipeFlow(R$;T[16];P[16]+0,01;m_dot_co2;D_161;L_161;RR_161:{h_T_161};
{h_H_161} ;DELTAP_161; {Nusselt_T_161}; f_161; Re_161)

P[1]=P[16]-DELTAP_161
"-----"

"!COP"
W_tot=3*W_comp_1+2*W_comp_2   "Total compressor work"
COP_e=Q_cooling/W_tot         "COP cooling"
COP_gc=(Q_cond+Q_sh+Q_ic)/W_tot "COP heating"
"-----"

```

G. Scientific Paper

Snow Production Equipment at Ambient Temperatures above 0°C

Jon-Brede R. DIESETH^(*)

^(*) Norwegian University of Science and Technology, Department of Energy and Process Engineering,
Kolbjorn Hejes vei 1D, Trondheim, 7049, Norway
jbdieset@stud.ntnu.no

ABSTRACT

Vacuum and flake ice systems with a production capacity of 50 tons/day was modelled in EES, to investigate the thermodynamic performance at different ambient temperatures. The flake ice model shows that SCS consumes less energy than TCS. The U-value and ice growth rate for the FID are highly dependent on the ice thickness, and the ice thickness dictates the heat transfer from water to CO₂. The vacuum model shows that TVS is more efficient than a SVS regardless of the ambient temperature. A vacuum/CO₂-cascade system is more energy intensive. The most efficient vacuum system consumes just 20,8% of the energy required by the least efficient flake ice system. COMSOL calculations reveal that increasing the number of refrigerant pipes in the FID above 200, do not affect the temperature distribution on the freezing surface too much. The thickness can be optimized regarding the structural strength, rather than the heat transfer.

1. INTRODUCTION

In the perspective of increasing global temperatures, it is important to produce snow at temperatures above 0°C to be able to maintain the snow activity close to the cities. Today, temperature independent snow machines(TIS) produce plate ice, flake ice and ice slurry in temperatures above 0°C. There are four manufacturers of TIS, IDE Technologies, TechnoAlpin(TA), SnowTech and SnowMagic Inc. The developed models are based on vacuum and flake ice technology, which uses water and CO₂ as refrigerant, respectively.

1.1. Vacuum ice maker

Water is one of the oldest refrigerants being used for refrigeration applications above 0°C (Kilicarslan and Müller, 2005). It is easily accessible, it is cheap and has excellent thermodynamic and chemical properties. It has ODP and GWP-values equal to zero, it is non-toxic, non-flammable and non-explosive. The low operating pressure of 611,7 Pa in the vacuum process results in a very large specific volume of the water vapour. Therefore, the compressor needs to handle large amounts of gas, which influence the construction of the compressor. The operating principal for the vacuum ice maker is to bring water to triple-point conditions (Orshoven et al., 1993). At triple-point conditions, the water starts to boil and some of it evaporates. The triple-point temperature is 0,01°C. Energy in the shape of heat is released, causing the temperature in the remaining water to decrease. Eventually it will freeze, and create an ice slurry. The latent heat of fusion and vaporization is 333 kJ/kg and 2500 kJ/kg, respectively, which means that the mass of ice produced is 7,5 times the mass of water vapour (Orshoven et al., 1993).

1.2. Flake ice maker with CO₂ refrigeration system

CO₂ was a commonly used working fluid in installations in late 1800's, but due the introduction of CFCs in the 1930s, CO₂ as a working fluid was almost forgotten until the end of the last century. CO₂ is one of the few natural working fluids, which is neither flammable nor toxic. It is widely available, inexpensive and have GWP and OPD-values equal to zero. Flake ice is harvested as dry subcooled ice flakes, typically up to 3 mm thick. The water is fed into a tank above the FID, from which it is evenly sprinkled onto the inner subcooled wall of the FID through a series of distribution tubes, resulting in an ice layer (Cao et al., 2015). The flake ice makers require a refrigeration system, unlike the vacuum system, where the refrigerant temperature is around -30°C.

1.3. Cascade. Vacuum ice maker with CO₂ refrigeration system

A cascade system based on the two latter system. The vacuum system condenses at a constant temperature, while the CO₂ refrigeration system adjusts the condensing temperature according to the ambient temperature. This system reduces the total number of compressors.

2. METHOD

The three simulation models are made in Engineering Equation Solver (EES). The main objective for the simulations is to investigate the thermodynamic performance at different ambient temperatures of the systems. The simulations include component and pipe design with pressure drop.

The area of the water-cooled counter current plate heat exchangers, is calculated based on the known Q , ΔT_{LMTD} and U -values. The number of plates are based on the size of commercially available plate heat exchangers from Alfa Laval.

$$U = \frac{1}{R_{warm} + R_{wall} + R_{cold}} = \frac{1}{\frac{1}{\alpha_{warm}} + \frac{\delta}{k_{wall}} + \frac{1}{\alpha_{cold}}} \quad (1)$$

$$A = \frac{Q}{U \Delta T_{LMTD}} \quad (2)$$

The following correlation is used to calculate the heat transfer coefficient, α_f , for single phase flow in the heat exchangers. (García-Cascales et al., 2007)

$$Nu = \frac{\alpha_f d_e}{k_f} = 0,122 \cdot Pr^{\frac{1}{3}} \cdot \frac{\mu_f^{\frac{1}{6}}}{\mu_{wall}} \cdot (f \cdot Re^2 \cdot \sin(2\beta))^{0,374} \quad (3)$$

The total pressure drop in the heat exchangers is the sum of several smaller pressure drops. To two latter contributions are positive for evaporation, and negative for condensation (Shah and Sekulić, 2007)

$$\Delta P_{tot} = \Delta P_{fric} + \Delta P_{man} \pm \Delta P_{acc} \pm \Delta P_{gr} \quad (4)$$

A built-in function in EES is used to calculate the pipe pressure drops

2.1. Vacuum ice maker

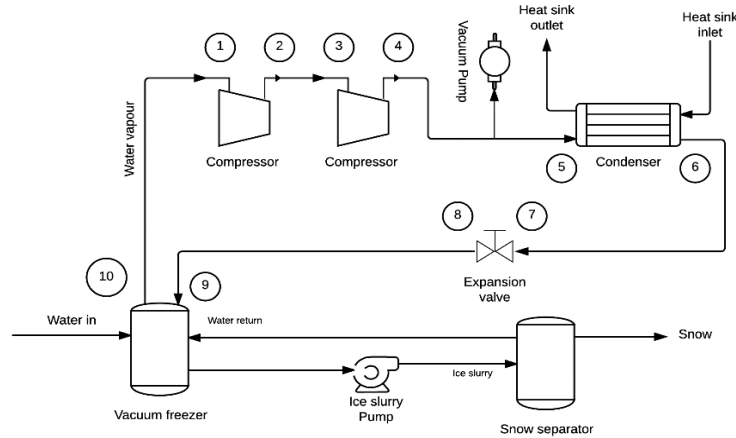


Figure 1 Vacuum ice maker. Two stage

The Knudsen equation (5) calculates the mass flux of vapour, from which the required evaporating surface area can be calculated. A 1 mBar difference between the gas and liquid is assumed (Eames et al., 1997).

$$G = f_{ec} \left(\frac{P_l}{\sqrt{T_l}} - \frac{P_g}{\sqrt{T_g}} \right) \sqrt{\frac{M}{2\pi R}} \rightarrow A_{surface} = \frac{\dot{m}_{gas}}{G} \quad (5)$$

The heat transfer coefficient for condensation of water is presented in equation (6) (Incropera et al., 2013)

$$Nu = \frac{\alpha_w d_e}{k_l} = 0,555 \cdot \left(\frac{\rho_l g (\rho_l - \rho_g) h'_{fg} d_e^3}{\mu_l k_l (T_{cond} + T_w)} \right)^{\frac{1}{4}} \quad (6)$$

2.2. Flake ice maker with CO₂ refrigeration system

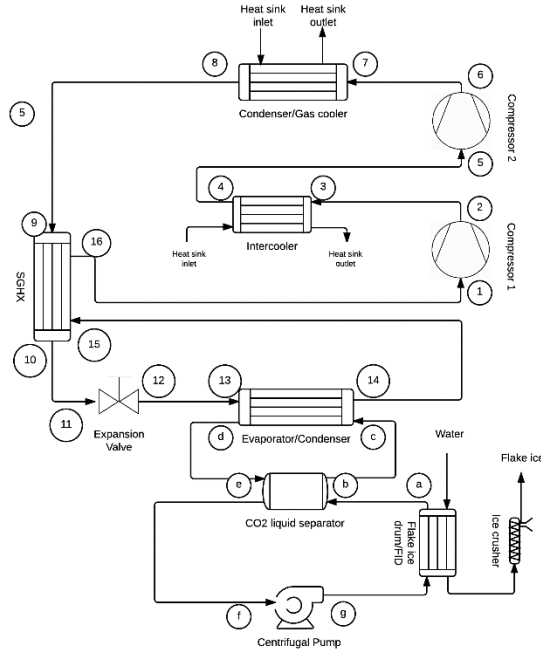


Figure 2 Flake ice maker with CO₂ refrigeration system. Two stage

The FID is a sandwich construction of steel-aluminium-steel, which is 2,6m high and 2,5m in inner diameter. CO₂ runs through 5mm straight pipes in the aluminium part of the structure.

To evaluate the overall heat transfer coefficient for the FID, the CO₂ evaporation heat transfer coefficient is calculated (Choi et al., 2007)

$$\alpha_{evap,CO_2} = S\alpha_{nb} + F\alpha_f \quad (7)$$

The heat transfer coefficient of the water in the FID is calculated by (Incropera et al., 2013)

$$\alpha_w = 0,037 \cdot \frac{k_w}{h} \left(\frac{u_w * h}{\nu_w} - B \right)^{\frac{4}{5}} Pr_w^{\frac{1}{3}} \quad (8)$$

To evaluate when the ice layer thickness on the FID reaches 3mm, the dynamic model ice growth process is modelled by applying heat and mass conservation. The boundary conditions are temperature continuity, eq. (9), and energy conservation, eq. (10).

$$T_i = T_w \quad (9)$$

$$q_{ice} - q_w = \rho_{ice} v_{ice} h_{ice} - \rho_w v_w h_w = 0 \quad (10)$$

Mass conservation, and the conduction and convection equations converts eq. (10) into (11), from which the ice thickness, x , and ice growth rate can be calculated.

$$\frac{T_{ice} - T_{ref}}{\frac{1}{\alpha_{evap,co2}} + \frac{\delta_{al}}{k_{wall}} + \frac{\delta_{sst}}{k_{wall}} + \frac{x}{\alpha_{ice}}} dt = \rho_w L dx + \alpha_w (T_w - T_{ice}) dt \quad (11)$$

The CO₂ condensation heat transfer coefficient in the condenser and condenser/evaporator is calculated by the correlation below, developed by Park and Hrnjak (2009).

$$\alpha_{cond,co2} = \frac{k_f^{\frac{2}{3}} C_{p,f}^{\frac{1}{3}}}{\mu_f^{\frac{1}{15}}} \cdot \left(\frac{1-z}{z} \cdot \left(\frac{\rho_f}{\rho_g} \right)^{0,5} + 1 \right) \quad (12)$$

3. RESULTS

The calculated size of heat exchangers is presented Table 1.

Table 1 Area of heat exchangers

| Heat exchanger | Model | Width [mm] | Height [mm] | # of plates | Q [kW] | \dot{m}_w [kg/s] | U-value [W/m ² K] | ΔT_{LMTD} [K] | Area [m ²] |
|------------------|----------|------------|-------------|-------------|--------|--------------------|------------------------------|-----------------------|------------------------|
| Condenser/evap | AC112 | 92 | 519 | 165 | 213,9 | - | 2764,0 | 5,0 | 15,5 |
| Intercooler | AC120EQ | 90 | 269 | 39 | 16,0 | 2 | 549,3 | 15,5 | 1,9 |
| Superheat HX | AXP112 | 150 | 519 | 62 | 90,4 | 10 | 384,0 | 24,5 | 9,6 |
| Condenser | AXP112 | 150 | 519 | 285 | 185,9 | 15 | 1277,0 | 3,3 | 44,4 |
| SGHX | AXP52 | 70 | 154 | 46 | 15,7 | - | 449,7 | 34,9 | 1,0 |
| Condenser Vacuum | AlfaCond | 1658 | 500 | 4 | 213,2 | 10 | 3243,0 | 11,2 | 5,9 |

Figure 3 presents the energy consumption per m³ produced snow of the systems modelled during the production period from September 1. to November 1.

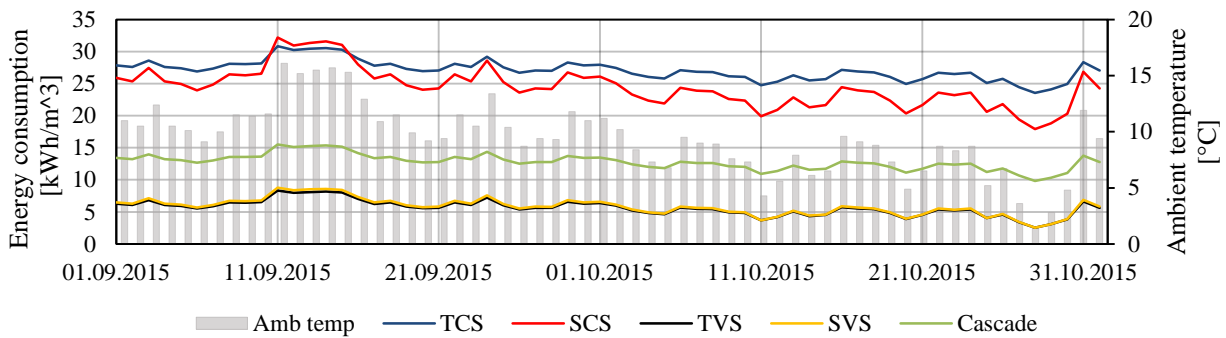


Figure 3 Energy consumption of the different solutions during the production period.

3.1. Vacuum ice maker

Figure 4 shows a comparison of the COP between the vacuum systems. The compressor outlet temperatures and pressure ratio is shown in Figure 5. Both are presented as a function of ambient temperature. The compressor is limited to a pressure ratio of 3.

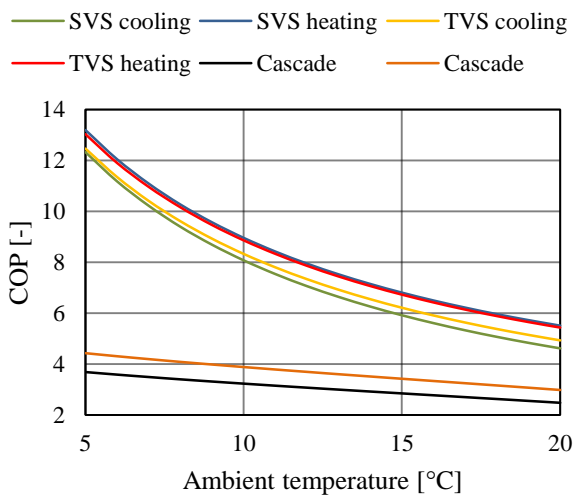


Figure 4 Comparison of COP. Vacuum systems.

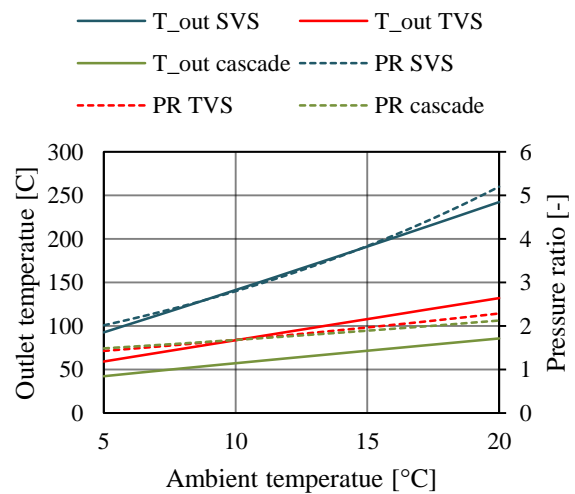


Figure 5 T_{out} and PR vs ambient temperature.

3.2. Flake ice maker with CO₂ refrigeration system

Figure 6 compare the work required for the SCS and TCS in the flake ice machine as a function of the ambient temperature, while Figure 7 shows the compressor outlet temperature and pressure ratio as a function of ambient temperature.

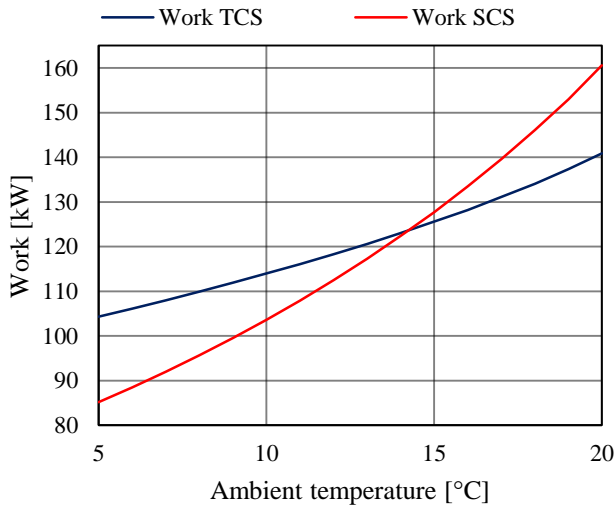


Figure 6 Comparison of work for SCS and TCS. $T_{CO_2} = -30^\circ C$

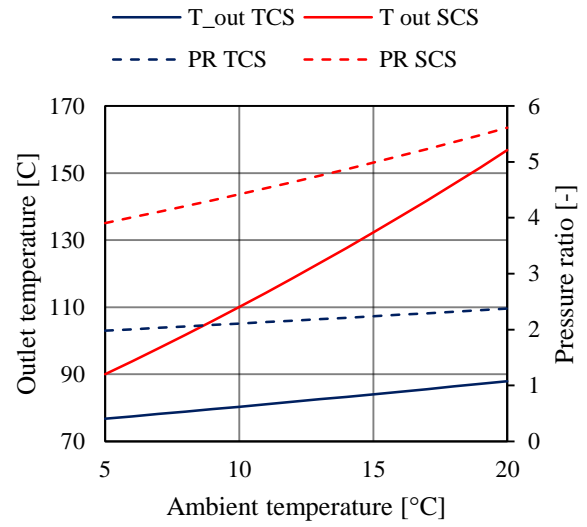


Figure 7 Comparison of outlet temperature and pressure ratio. $T_{CO_2} = -30^\circ C$

In Figure 8, the overall heat transfer coefficient as a function of production time is shown. The ice growth rate as function of time is presented in Figure 9. The figures compare CS, SST and Al as construction material for the FID.

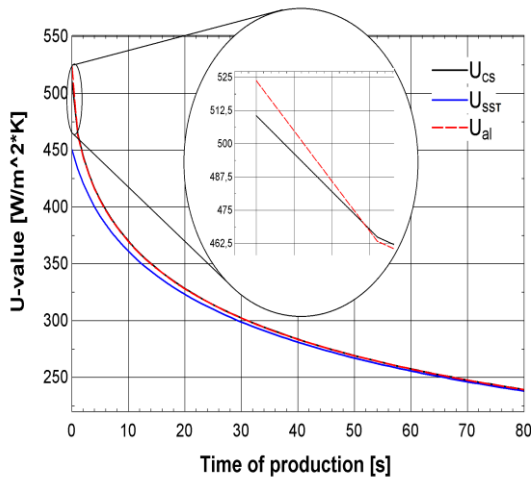


Figure 8 Variation of the overall heat transfer coefficient in the FID. $T_{ref} = -30^\circ C$

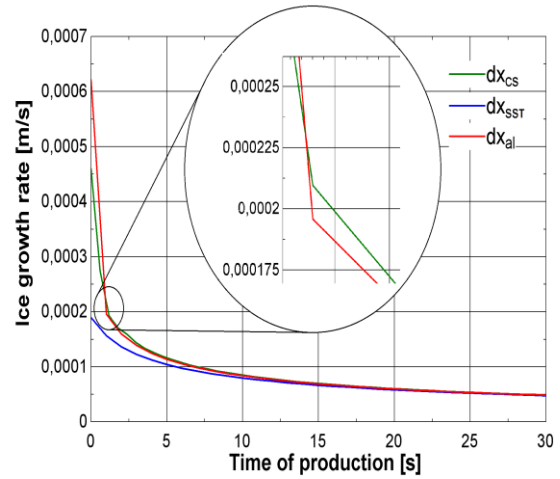


Figure 9 Ice growth rate vs time. $T_{ref} = -30^\circ C$

The temperature distributions for varying width of the model calculated in COMSOL is presented in Figure 10. The temperature distributions are time dependent, but are stabilized within 60 seconds.

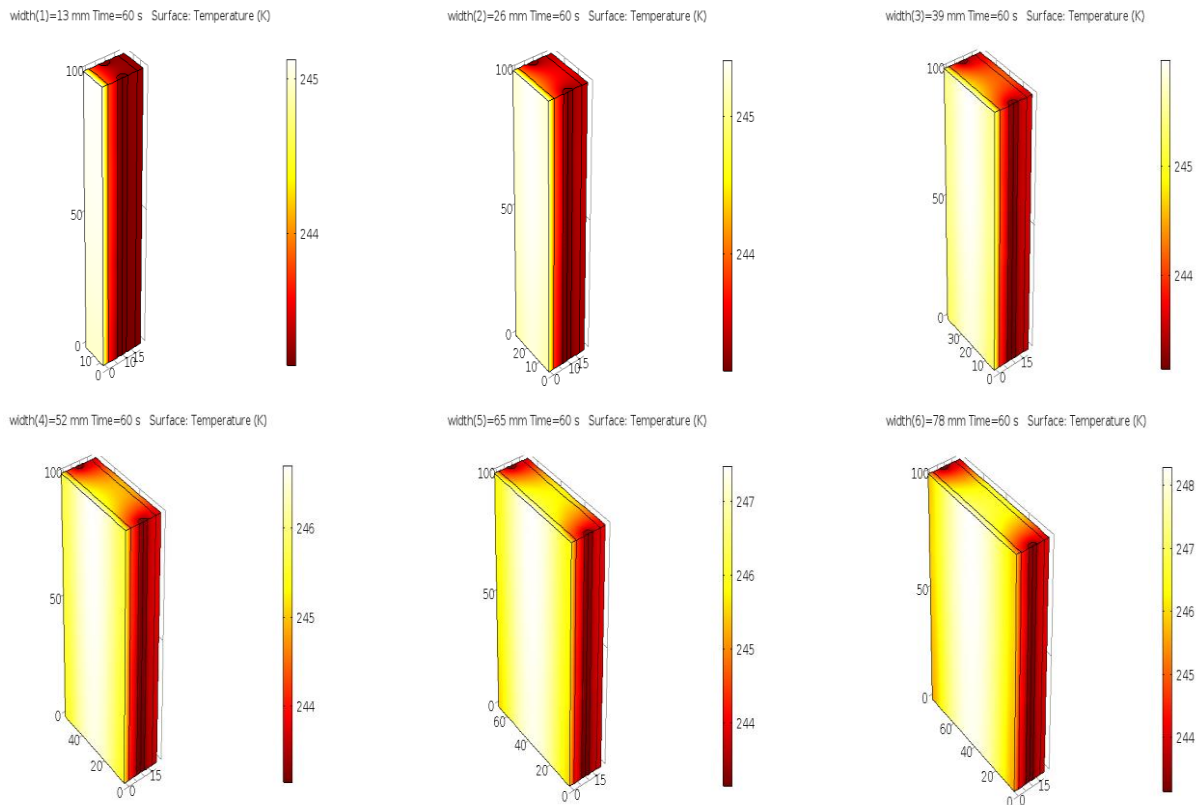


Figure 10 Temperature distribution between the refrigerant pipes with different width. Width: 13mm, 600 pipes. Width: 26mm, 300 pipes. Width: 39mm, 200 pipes. Width: 52mm, 150 pipes. Width: 65mm, 120 pipes. Width: 78mm, 100 pipes. $T_{ref}=-30^{\circ}\text{C}$

4. DISCUSSION

Due to the high enthalpy of vaporization in the vacuum system, the refrigerant mass flow is very low compared to the CO_2 unit in the cascade system. This is the main reason why the vacuum systems have higher COP and consumes less energy than the cascade system. To reduce the energy consumption of the cascade system, it is possible to run the vacuum part at higher $T_{\text{cascade,cond}}$. The average energy consumption is $12,8 \text{ kWh/m}^3$ for the cascade. The efficiency of the TVS is slightly better than the SVS, using $5,64 \text{ kWh/m}^3$ compared to $5,8 \text{ kWh/m}^3$, and the cooling COP is higher throughout the temperature range. The high outlet temperature of the SVS is a result of the high pressure ratio. In ambient temperatures above 11°C the required pressure ratio is too high for the compressor to handle. Thus, to be able to operate at higher T_{amb} several compressor stages are necessary. The special compressor, both in size and construction, will lead to very large, complex and expensive systems.

Assuming an average price of $0,8 \text{ kr/kWh}$, including electricity, grid rent and taxes, the costs are $4,51 \text{ NOK}$, $4,64 \text{ NOK}$ and $10,24 \text{ NOK}$ per 1 m^3 of snow for the SVS, TVS and cascade respectively, meaning the TVS is the most reasonable vacuum system to operate.

The calculated energy consumption is much less than the existing machine from IDE Technologies. A comparison is difficult, since the configuration of the existing machine is not available to the public.

The calculated evaporation area required in the vacuum system, is unreliable due to f_{ec} . In a perfect vacuum, f_{ec} has a value of 1, while in ambient pressure the coefficient may just be a fraction of unity. A value of 0,2 is assumed, leading to a diameter of the vacuum vessel of 1,91m.

During the production period, the SCS consumes less energy than the TCS most of the time. Therefore, the SCS is the desired system configuration when operating sub-critically and the ambient temperatures is rather low. The average energy consumption is 24,47 kWh/m³ and 27,1 kWh/m³ for the SCS and TCS, respectively. However, at an ambient temperature of 18,7°C the compressor outlet temperature reach above the maximum temperature of 150°C and limits the operation of the SCS. Problems related to the compressor lubrication oil is limiting the system. Thus, if heat recovery or operation in high ambient temperatures is desirable, a system with two compressor stages is inevitable. The SCS and TCS operates with the same efficiency at T_{amb}=14°C.

In principle, Al-constructions have higher overall heat transfer coefficient than CS-constructions, due to higher thermal conductivity. However, the results show that the average U-value for the FID is larger for CS-constructions most of the time. The thermal resistance of ice is high due to low heat conduction through the ice layer. The ice growth rate is initially high for aluminium construction, leading to a rapid increase of the ice thickness. Due to a thicker ice layer on the Al-construction, the U-value is smaller than for CS. Therefore, it is the thickness of the ice layer rather than the properties of chosen material that decides the heat transfer. The ice layer of Al-constructions reaches 3mm after 32s, while CS and SST-constructions need 34s and 45s, respectively. Al-constructions reach 3mm first, due to the high initial growth rate, even though the ice growth rate is slightly lower the for CS-constructions.

Regarding the operating costs, the SCS is more reasonable than the TCS. The costs from September 1. to November 1. is 19,6 NOK/m³ for the SCS, while it is 21,7 NOK/m³ for the TCS. This means that the TCS are 10,7% more expensive to run.

It is desirable with low temperature variation at the freezing surface of the FID to avoid an uneven ice layer. The temperature distribution changes only with 0,8°C for a pipe width up to 39mm. This means that constructions with 200 refrigerant pipes or more, have more or less the same temperature distribution. Changing the thickness of the model will only result in a small reduction of the surface temperature, and production capacity will not suffer too much.

Based on the calculations, both the SCS and TCS is more energy efficient than the SF100 from TA. The energy consumption is 3,4% and 1,8% lower for the SCS and TCS, respectively.

Comparing the average energy consumption of vacuum and flake ice systems, show that the most efficient vacuum system consumes just 20,8% of the energy required by the least efficient flake ice system. In terms of operation costs, the snow from the flake ice system is 4,8 times more expensive than from the vacuum systems.

5. CONCLUSIONS

The flake ice model shows that SCS consumes less energy than a TCS in ambient temperatures below 14°C. The U-value and ice growth rate for the FID are highly dependent on the ice thickness. Ice has high thermal resistance, and dictates the heat transfer from water to CO₂ rather than the metals or refrigerants. The vacuum model shows that a TVS is more efficient than a SVS regardless of the ambient temperature. A cascade system with CO₂ is more energy intensive than the two previous systems.

The most efficient vacuum system consumes just 20,8% of the energy required by the least efficient flake ice system. In terms of operation costs, the snow from the flake ice system is 4,8 times more expensive than from the vacuum systems. However, the investment costs are much higher for the vacuum system. Therefore, the life-cycle cost is important to evaluate when choosing the right system.

Both the SCS and TCS is more energy efficient than the TA SF100. A comparison between the vacuum models and existing machines is difficult, due to little known information about the existing machine.

The COMSOL calculations reveal that increasing the number of refrigerant pipes in the FID above 200, do not affect the temperature distribution on the freezing surface too much. In addition, the thickness can be optimized regarding the structural strength, rather than the heat transfer.

NOMENCLATURE

Latin letters and abbreviations

| | | |
|-----------------|---|------------------------|
| A | Area | [m ²] |
| B | Constant, water heat transfer | [-] |
| CFC | Chlorofluorocarbon | [-] |
| COP | Coefficient of performance | [-] |
| C _p | Specific heat capacity | [kJ/kg·K] |
| d | Diameter | [m] |
| F | Correction factor evaporating CO ₂ | [-] |
| f _{ec} | Evaporation coefficient | [-] |
| FID | Flake ice drum | [-] |
| G | Mass flux | [kg/m ² ·s] |
| GWP | Global warming potential | [-] |
| h | Height | [m] |
| k | Thermal conductivity | [W/m·K] |
| L | Latent heat of fusion | [kJ/kg·K] |
| M | Molecular weight | [kg/kmol] |
| Nu | Nusselt number | [-] |
| ODP | Ozone depletion potential | [-] |
| P | Pressure | [Pa] |
| Pr | Prandtl number | [-] |
| PR | Pressure ratio | [-] |
| Q | Heat transfer | [kW] |
| q | Heat flux | [kW] |
| R | Thermal resistance | [K/W] |
| S | Nucleate boiling suppression factor | [-] |
| SCS | Single-stage flake ice | [-] |
| SVS | Single-stage vacuum system | [-] |
| T | Temperature | [C] |
| TCS | Two-stage flake ice | [-] |
| TVS | Two-stage vacuum system | [-] |
| U | Overall heat transfer coefficient | [W/m ² ·K] |
| x | Ice thickness | [m] |
| z | Gas quality | [-] |

Greek letters

| | | |
|---|---------------------------|-----------------------|
| α | Heat transfer coefficient | [W/m ² ·K] |
| β | Chevron angle | [deg] |
| δ | Wall thickness | [m] |
| μ | Dynamic viscosity | [kg/m·s] |
| ρ | Density | [kg/m ³] |

Subscripts

| | |
|------|-----------------------------|
| Al | aluminium |
| CS | carbon steel |
| e | equivalent |
| f | fluid |
| fg | liquid-gas phase transition |
| g | gas |
| gr | gravity |
| i | initial |
| l | liquid |
| LMTD | log mean temp difference |
| nb | nucleate boiling |
| SST | stainless steel |
| w | water |
| out | outlet |

REFERENCES

- CAO, W., BEGGS, C. & MUJTABA, I. M. 2015. Theoretical approach of freeze seawater desalination on flake ice maker utilizing LNG cold energy. *Desalination*, 355, 22-32.
- CHOI, K.-I., PAMITRAN, A. S. & OH, J.-T. 2007. Two-phase flow heat transfer of CO₂ vaporization in smooth horizontal minichannels. *International Journal of Refrigeration*, 30, 767-777.
- EAMES, I. W., MARR, N. J. & SABIR, H. 1997. The evaporation coefficient of water: a review. *International Journal of Heat and Mass Transfer*, 40, 2963-2973.
- GARCÍA-CASCALES, J. R., VERA-GARCÍA, F., CORBERÁN-SALVADOR, J. M. & GONZÁLEZ-MACIÁ, J. 2007. Assessment of boiling and condensation heat transfer correlations in the modelling of plate heat exchangers. *International Journal of Refrigeration*, 30, 1029-1041.
- INCROPERA, F. P., DEWITT, D. P., BERGMANN, T. L. & LAVINE, A. S. 2013. *Principles of Heat and Mass Transfer*.
- KILICARSLAN, A. & MÜLLER, N. 2005. A comparative study of water as a refrigerant with some current refrigerants. *International Journal of Energy Research*, 29, 947-959.
- ORSHOVEN, D. V., KLEIN, S. A. & BECKMAN, W. A. 1993. An Investigation of Water as a Refrigerant. *Journal of Energy Resources Technology*, 115, 257-263.

- PARK, C. Y. & HRNJAK, P. 2009. CO₂ flow condensation heat transfer and pressure drop in multi-port microchannels at low temperatures. *International Journal of Refrigeration*, 32, 1129-1139.
- SHAH, R. K. & SEKULIĆ, D. P. 2007. Fundamentals of Heat Exchanger Design. *Fundamentals of Heat Exchanger Design*. John Wiley & Sons, Inc.